2007

CHARACTERIZATION OF CARBON NANOTUBES BASED RESISTIVE AND CAPACITIVE GAS SENSORS

Ning Ma
University of Kentucky, nma2@uky.edu

ABSTRACT OF DISSERTATION

Ning Ma

The Graduate School

University of Kentucky

2007

CHARACTERIZATION OF CARBON NANOTUBES BASED RESISTIVE AND CAPACITIVE GAS SENSORS

ABSTRACT OF DISSERTATION

A dissertation submitted in partial fulfillment of the requirements for the degree of Ph. D. in Electrical and Computer Engineering in the College of Engineering at the University of Kentucky

By

Ning Ma

Lexington, Kentucky

Director: Dr. Janet K. Lumpp, Associate Professor of Electrical and Computer Engineering

Lexington, Kentucky

2007

ABSTRACT OF DISSERTATION

CHARACTERIZATION OF CARBON NANOTUBES BASED RESISTIVE AND CAPACITIVE GAS SENSORS

A preliminary gas detection study was conducted on as-grown multi-walled carbon nanotubes and anodized aluminum oxide (MWNTs/AAO) template. The material demonstrated room temperature gas sensitivity and p-type semiconductor characteristics. Plasma-etched MWNTs/AAO templates were employed to construct capacitive gas sensors. The capacitances of the sensors were sensitive to both reducing and oxidizing gases at room temperature. Single-walled carbon nanotubes (SWNTs) dispersed in binder α-terpineol were applied on sensor platforms to form resistive gas sensors. The sensors demonstrated excellent sensitivity to low concentrations of reducing and oxidizing gases at room temperature, which suggests the p-type semiconducting behavior of SWNTs. The sensor recovery was found to be incomplete at room temperature in flow of nitrogen and air, thus possible solutions were investigated to enhance sensor performance. The sensor operating principles and suggestions for possible future work are discussed. The room temperature and air background functionality of the sensor suggest that SWNT is a promising gas sensing material for application in ambient conditions.

KEYWORDS: carbon nanotube, gas, sensor, sensitivity, recovery

Ning Ma

12/04/07

CHARACTERIZATION OF CARBON NANOTUBES BASED RESISTIVE AND CAPACITIVE GAS SENSORS

By

Ning Ma

Janet K. Lumpp

Director of Dissertation

YuMing Zhang

Director of Graduate Studies

12/04/07

RULES FOR THE USE OF DISSERTATION

Unpublished dissertations submitted for the Doctor's degree and deposited in the University of Kentucky Library are as a rule open for inspection, but are to be used only with due regard to the rights of the authors. Bibliographical references may be noted, but quotations or summaries of parts may be published only with the permission of the author, and with the usual scholarly acknowledgments.

Extensive copying or publication of the dissertation in whole or in part also requires the consent of the Dean of the Graduate School of the University of Kentucky.

A library that borrows this dissertation for use by its patrons is expected to secure the signature of each user.

Name	Date

DISSERTATION

Ning Ma

The Graduate School

University of Kentucky

2007

CHARACTERIZATION OF CARBON NANOTUBES BASED RESISTIVE AND CAPACITIVE GAS SENSORS

DISSERTATION

A dissertation submitted in partial fulfillment of the requirements for
the degree of Ph. D. in Electrical and Computer Engineering
in the College of Engineering
at the University of Kentucky

By

Ning Ma

Lexington, Kentucky

Director: Dr. Janet K. Lumpp, Associate Professor of Electrical and Computer Engineering

Lexington, Kentucky
2007

DEDICATION

To my parents Chuanli Ma and Shuzhen Hou, for your love and support.
I could not have done it without you.

ACKNOWLEDGEMENTS

The author wishes to express his sincere gratitude and appreciation to his advisor Dr. Janet Lumpp, for her constant encouragement, invaluable guidance and advice throughout this research work.

The author is very much obliged to Dr. Vijay Singh for accepting to be one of the dissertation committee members, for his advice and assistance during the first part of this work. And the author is also thankful to Dr. Rodney Andrews, Dr. James Lumpp and Dr. John Selegue for accepting to be the committee members.

Appreciation also goes to colleagues Dr. Suresh Rajaputra, Patricia Clore, Jing Li, Piao Liu, George Spiggle and Larry Rice for their assistance, inspiration and kindness.

The author wishes to acknowledge the financial support for this project from Army Research Laboratory under Cooperative Agreement Number W911NF-04-2-0023. The authors also would like to thank CoorsTek and Heraeus for their donation of the materials during sensor fabrication.

Finally, the author thanks his family for their love, encouragement, patience and assistance.

TABLE OF CONTENTS

LIST OF TABLES

LIST OF FIGURES

LIST OF FILES

CHAPTER1: INTRODUCTION AND OVERVIEW

1.1 Introduction

1.1.1 A brief overview of chemical gas sensors

By definition, a chemical gas sensor is a device capable of altering its physical properties (electrical conductance, capacitance, or mass) upon exposure to a gaseous chemical compound or mixture of chemical compounds. The change in properties is observed as an electrical signal and then used to detect the species. Generally, gas sensors are required to perform within required ambient and process conditions with fast response time and acceptable accuracy. They must conform to size, weight, and cost constraints of individual applications and measure the properties within the required range over an acceptable lifetime.

Gas sensors can be classified according to their operating principles as metal oxide semiconductor sensor, electrochemical sensor, gas sensitive field-effect transistors (FETs), solid electrolyte, pellistor catalytic gas detector, bulk and surface acoustic wave devices (BAW and SAW), and conducting polymer, etc. The operating principle and features of a few most commonly used types will be briefly summarized in the next chapter.

Currently, chemical gas sensors find extensive applications in toxic and combustible gas monitoring, automobile combustion control, medical analysis and energy and drying operations markets. The emerging markets include defense, consumer products, automobiles, wastewater treatment, and food and beverage processing, etc [1]. The entire US gas sensor market is projected to be over $2.8 billion in sales in 2008 [2].

The major advantages of the commercially available gas sensors are low cost, small size and simplicity in function. The size is typically measured in centimeters to micrometers and the cost is minimized by large scale, batch fabrication. In contrast to

some of the conventional laboratory scale analytical instruments, for example, gas chromatography, ion mobility spectroscopy and mass spectroscopy; gas sensor devices require much simpler equipment to run an analysis and the cost of operation is much lower. Gas sensor devices are effective in real-time in situ applications.

1.1.2 Motivations and contributions

Despite the attractive features listed in the previous section, gas sensors in the market do have some drawbacks which impair their long term performance. The common concerns of most gas sensors are stability, reproducibility, selectivity and sensitivity [1]. However, the specific objective of this dissertation is to address one of the major disadvantages of gas sensors, i.e., their lack of functionality at room temperature. Most of the gas sensors in the market are operated at 200 to 600ºC thus a built-in heater is very common in the sensor structure. Unfortunately the built-in heater will increase the design complexity and power consumption of the sensor device. As a result, searching for new gas sensing materials with acceptable performance at room temperature has been an interesting research topic.

Recently, carbon nanotubes (CNTs) have shown promise for gas sensing due to their high surface area and their capability to change electrical properties at room temperature upon exposure to different gases [3]. Gas sensing studies have been based either on single-walled carbon nanotubes (SWNTs) or on multi-walled carbon nanotubes (MWNTs). In this dissertation both approaches were investigated for room temperature gas sensing application. First, a highly automated gas sensor testing system was designed and implemented, which features a PC controlled gas delivery system, real time electrical signal measurement, data acquisition configuration, LabVIEW program and user-friendly interface. Next, resistive and capacitive gas sensors based on vertically aligned MWNTs were fabricated and tested. These aligned MWNTs were prepared by chemical vapor deposition (CVD) through anodized porous alumina oxide template (AAO). The work described here is the first report to construct a gas sensor device based on this unique CNT structure. A conference paper based on this work was accepted and presented at 39th International Microelectronics and Packaging Symposium in October 2006. Then,

the performance of a resistive sensor based on the mixture of low loading SWNTs and organic binder was studied. To date, this is the lowest reported SWNT loading (1 wt %) for this type of sensor with excellent response. A journal paper manuscript based on this part of the work has been submitted to Sensors and Actuators for peer review. The main purpose of this dissertation is to evaluate MWNTs and SWNTs as gas sensing materials at room temperature.

1.1.3 Collaborative activities

The research covered in this dissertation is a part of the Advanced Carbon Nanotechnology Program (ACNP) which is financially supported by the Army Research Laboratory under the Cooperative Agreement Number W911NF-04-2-0023. The synthesis of the nanotube materials described in chapter 3 was performed by Dr. Vijay Singh's research group using the facilities at the Center for Applied Energy Research of University of Kentucky. The collaboration with Dr. Singh's group has produced several journal papers and conference papers, which are either accepted or under review.

1.2 Overview of the Dissertation

There are three major objectives in this dissertation. The first objective is to review the major gas sensing technologies and recent development of carbon nanotubes for gas sensing applications. The second objective is to fully describe the experimental and theoretical work on gas sensors based on both aligned multi-walled carbon naotubes and single-walled carbon nanotube powders. The third objective is to analyze the performance and limitations of these carbon nanotube gas sensors, and suggest future improvements.

Chapter 2 reviews the techniques and mechanisms of major gas sensors on the market, the emerging of carbon nanotubes as potential gas sensing material, and the development of carbon nanotube based gas sensing research. The current status of gas sensors and gas sensing potentials of nanotubes are the motivations of this dissertation.

Chapter 3 briefly introduces the preparation and the features of the aligned MWNTs/AAO template. Using the as-grown MWNTs/AAO template, resistive gas sensing tests demonstrate response to NH_3 and CO_2 at room temperature. In chapter 3, a capacitive sensor design is described and the results of gas detection are presented. The gas sensing mechanism of the MWNTs based capacitive sensor is explained and a sensor model is proposed. The concept of inductor-capacitor resonant sensor is verified experimentally using both a commercial humidity sensor and MWNTs capacitive sensor.

Chapter 4 describes a resistive gas sensor based on SWNTs. The gas sensing material is prepared by mixing the SWNT powders with organic binder and then coating on the sensor platform. After annealing, the sensor is employed to detect both reducing and oxidizing agents at room temperature. The response demonstrated by the SWNT sensor indicates p-type semiconductor characteristic and great potential as room temperature gas sensing material. The limitation of sensor recovery is illustrated and the detailed sensing and recovery mechanisms are discussed in chapter 4. The techniques to improve sensor performance are applied and the results are demonstrated and explained. Finally, the sensor performances in a background of air as well as temperature and humidity dependencies are discussed.

In chapter 5, summaries for the entire dissertation are given and the possible directions for future research are identified.

CHAPTER2: LITERATURE REVIEW

2.1 Introduction

Chapter 2 reviews common gas sensor operating principles as well as advantages and disadvantages of each technology. The exceptional physical properties of carbon nanotubes (CNTs) are described and explained as they pertain to the gas sensing application. A brief review of the research of CNTs in the development of chemical gas sensing is provided in the last part of this chapter.

2.2 Techniques and Mechanisms in Gas Sensing

Table 2.1 lists some common health hazardous gases and human exposure limits recommended by U.S. Department of Labor [4]. One can see that the gas sensor detection limit for some extremely dangerous substances could be as low as 0.05 parts per million (ppm). By utilizing various sensing materials and operating principles, the gas sensors in the market have satisfied most of the demands by industry. In this section brief reviews are given for the most commonly used gas sensors and some of the key factors to evaluate sensor performance are introduced.

2.2.1 Gas sensor characteristics

Section 2.2.1 defines technological aspects used through out this dissertation to evaluate gas sensor characteristics and to compare sensor performance.

Sensitivity is the ratio of the change in sensor output in response to the change in sensor input in the presence of target gas. By definition if a sensor output y is related to the input x by the function y = f(x), then the sensitivity $S(x_a)$ at point x_a is [5]:

$$S(x_a) = \frac{dy}{dx}\Big|_{x=x_a} \tag{2.1}$$

In this dissertation, for a resistive gas sensor, the sensitivity S is defined as:

$$S(\%) = \frac{R_{gas} - R_0}{R_0} \times 100 \tag{2.2}$$

where R_0 is the sensor resistance in the presence of carrier gas, R_{gas} is the sensor resistance in the presence of target gas, and S is the resistance sensitivity in percentage. The sensitivity S of a capacitive sensor in this dissertation is defined as:

$$S(\%) = \frac{C_{gas} - C_0}{C_0} \times 100 \tag{2.3}$$

where C_0 is the sensor capacitance in the flow of carrier gas, C_{gas} is the sensor capacitance in the presence of target gas, and S is the capacitance sensitivity in percentage.

Response time is typically defined as the time for the output of a gas sensor to reach a certain percentage of full scale after being exposed to target gas. For example, T_{90} = 60 seconds means that it takes the sensor 60 seconds to reach 90% of its full scale output after being exposed to a full scale gas concentration.

The time for the output of a gas sensor to return to its baseline value after the removal of the target gas is defined as sensor recovery time. In the sensor industry it is usually specified as time to fall to 10% of steady state value after the removal of the measured gas. Figure 2.1 shows an example of gas sensor response time and recovery time.

Selectivity is the ability of a gas sensor to detect a target gas without being affected by the presence of other interference gases. Most gas sensors are sensitive to a family of gases and it is difficult to produce a sensor specific to only one gas. Moreover, temperature and humidity may also affect sensor performance. A common practice for manufactures of gas sensors is to provide data indicating the changes of different gases on the sensor output in the presence of common interference gases.

Repeatability is defined as the ability of a sensor to repeat the measurements of gas concentrations when the same measurand is applied to it consecutively under the same conditions.

The closeness between the calibration curve and a specified straight line is defined as linearity [5]. Generally the initial response of a gas sensor is nearly linear and it tends to saturate as the gas concentration increases. A typical gas sensor response curve, which consists of near linear region, nonlinear region and saturation region, is shown in Figure 2.2. One can see that the sensor output provides better linearity at lower concentration than at higher concentration.

Gas concentration is expressed as volume percent (%) or ppm (parts per million by volume) throughout this dissertation. These are unitless expressions as they simply express the ratio of gases in relation to the balance or carrier gas, such as air or nitrogen (N_2). For example, 100 ppm NH_3 in N_2 means 100 parts of NH_3 diluted in 999,900 parts of N_2.

2.2.2 Metal oxide semiconductor gas sensor

Metal oxide semiconductor gas sensors were first developed by Seiyama and Taguchi in the 1960s. Seiyama found the gas sensing effect of metal oxides [6] and later Taguchi brought semiconductor gas sensors based on metal oxides to an industrial product [7][8][9]. Therefore, a metal oxide semiconductor sensor is also known as Taguchi sensor. Under suitable conditions many metal oxide semiconductor show gas sensitivity, including tin dioxide (SnO_2), zinc oxide (ZnO), tungsten oxide (WO_3), iron oxide (Fe_2O_3), and titanium dioxide (TiO_2) [1]. Among them the most widely used material is SnO_2 doped with small amounts of catalytic additives such as palladium (Pd) or platinum (Pt). By choosing different catalyst and operation conditions, Taguchi sensors have been developed for various applications such as domestic safety (CO and methane), industry safety (NH_3, O_2, H_2, and H_2S), air quality control (CO_2), and automotive (general air contaminants) [10].

The basic structure of a 3-dimensional Taguchi sensor consists of a ceramic supporting tube with a platinum heater coil and a sintered semiconducting SnO_2 coating on the outside as shown in Figure 2.3. The schematic shows that the heater is embedded in a

ceramic tube and the semiconductor material SnO_2 is deposited on the tube with two printed gold electrodes. The purpose of the heater is to achieve the typical sensor working temperature range of 200-550˚C and the two gold electrodes are for the measurement of gas sensitive changes in electrical conductivity. The sensitivity results from conductivity change caused by reactions occurring on the surface of SnO_2 particles. 2-dimensional, planar metal oxide semiconductor gas sensors are fabricated by using screen-printing techniques. SnO_2 films are printed to a thickness in the range of 50-500 μm over interdigitated electrodes evaporated onto ceramic substrates. A thin metal heater track is printed on the back side of the substrate. Figure 2.4 shows the basic structure of a typical 2-dimensional planar SnO_2 sensor [12].

The operation principle of Taguchi sensor can be described as follows: when n-type semiconductor SnO_2 is heated at a certain temperature in air, oxygen is adsorbed on its surface. The majority carrier electrons in the metal oxide semiconductor are transferred to the adsorbed oxygen molecules as the result of following reaction:

$$2e^- + O_2 \rightarrow 2O^- \tag{2.4}$$

The chemisorption of oxygen takes electrons out of semiconductor bulk, leave positive charges and form a space charge layer at the surface of SnO_2. At SnO_2 grain boundaries, a space charge layer (potential barrier) prevents charge carriers from moving freely, therefore surface conductivity decreases. Figure 2.5 describes the model of inter-grain potential barrier and shows that the surface potential formed serves as a potential barrier against electron flow. Since the sensing material, SnO_2, is in the form of a compressed powder, i.e. sintered particles, the space charge induced by the oxygen adsorption can be a significant fraction of the whole grain; therefore the adsorption causes the resistance of the SnO_2 film to increase considerably.

When reducing gas molecules react with the adsorbed oxygen species at high temperature they oxidized and acting as electron donor during the reduction-oxidation process. The reaction can be described as Eq 2.5 where R denotes reducing gas:

$$R + O^- \rightarrow RO + e^- \tag{2.5}$$

As the result, the surface density of negatively charged oxygen decreases, so the height of potential barrier at grain boundary is reduced along with the sensor resistance.

The operating temperature for metal oxide semiconductor gas sensors is between 200ºC and 550ºC [11]. There are two reasons why the sensor is operated at elevated temperatures. First, at temperature below 100ºC the metal oxide surface will be covered by a layer of water molecules (ambient humidity) which prevents the reaction of the gas with the oxide surface. Second, the reaction rate at the oxide surface will be very slow if operated at temperatures below 200ºC. The advantages of metal oxide semiconductor sensors are their high sensitivity to most combustible gases including saturated hydrocarbons, NO and CO, simple sensor structures, fast response time, good reliability, and low production cost. Disadvantageous are the relatively poor selectivity and high operation temperature. The selectivity can be modified by doping the metal oxide with catalytic additives, by changing the operation temperature, or by modifying the grain size. As a consequence of high operating temperature the power consumption of metal oxide semiconductor sensor is relatively high. A typical commercial Taguchi sensor has power consumption of approximately 800 mW. This level of power consumption is too high for applications where battery operation is required.

2.2.3 Electrochemical gas sensor

The operating principles of electrochemical gas sensors are the same as liquid electrolytic fuel cells. They are based on the electrochemical oxidation or reduction of the analytic gas at a catalytic electrode surface. Basically, they detect gases by producing a chemical reaction between the gas and oxygen contained in the sensor. The reaction produces a small current, which is proportional to the concentration of the gas present. Commercial electrochemical gas sensors are used for a variety of applications including medical and gas purity application, air quality monitoring, industry control, and toxic gas monitoring.

The simplest form of a fuel cell electrochemical sensor and the schematic diagram of the cross section of a sensor structure are shown in Figure 2.6. A typical electrochemical

sensor consists of a sensing electrode and a counter electrode separated by a thin layer of electrolyte. The electrode is normally made of catalytic metal and the electrolyte is a concentrated, ion-conducting aqueous solution such as sulfuric acid or potassium hydroxide depending on the sensor chemistry [13]. External gases have relatively easy access to the sensing electrode whereas the counter electrode is located in the bulk of the electrolyte within the body of the sensor, where diffusion access by ambient atmospheric gases is severely restricted. The diffusion barrier can be a capillary or a membrane and it controls the diffusion of reactant gas to the sensing electrode [14]. To measure the output current of the sensor, a load resistor connects the sensing electrode and the counter electrode to provide a voltage output across the load.

The target gas present in the ambient air diffuses through the capillary inlet or the pores of hydrophobic membrane and then reacts on the catalytic sensing electrode surface at the three-phase boundary between the electrode, the electrolyte, and the gas. The reaction causes the potential of sensing electrode to shift. The reactions at the sensing electrode for several gases are as follows:

$$CO + H_2O \rightarrow CO_2 + 2H^+ + 2e^- \tag{2.6}$$

$$H_2S + 4H_2O \rightarrow H_2SO_4 + 8H^+ + 8e^- \tag{2.7}$$

$$NO + 2H_2O \rightarrow HNO_3 + 3H^+ + 3e^- \tag{2.8}$$

$$H_2 \rightarrow 2H^+ + 2e^- \tag{2.9}$$

Simultaneously, the reactions at the counter electrode need oxygen molecules to complete the process:

$$O_2 + 4H^+ + 4e^- \rightarrow 2H_2O \tag{2.10}$$

Electrochemical reduction of a reactant gas at the sensing electrode is also possible, for example NO_2 sensing:

$$NO_2 + 2H^+ + 2e^- \rightarrow NO + H_2O \tag{2.11}$$

As the result of the potential difference between the sensing electrode and counter electrode, current will start to flow in the external circuit. The current is sustained by electrochemical oxidation of the reactant gas at the sensing electrode and an equivalent amount of oxygen reduction at the counter electrode. One can see from Eq 2.10 that an

oxygen supply must be provided to the counter electrode to maintain the current. Oxygen is found dissolved in the electrolyte. Replenishment of the oxygen used in the reaction can be provided by oxygen in the sample gas or by diffusion of oxygen through the housing of the sensor. However for some particular applications such as indicated by Eq 2.11, oxygen is not necessary for electrochemical sensor to maintain proper operation.

The most attractive feature of electrochemical sensors is that they provide a direct relationship between the output signal and the target gas concentration, i.e., the output current is proportional to the gas concentration. Electrochemical sensors also have the advantages that they operate at room temperature, are robust and have 1 to 2 years of life expectancy. Electrochemical sensors require very little power to operate. In fact, their power consumption is the lowest among all sensor types available for gas monitoring. Generally electrochemical sensors are quite sensitive to temperature therefore it is necessary to keep the sample temperature as stable as possible. Oxygen detection by electrochemical sensing has the best selectivity whereas detections of other gases are subject to interference from background gases [13].

2.2.4 Solid electrolyte – lambda sensor

The best known solid electrolyte based gas sensor is zirconia (ZrO_2) oxygen sensor, which is mainly used for monitoring the air-to-fuel ratio in combustion engines. In the automotive industry, a zirconia oxygen exhaust sensor is also called a lambda sensor or lambda probe. Figure 2.7 illustrates the basic structure of a simplified zirconia oxygen sensor. The potential between the two electrodes depends on the ratio of the partial pressure of oxygen at each electrode, separated by the oxygen ion conductor zirconia. The chemical reactions (electron transfer) at each electrode are the same but in reverse, i.e. at one electrode the reduced form of the chemical particle is being oxidized (releasing electrons) and at the other electrode the oxidised form is being reduced (accepting electrons). The reactions at the electrodes are as follows:

$$4e^- + O_2 \rightarrow 2O_2^{2-} \tag{2.12}$$

$$2O_2^{2-} \rightarrow 4e^- + O_2 \tag{2.13}$$

The potential difference between two electrodes is defined by Nernst equation [1]:

$$E = \left(\frac{RT}{4F}\right)\ln\left[\frac{P_{O_2(ref)}}{P_{O_2(test)}}\right] \tag{2.14}$$

where T is temperature, R is the gas constant, F is the Faraday constant, and P is partial pressure. Therefore a higher concentration of oxygen on one side of the zirconia electrolyte leads to a potential difference which, according to the Nernst equation, is proportional to the ratio of the two oxygen concentrations.

In order for a ZrO_2 sensor to function properly, the zirconium dioxide is often doped with yttrium oxide (Y_2O_3) and heated above 500ºC [1]. Yttrium oxide dopants are able to create more defects so that the ionic conductivity is enhanced. ZrO_2 sensors can be tailored to have excellent O_2 selectivity by choosing optimized electrode material. However, the limitation of its operating principle makes it impossible to use lambda sensor for lower temperature applications.

2.2.5 Pellistor

Pellistors, also known as catalytic combustion sensors, are detectors for combustible gases such as methane. The sensing elements consist of small pellets of catalyst-loaded ceramic whose resistance changes in the presence of the target gas. The term 'pellistor' is the combination of 'pellet' and 'resistor'. As shown in Figure 2.8, the typical pellistor sensing element consists of a platinum wire spiral supported within a porous alumina bead. Particles of precious metal catalyst are added into alumina to accelerate the oxidation reaction. There is a number of catalyst materials available, typically platinum or palladium, and they are carefully chosen to optimize sensor performance. The platinum wire is used to heat the catalyst bead above 500ºC to facilitate the combustion reaction. It also serves as resistance thermometer to measure the temperature of the catalyst bead [11].

The commercial pellistor system typically consists of a pair of sensing elements operated in a Wheatstone bridge circuit, referred to as a detector and compensator

(reference element). The detector is a platinum wire spiral embedded within a bead of catalytic material (Figure 2.8). The compensator is similar except that the bead is alumina without any catalytic material. Oxidation occurs at approximately 500ºC when a combustible gas is present at the detector. The burning increases the temperature of the element and the generated heat is transmitted to the platinum wire which causes the wire resistance to increase. At the same time, the inert compensator stays at a constant temperature. An electrical imbalance occurs in the bridge circuit and a voltage output is obtained. The output voltage level depends on the type of the detected gas and it is normally proportional to the gas concentration.

Pellistors are capable of detecting various combustible vapours and flammable gases at concentration as low as 500 ppm with relatively fast response times (20 seconds) [11]. They have robust construction and life expectancy is of a few years. However, they have high power consumptions (typically 350 mW) due to the elevated operating temperature. Another disadvantage of pellistors is that they tend to be 'poisoned' by volatile compounds which leave involatile oxidation products covering the catalyst surface impeding sensor performance.

2.2.6 Gas sensitive FET

Field-effect gas sensors are based on metal insulator semiconductor field effect transistor (MISFET) structures in which the metal gate is a gas sensitive catalyst such as platinum (Pt), palladium (Pd), and iridium (Ir). MISFETs operate in a temperature range of 200ºC to 600ºC [1].

The basic structure of a MISFET gas sensor is depicted in Figure 2.9 (adapted from [1]). Conduction between the source and drain of the transistor is controlled by charge or potential on the gate electrode. Charge present at the gate gives rise to a reflected charge induced in the channel and this modifies the conductance between source and drain. Any process that changes either the charge on the gate or its potential will alter the conduction of the channel and this can be detected as an electrical signal. A MISFET sensor with catalytic metal gate was first reported sensitive to hydrogen at

1975 [16]. In detection mode, hydrogen molecules decompose to H atoms by dehydrogenation on the catalytic metal gate surface. The H atoms then diffuse to the metal/insulator interface and influence the charge in the semiconductor, thereby changing the drain source current.

Since the dehydrogenation and catalytical process are temperature dependent, selectivity to different gases can be achieved by changing the operating temperature, the catalytic metal gate material, and the thickness and morphology of the gate metal [17]. MISFET sensors can thus be made sensitive to a broad range of hydrogen-containing or polar compounds such as hydrogen [16], ammonia [18], hydrogen sulfide [19], and alcohol [20]. The sensors are stable and exhibit a relatively low sensitivity to moisture. Due to the well-established MISFET fabrication processes in the semiconductor industry, MISFET sensors can be manufactured in large batches with high reproducibility and low cost.

Besides conventional MISFET, suspended gate FETs, which were first described by Blackburn *et al.* [21], are also popular for chemical gas sensing. In the suspended gate FET (SGFET) the gate metal is suspended above the gate insulator (SiO_2) by a narrow gap with access holes for gas molecules. This construction makes it possible to develop gas sensors sensitive to gases other than hydrogen because the metal/gaseous-insulator interface is now freely accessible to the gas instead of the gas having to diffuse through the gate material as in the case of the Pd gate MISFET. The basic structure of a SGFET is schematically described in Figure 2.10 [22].

2.2.7 Others

Conducting polymers have been used primarily as chemiresistor structures (Figure 2.11), although their uses in acoustic wave devices, in suspended gate FETs, and as capacitive sensors have also been investigated [23][24][25][26]. The most commonly used polymers for gas sensing are those based on pyrrole, aniline, or thiophene monomers. Chemiresistors based on conducting polymers can be fabricated by deposition of a thin polymer film on an insulating substrate with a narrow electrode gap.

While operating at room temperature, the adsorption of gases into the polymer matrix and the interaction with the matrix causes a change in the conductivity of the polymer. The conductivity of the polymer is simply measured at a constant current or voltage, so called chemiresistor. The advantages of conducting polymer gas sensors are room temperature operation, relatively high sensitivity, and simple sensor structure. However, lack of reproducibility of fabrication, strong humidity interference, and the base line drift over time have been concerns associated with the further development of conducting polymer chemiresistor gas sensors.

Acoustic wave gas sensors operate by monitoring the effect of adsorbed gas molecules on the acoustic wave propagation. There are two types of acoustic wave sensors: bulk acoustic wave sensor (BAW) and surface acoustic sensor (SAW). Both share a similar device structure which consists of a piezoelectric crystal substrate (such as quartz) coated with a coating for gas adsorption. The adsorption of gas molecules changes the velocity of the acoustic wave hence the effect of wave propagation on the sensor frequency can be detected [14]. The schematic diagram of a basic SAW device is shown in Figure 2.12. A pair of interdigitated (IDT) electrodes is patterned on a single piece of quartz coated with polymer film. Acoustic wave propagation is stimulated by applying an a.c. voltage to one set of IDT (transmitter) and detected by a second set (receiver). The delay between launching and receiving the wave depends on the velocity of the surface acoustic wave. SAW is preferred over BAW in gas sensing applications because they can be operated at higher frequency (up to 300 MHz) to achieve higher sensitivity. Typical detection limits of SAW sensors are 50 ppm for hydrogen, 10 ppm for H_2S and 0.5 ppm for NO_2 [27].

2.3 Properties of Carbon Nanotubes

A considerable amount of research in new gas sensors has been carried out in order to meet the increasing demand for gas detection technologies. Recent developments in nanotechnology provide the opportunity to dramatically improve sensor performance. Nanotechnology is referred to any process or product that involves sub-micron dimensions, but a more concise definition is any fabrication technology in which objects

are built by the specification and placement of individual atoms or molecules or where at least one dimension is less than 100 nm [28]. Since early the 1990s, research interest in nanotechnology has grown rapidly ranging from new high-performance nanomaterials to nano-scale electronics and Micro-Electro-Mechanical Systems (MEMS). The sensor research community has also benefited from nanotechnology, especially through the development of advanced nanomaterials. One of the most widely studied new nanomaterials is carbon nanotube (CNT).

Ijiima at the Japanese NEC Corporation first discovered CNTs in 1991 [29]. CNTs have special structures that are different from graphite and carbon fibers. There are two types of nanotubes: single-walled carbon nanotubes (SWNTs) and multi-walled carbon nanotubes (MWNTs). Single-walled nanotubes consist of a single layer of graphite sheet wrapped into a cylindrical tube seamlessly. Multi-walled carbon nanotubes comprise an array of single-walled nanotubes that are concentrically nested like rings of a tree trunk [30]. The typical diameter of CNTs ranges from 1 to100 nm and lengths up to millimeters. Carbon arc discharge, laser ablation of carbon, and chemical vapor deposition (CVD) on catalytic particles are the most commonly used methods for CNTs synthesis.

SWNTs may be either metallic or semiconducting, depending on the direction in which the graphite sheet twists to form the seamless nanotube cylinder. The diameter and helicity of a SWNT are characterized by the vector [31]:

$$C = na_1 + ma_2 \equiv (n, m) \tag{2.15}$$

where a_1 and a_2 are graphene lattice vectors and n and m are integers to represent nanotube type. Depending on the appearance of the belt of the nanotube diameter, the nanotube is either armchair (n = m), zigzag (n = 0 or m = 0), or chiral (any other n and m). All armchair SWNTs and those with n-m = 3k (k is a non-zero integer), are metallic. All others are semiconductors with the band gap inversely depend on the diameter [30].

A brief summary of some extraordinary electrical, mechanical and thermal properties of CNTs is provided in Table 2.2 [32]. With the nearly one-dimensional structures,

electronic transport in CNTs was found to take place through quantum effects and to be ballistic along the nanotube axis without scattering. Consequently they are capable of conducting high current density without dissipating heat [33][34]. In theory, metallic CNTs can have a current density 1000 times higher than that of metals such as silver and copper [35].

CNTs are excellent thermal conductors along the tube axis due to the effect of ballistic electron conduction. Kim, *et al*. [36] reported a measured room temperature thermal conductivity of 3000 W/m·K for an individual MWNT, which is greater than that of natural diamond and the basal plane of graphite (~ 2000 W/m·K). It is predicted that the thermal conductivity of CNTs could reach 6000 W/m·K at room temperature. Comparing this to copper, a metal well-known for its high thermal conductivity, CNTs offer a fifteenfold increase [35]. Superconductivity in CNTs has been observed at low temperatures. For example, 0.55 K transition temperature for SWNTs with 1.4 nm diameters and 5 K transition temperature for those with 0.5 nm diameters have been reported [37][38].

CNTs are one of the strongest and stiffest materials known, featuring high Young's modulus and high tensile strength. The mechanical strength is the result of the covalent sp^2 bonds formed between the individual carbon atoms along the walls of CNTs. Gao *et al.* [39] reported the calculated Young's modulus for an individual (10,10) SWNT is approximately 0.64 TPa (1012 Pa), which is consistent with measured results [40]. Yu *et al.* measured a tensile strength of 63 GPa for MWNTs [41]. In comparison, the tensile strength of MWNT is approximately 50 times greater than that of high-carbon steel [42].

In recent years, the high mechanical strength and unique electrical properties of CNTs have attracted considerable interest for various applications utilizing individual or ensembles of CNTs including: as atomic force microscope (AFM) tips [43][44], field emission devices and displays [45][46], electromechanical actuators [47], CNT-based field effect transistors (CNTFET) [48][49][50][51], and CNT composite materials [52][53][54] etc.

2.4 Development of Carbon Nanotubes as Gas Sensing Materials

Since the year 2000, the potential for CNT chemical gas sensing applications has attracted extensive research effort for three significant reasons. First, CNTs are surface reacting materials, i.e., they are composed entirely of surface atoms where adsorbed gas molecules can dramatically change CNT electrical properties at room temperature. Next, the ballistic electronic transport along the CNT axis provides excellent transmission of the altered electrical signal to the external contact. Third, the long-term performance of CNTs based sensor may be stable due to their chemically robust graphitic surface. CNTs for gas sensing at room temperature are of great interest because most currently available sensors operate at elevated temperatures. A brief review of research on CNTs for gas sensing is given in this section. Due to the nature of this dissertation research, the discussion will focus on non-functionalized as-grown CNT based gas sensors.

2.4.1 Conductance-based detection

The pioneer works by Kong, *et al*. [55] and Collins, *et al*. [56] were the first to report that the adsorption of certain gas molecules can dramatically change the electrical conductance of SWNTs. Kong and coworkers investigated individual p-type semiconducting SWNT as a resistive sensor for NO_2 and NH_3 detection at room temperature in air or argon. They demonstrated that the oxidizing agent NO_2 (an electron acceptor) causes the conductivity of p-type SWNT to increase while the reducing agent NH_3 (an electron donor), causes a reduction in conductance [55]. The detection limit of their SWNT sensor was found to be ~ 2 ppm for NO_2 and ~ 0.1% for NH_3. They concluded that the sensing mechanism is based on the charge transfer between the p-type semiconducting SWNT and electron-withdrawing NO_2 and electron-donating NH_3 gas. The recovery time of the sensor was found to be 12 hours and it was significantly reduced by heating the sample in air at 200ºC [55]. Using transport measurement and scanning tunneling spectroscopy, Collins and coworkers demonstrated that the electrical resistance, thermoelectric power and local density of states of SWNT are sensitive to air or oxygen exposure. By alternating the medium between air (or oxygen) and vacuum, a reversible change in SWNT resistance was observed [56]. They attributed this variation in

resistance to the charge transfer between adsorbed oxygen molecules and SWNTs. However, in order to fully recover, the sample had to be heated above 110ºC for several hours in vacuum for oxygen to be desorbed [56]. The authors also suggested that any intrinsic properties measurement on as-prepared CNTs could be compromised by extrinsic air exposure (oxygen exposure). Therefore they claimed that the electronic properties of a given nanotube are not only specified by its chirality and diameter but also depend on gas exposure history.

Li, *et al*. investigated an SWNT based sensor for the detection of NO_2 and nitrotoluene vapors at room temperature [57]. Randomly orientated SWNTs were dispersed in dimethylformamide (DMF) and drop-deposited on a sensor platform with interdigitated electrodes patterned on top. The SWNT sensor responded in seconds to the presence of NO_2 within the concentration range of 6-100 ppm while pure nitrogen was used as carrier gas for dilution and purging. The conductance of the SWNT sensor was increased significantly by exposure to the oxidizing agent NO_2. Due to the high bonding energy between SWNT and NO_2, the sensor recovered slowly with a recovery time on the order of 10 hours, which is consistent with the results reported by other researchers [55]. Li and coworkers applied ultraviolet (UV) light illumination during recovery and successfully accelerated the recovery time to 10 min [57]. They reported that the UV illumination lowered the desorption energy barrier of CNTs thus facilitating the NO_2 desorption. Chen, *et al.* were the first to discover the photo-induced molecular desorption in molecule-CNT systems [58]. They found that UV light induced desorption of oxygen, NO_2, and NH_3 molecules can drastically alter the electrical characteristics of semiconducting SWNTs. Although the mechanism has not been fully understood, they suggested that the photodesorption in CNTs is a non-thermal process and wavelength dependent.

Parallel theoretical studies have also predicted significant variation of the electronic properties of CNTs as the result of gas molecules adsorption. Zhao, *et al*. have performed first principles calculations on the electronic properties of SWNT upon adsorption of various gas molecules, such as NO_2, O_2, NH_3, N_2, CO_2, CH_4, H_2O, H_2 and

Ar [59]. The authors found all molecules, either electron donor or electron acceptor, are weakly adsorbed on SWNT with small charge transfer. They also obtained the equilibrium position, adsorption energy, charge transfer, and electronic band structures for SWNTs with various structures [59].

Bradley and coworkers used SWNT field-effect transistor to detect NH_3 through the shift of gate voltage [60]. They determined that the shift of gate voltage is due to the charge transfer between SWNT and adsorbed NH_3 molecules. Their experiments measured the amount of charge transfer to be approximately 0.04 electrons per NH_3 molecule [60]. Qi, *et al*. fabricated arrays of electrical devices with each comprising ensembles of SWNTs bridging metal electrodes for NO_2 detection. The sensor is capable of detecting NO_2 at less than 1 ppb (parts per billion) concentration [61]. Their calculations indicate that NO_2 binds to the SWNT surface with energy of 0.8 eV and withdraws approximately 0.1 electrons per molecule [61]. Chang and coworkers investigated the adsorption of NH_3 and NO_2 molecules on semiconducting (10,0) SWNTs through density function theory [62]. Their calculation shows that the binding energies are less than 0.5 eV for both molecules (0.18 eV for NH_3 and 0.42 for NO_2) [62]. Therefore they claim that both NH_3 and NO_2 molecules bind to nanotubes by physisorption and the electron charge transfer is the major mechanism for the change of conductivity.

Although most of the attention has focused on SWNTs for gas sensing, MWNTs do present one attractive feature with respect to SWNTs, i.e., low production cost. Recently, there have been increasing numbers of reports on the studies of MWNTs for gas detection. Cantalini, *et al*. [63] reported the influence of the catalyst geometry on the growth of MWNTs and their electrical response to NO_2 of 10-100 ppb concentrations at different operating temperatures ranging from 25 to 215ºC. The resistive gas sensor was fabricated by PECVD depositing MWNTs on Pt interdigitated electrodes based on Si/Si_3N_4 substrate [63]. The maximum response was found at 165ºC and the sensor showed fast dynamic response and reproducible electrical properties. Based on a similar sensor structure, Valentini and coworkers studied CH_4 detection by MWNTs grown on a

Ni catalyst [64]. They demonstrated that oxygen molecules are chemisorbed when CNT walls contain defects and this caused the electrical response to CH_4. The authors also suggest that the semiconducting CNTs could be converted from p-type to n-type by adsorption of oxygen molecules at elevated temperature.

Wang, *et al*. investigated the effect of MWNTs resistive sensor for NH_3 detection at room temperature [65]. The sensor was fabricated by patterning Ti/Au electrode on top of ultrasonically dispersed MWNTs using evaporation and lift-off techniques. They observed a significant decrease in sensor conductance upon exposure to 1% NH_3 gas. The authors also demonstrated that the sensitivity is linearly proportional to the NH_3 concentration ranging from 10 to 200 ppm. While in vacuum, the sensor required more than 6 hours at 250ºC to recover to baseline condition, therefore they conclude that the sensor response involved both physisorption and chemisorption [65].

2.4.2 Non conductance-based detection

Snow, *et al*. showed that the capacitance of SWNTs is sensitive to a broad range of chemical vapors [66]. Their SWNT sensor was fabricated by patterning Pd interdigitated electrodes on top of SWNT networks [66]. More importantly, they demonstrated that the capacitive SWNT sensor is sensitive to 0.5 s pulses of dimethyl methylphosphonate (DMMP), a simulant for chemical warfare agents [67]. The DMMP was diluted in dry air at a concentration of 500 ppm and the sensor response is dynamic and reversible. Snow and coworkers believe that the SWNT surface will generate a large fringing electrical field while applying a gate bias and this electrical field will then polarize the adsorbed molecules on the SWNT surface. By calculation, they found that SWNTs capacitance was affected by both dielectric polarization and charge transfer upon exposure to chemical vapor molecules but the charge contribution is less than 10% [67]. Therefore they attribute the capacitance response to field-induced polarization of surface dipoles. They also demonstrated that the effect of humidity on the sensor response is negligible due to the weak interaction between water molecules and SWNTs.

Varghese, *et al*. applied an impedance spectroscopy method to investigate the gas sensing behavior of both capacitive and resistive MWNTs sensors at ambient temperature [68]. The capacitive sensor consists of gas sensing MWNT-SiO_2 composite on top of insulating SiO_2 layer and interdigitated electrodes. The sensor was found sensitive to water vapor and NH_3, with the response to water vapor being reversible. Varghese and coworker used an equivalent circuit model to simulate the sensor and the results indicated that chemisorption of gases on the surface of the p-type semiconducting MWNTs is the dominant sensing mechanism. As a result the chemisorption induced charge transfer between MWNTs and gas molecules is responsible for the variation in capacitance [68]. An identical capacitive sensor was utilized to form an inductor-capacitor (LC) wireless remote query gas sensor by the same team [69]. The fabricated sensor consists of a planar LC resonant circuit covered by a layer of SiO_2 and the mixture of MWNTs and SiO_2 [69]. Upon exposure to various gases, the complex permittivity of the MWNTs varies, therefore changing the resonant frequency of the sensor. The sensor response was detected by measuring the impedance spectrum of a loop antenna used to monitor the sensor remotely. Ong and coworkers demonstrated that the LC sensor response to CO_2 and O_2 is linear and reversible. However both reversible and irreversible response was observed for NH_3 detection [69], which indicated the presence of both physisorption and chemisorption.

Chopra and coworkers reported a gas sensor based on the downshift in resonant frequency of circular electromagnetic resonator for NH_3 detection at ambient temperature [70]. The sensor was constructed by physically coating a copper resonator with either SWNTs or MWNTs using conductive epoxy. The detection mechanism relies on the interaction between CNTs and the NH_3 molecules, which results in a change in the resonant frequency of the sensor. They describe that it is the change in the dielectric constant of CNTs that caused a shift in the resonant frequency of the resonator. The resonant sensor demonstrated sensitivity to NH_3 gas concentration as low as 100 ppm with a response-recovery time of 10 min, which is attractive considering the generally slow recovery of CNTs-based gas sensor [70]. They reported that the resonant sensor coated with SWNTs is more sensitive than the sensor coated with MWNTs and this

difference in nanotube sensing ability is consistent with the observation by others. Chopra and coworkers later reported using the SWNTs coated resonant sensor to detect the presence of other gases such as CO, N_2, He, O_2, and Ar [71]. They showed the sensor can be selective as to give different resonant frequency shifts to different gases.

In summary, in the past 7 years CNTs have attracted a great amount of attention for potential applications in chemical gas sensing at room or moderate temperatures. Although the exact sensing mechanisms are not yet fully understood, it is commonly believed that sensing involves charge transfer and dielectric response. Gas sensors based on SWNTs or SWNT composites detect the target gas by altering electrical conductance, and comprise the majority of the research work. However gas sensing device based on MWNTs, operating by dielectric response or mass sensitive principles, has also been reported. The challenges facing the development of CNTs based gas sensing devices need to be continuously addressed before practical applications can be realized. The challenges include the development of inexpensive and reliable devices, reproducible sensor performance, reasonable selectivity and sensitivity, robust devices, and recovery ability.

Table 2.1: Common health hazardous gases and their OSHA permissible exposure limit, adapted from [4].

Substance	OSHA Permissible Exposure Limits (ppm)
ammonia (NH_3)	50
arsine (AsH_3)	0.05
bromine (Br_2)	0.1
carbon dioxide (CO_2)	5000
carbon monoxide (CO)	50
chlorine (Cl_2)	1
chlorine dioxide (ClO_2)	0.1
diborane (B_2H_6)	0.1
fluorine (F_2)	0.1
hydrogen chloride (HCl)	5
hydrogen cyanide (HCN)	10
hydrogen fluoride (HF)	3
hydrogen selenide (H_2Se)	0.05
hydrogen sulfide (H_2S)	20
nitrogen dioxide (NO_2)	5
nitric oxide (NO)	25
ozone (O_3)	0.1
phosphine (PH_3)	0.3
sulfur dioxide (SO_2)	5

Table 2.2: Summary of important electrical, mechanical and thermal characteristics of carbon nanotubes, adapted from [32].

Electrical and mechanical characteristics of CNTs	
Electrical Conductivity	Metallic or semiconducting
Electrical Transport	Ballistic, no scattering
Energy gap (semiconducting)	E_g [eV] ~ 1/d (nm)
Maximum current density	~ 10^{10} A/cm^2
Maximum strain	0.11% at 1V
Thermal conductivity	6000 W/m·K
Diameter	1 – 100 nm
Length	Up to millimeters
Young's modulus	1000 GPa
Tensile strength	63 GPa

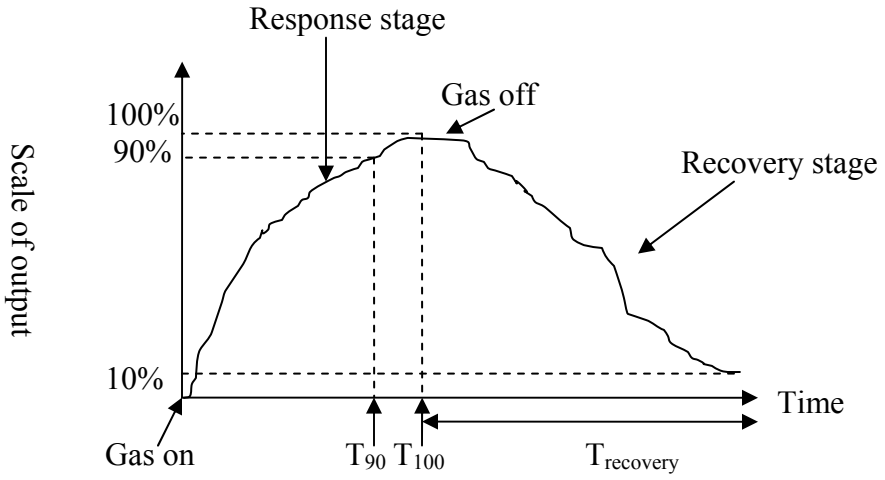

Figure 2.1: Schematic description of gas sensor response and recovery.

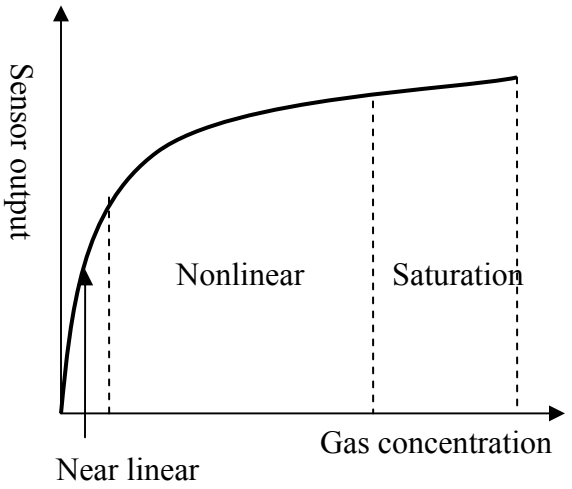

Figure 2.2: Typical gas sensor output curve. It consists of near linear, nonlinear and saturation regions.

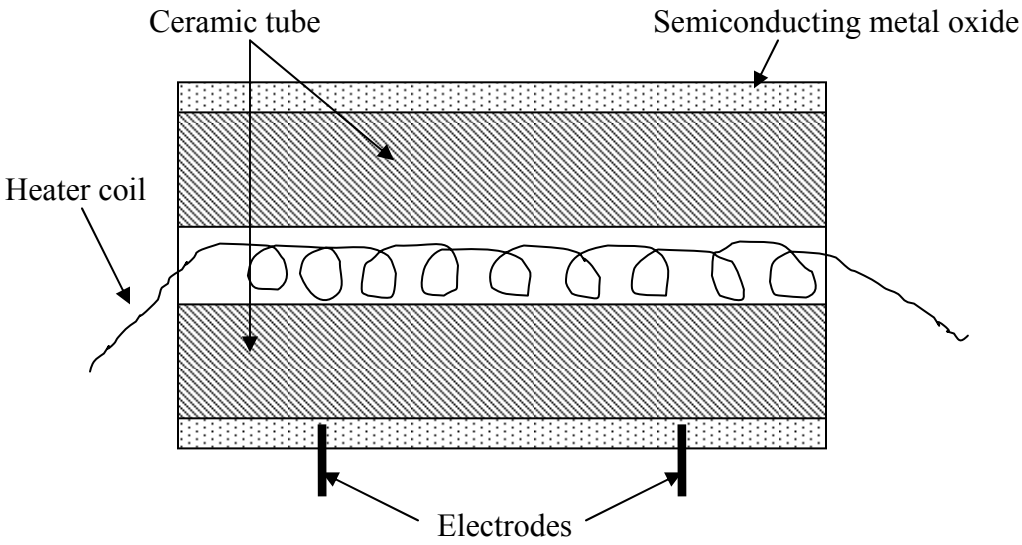

Figure 2.3: Schematic diagram of the cross-section view for a 3-dimensional Taguchi gas sensor.

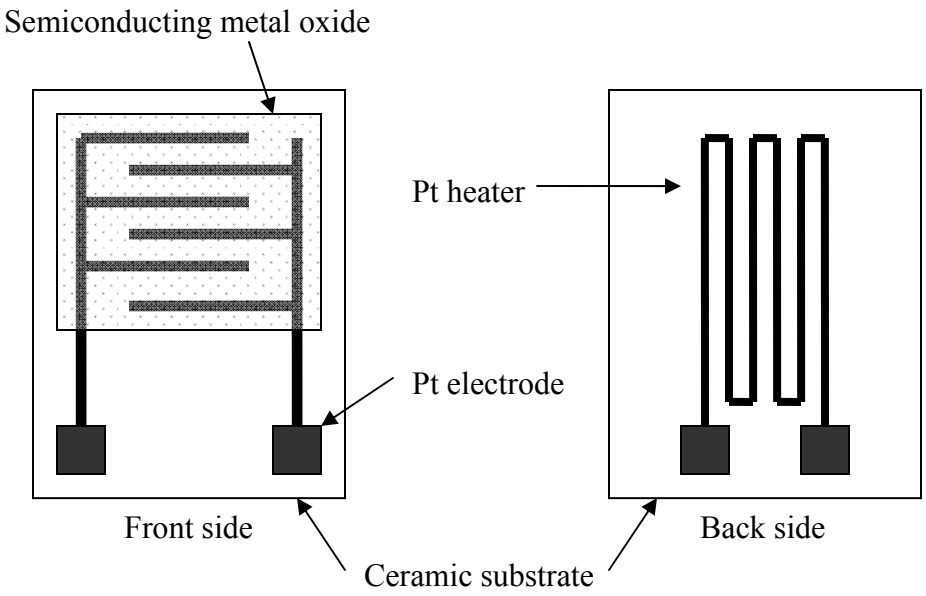

Figure 2.4: Schematic diagram of 2-dimensional planar metal oxide semiconductor gas sensor, adapted from [12].

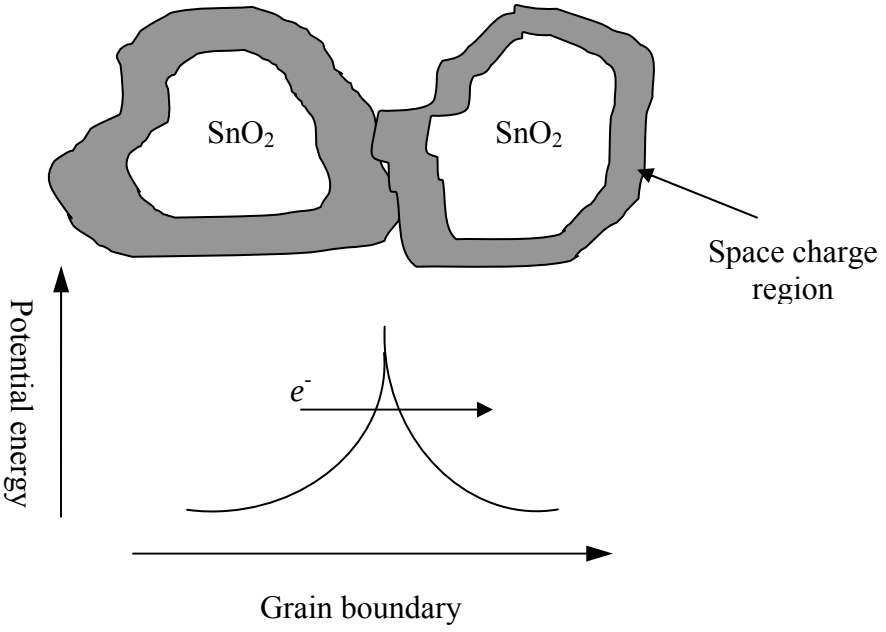

Figure 2.5: Model of inter-grain potential barrier in resistive metal oxide gas sensors.

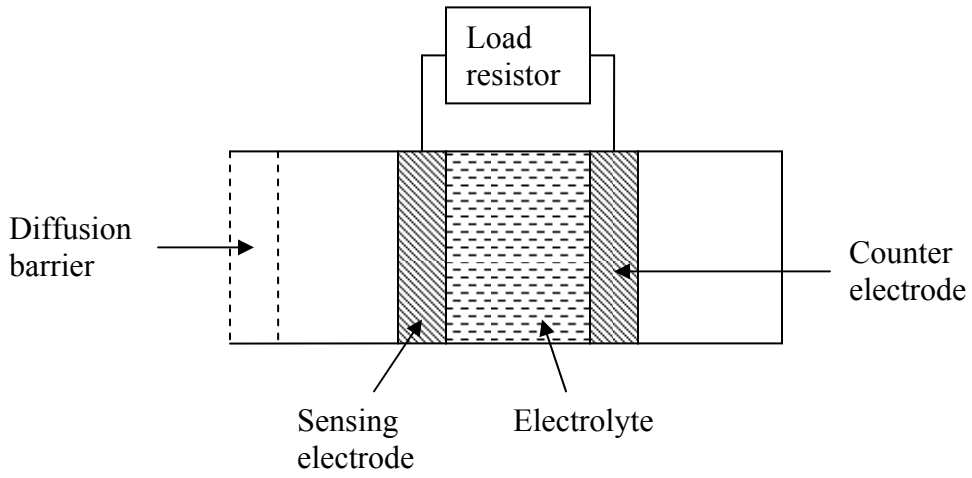

Figure 2.6: Schematic diagram of the basic element of an electrochemical gas sensor.

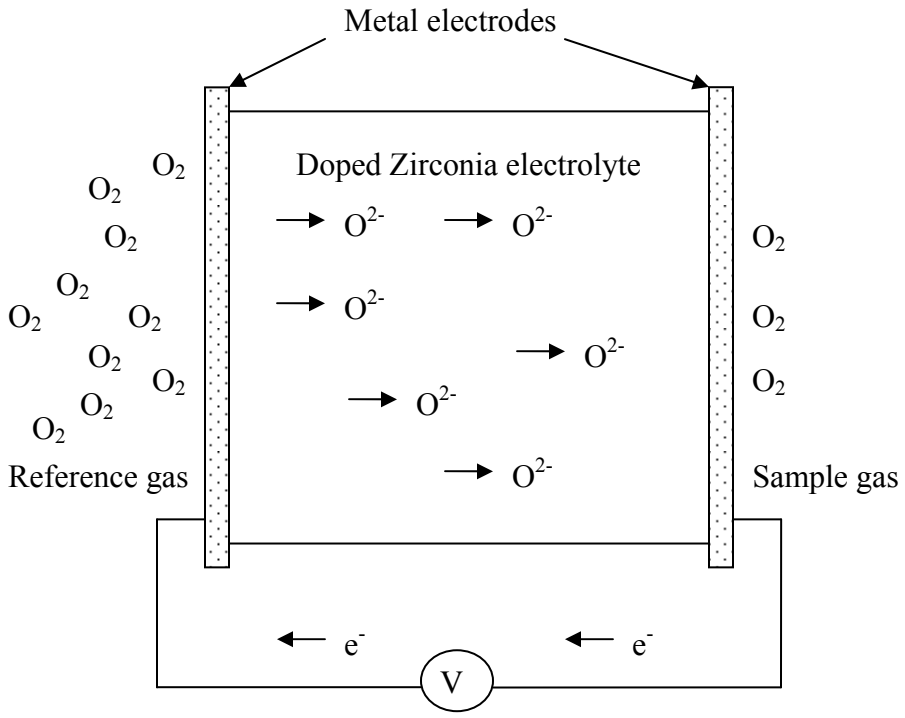

Figure 2.7: Schematic diagram of simplified zirconium oxide sensor (lambda sensor).

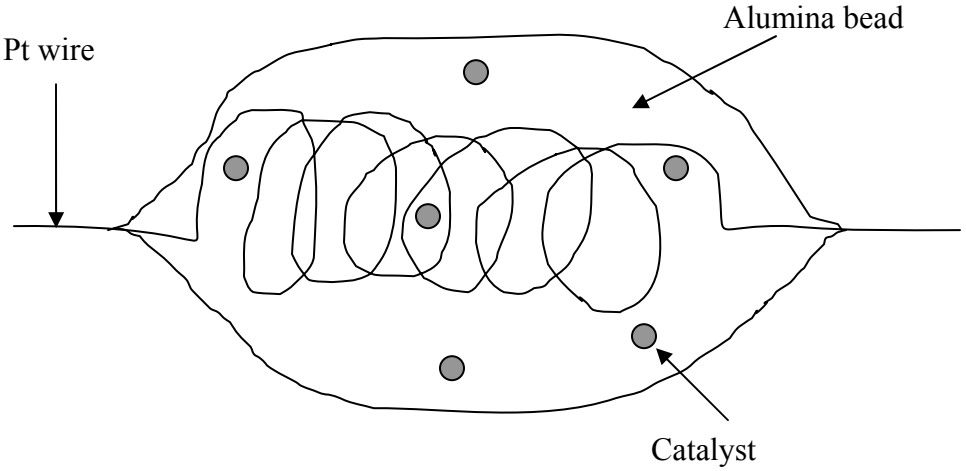

Figure 2.8: Schematic diagram of the basic sensing element of a pellistor (catalytic gas sensor), adapted from [15].

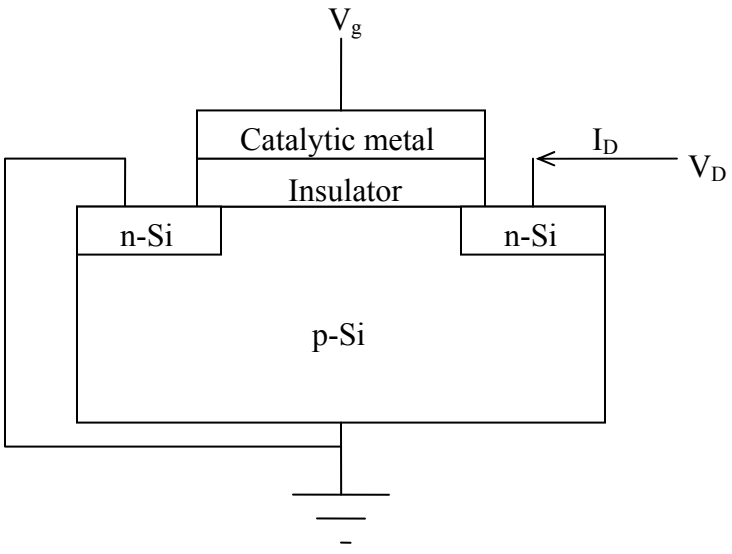

Figure 2.9: Schematic diagram of the gas sensitive metal insulator semiconductor field effect transistor (MISFET) device structure. V_g represents the gate voltage, V_D the applied junction bias, I_D the drain current, adapted from [1].

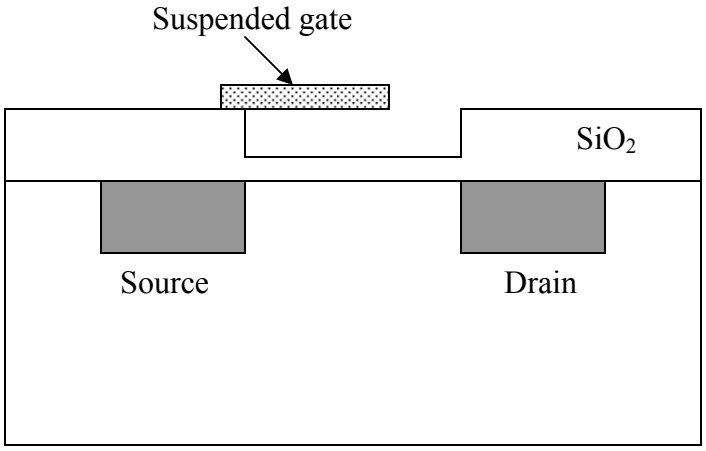

Figure 2.10: Schematic diagram of MOSFET sensor with a suspended gate (SGFET), adapted from [22].

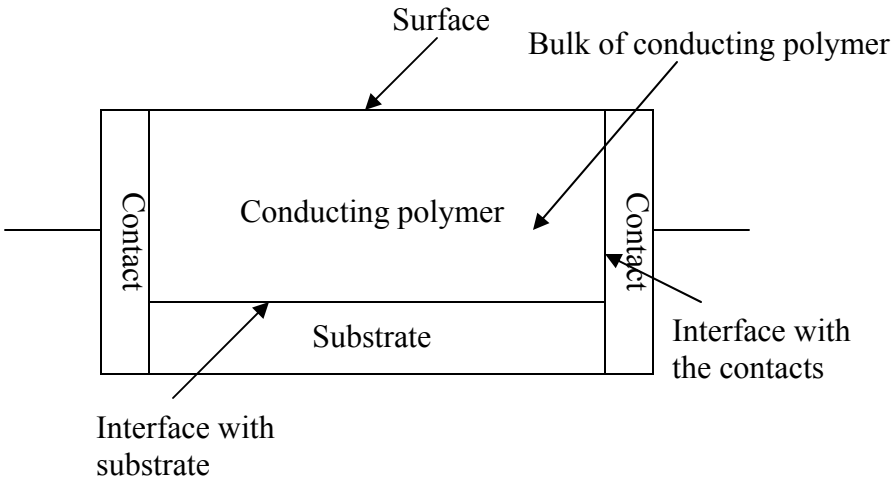

Figure 2.11: Schematic diagram of a conducting polymer based chemiresistor.

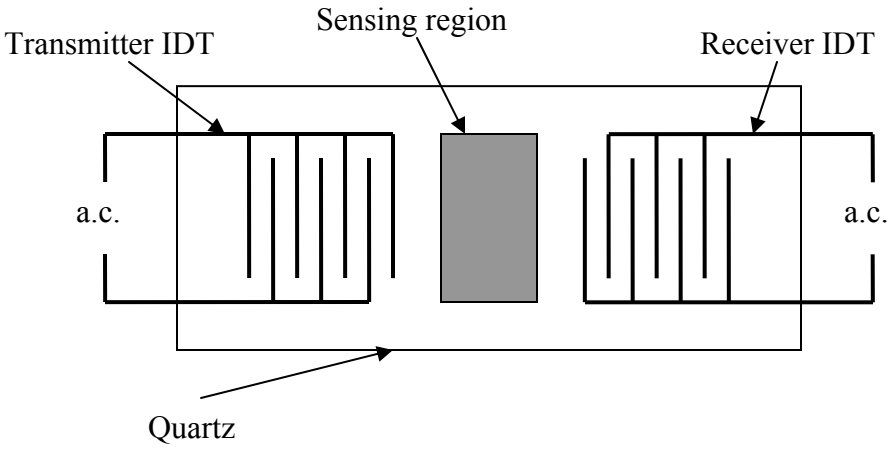

Figure 2.12: SAW sensor consists of a pair of interdigitated (IDT) electrodes and a quartz substrate.

CHAPTER3: GAS SENSORS BASED ON MWNTS

3.1 Introduction

CNTs have great potential for application as chemical gas sensing devices with excellent sensitivity and fast response time because of their special geometry (all surface reacting material) and their tendency to change electrical properties at room temperature in the presence of certain gases [55][56][57]. The majority of research works on CNTs for gas sensing materials are based on SWNTs. The reasons that MWNTs have not been attractive for this application are low purity in CNTs volume, less semiconductor characteristics (most MWNTs are metallic) and hence low sensitivity [65]. However, MWNTs can be produced in large scale thus the production cost is much lower than SWNTs. In recent years, the interest in MWNTs as potential gas sensing materials has increased [63][64][65][68][69][70].

The investigation of MWNTs as potential gas sensing materials is discussed in this chapter. A unique material structure aligned MWNTs arrays based on porous anodized alumina template, was utilized to construct resistive and capacitive gas sensing device. By anodizing aluminum foil or tape into porous anodized aluminum oxide (AAO) template, MWNTs are grown inside the porous matrix through CVD process. The gas sensing devices are fabricated by depositing metal electrodes on the surface of MWNTs arrays. As the sensor is exposed to target gas, either the conductivity or the complex permittivity of the CNTs varies, alters the resistance or capacitance of the sensor. For example, the sensors have shown response to NH_3 and CO_2.

The synthesis method of the aligned MWNTs, the design and fabrication of the sensor device, and the experimental procedure are described in the following sections. The experiment results as well as the data analysis and discussions are also presented.

3.2 Experimental

3.2.1 Fabrication of aligned MWNTs

Aligned MWNT arrays were fabricated inside porous alumina templates which allowed for the control of spatial density and the aspect ratio of the nanotubes. CNTs were then synthesized without the use of a catalyst and the tubes were open ended on both sides. The aligned MWNTs were fabricated by Dr. Vijay Singh's research group using a chemical vapor deposition (CVD) method and the synthesis techniques are briefly described here. The technical details and most of the microscopic images in this section are provided by Dr. Singh's group.

First, porous alumina templates were prepared by anodizing high purity aluminum (Al) foil (~ 2 μm thickness) or tape (~ 10 μm thickness) in an oxalic acid medium at a voltage of 40-45V. Anodizing was performed at constant voltages for a sufficient time to develop steady-state morphology in different concentrations of sulfuric acid or oxalic acid solutions. The setup for Al anodization is schematically depicted in Figure 3.1. After cleaning and degreasing the Al foil or tape was used as anode and a Pt sheet was used as the cathode. The anodization was completed after 40-50 min at room temperature [72]. The anodization process followed by pore opening which involves dipping the Al foil or tape in a solution with less oxide dissolving ability than the anodizing electrolyte [72]. Here they use phosphoric acid for pore opening. By either varying the anodization voltage or varying the time duration of pore opening process, the diameter of the pore and the total area of the pores per unit surface area can be controlled. Figure 3.2 shows the SEM images of porous anodized alumina template with different pore size.

Next, aligned, open-ended MWNTs arrays were synthesized within the pores of the porous AAO templates using a CVD system. The CVD system was based on a 96 mm diameter Lindberg furnace, with a specially designed gas-flow injector to minimize turbulent flow as described previously by Andrews, *et al*. in [73]. The CVD process for aligned MWNTs growth is similar except that, pure xylene was used as hydrocarbon

source and a stream of Ar/N_2 was replaced with N_2 gas [73]. The growth procedure was as follows: first, the sample was heated to 700ºC in N_2 over the course of half hour; next, xylene was injected into the preheater (maintained at 250ºC) using a syringe pump. As the xylene vapors emerged at the outlet of the preheater, a stream of N_2 gas swept the vapors into the furnace (maintained at 700ºC) where xylene is decomposed to produce MWNTs within the nano-sized pores. The growth of nanotubes was performed at 700ºC for 1-2 hours by pyrolysis of xylene without the need for any catalyst and thus simplifying the synthesis procedure. The sample was then allowed to slowly cool in N_2.

The nanotubes arrays were characterizes by scanning electron microscopy (SEM) and transmission electron microscopy (TEM). The SEM observations in Figure 3.3 indicate that products of CVD process are spatially well separated, free standing, and open-ended nanotubes protruding from both top and bottom surfaces of the AAO template. TEM investigation further revealed the structure of multi-walled nanotubes. Figure 3.4 shows the TEM images of MWNTs with 25 nm (A) and 2 nm (B) inner core diameters. For the sample shown in Figure 3.4 (A), the outer diameter of the nanotube is 35 nm (wall thickness is 5 nm on both side and the inner diameter is 25 nm), which corresponds to the 35 nm pore diameter of the porous AAO sample MWNTs based on. Similarly for the sample in Figure 3.4 (B) the outer diameter is 12 nm (5 nm wall thickness on both side and the inner diameter is 2 nm), which is consistent with the 12 nm pore diameter of the porous AAO template. In fact, Dr. Singh's group discovered that the MWNT wall thickness remains the same (5 nm on both side) for a given CVD reaction time. The AAO pore diameter, MWNT inner core diameter, and MWNT wall thickness of a series nanotube samples are listed in Table 3.1. These samples were synthesized by CVD for 1 hour duration. The TEM observations indicated that the distance of two neighboring fringes is approximately 3.4 Å, which is in agreement with the inter-planar separation of graphite (3.35 Å). It was believed that the nanotube growth is initiated by the walls of the AAO template, hence alumina acts as catalyst.

3.2.2 Resistive sensing with as-grown MWNTs

Four-point-probe resistance measurement revealed that the surface of the as-grown aligned MWNTs/AAO template is not perfectly insulating, indicating the existence of conductive paths along the surface. This observation is a contradiction from the design of the aligned MWNTs/AAO structure consisting of free standing MWNTs spatially well separated by electrical insulating alumina. Amorphous carbon, a potential by-product of the nanotube growth CVD process, was observed previously by other researchers [74][75] and believed to be the cause of the existing conductive paths on the sample surface.

The surface conductivity of the aligned MWNTs/AAO template was utilized to construct resistive sensor for preliminary gas testing. Figure 3.5 illustrates the schematic diagram of the resistive sensor structure (Note: amorphous carbon is not shown) and Figure 3.6 shows its photograph. Silver (Ag) electrodes with the thickness of 200 nm were deposited on both ends of the MWNTs/AAO template surface through a shadow mask using Kurt Lesker EPS-2000 thermal evaporator. The shadow mask was prepared by cutting through a piece of transparency film using a Lambda Physik COMPex 102 excimer laser system. The dimension of the metal contact is 15 mm by 2 mm. By monitoring its resistance variation, the response of the sensor to target gases at room temperature was determined.

3.2.3 Capacitive sensing with plasma-etched MWNTs

Although the amorphous carbon on the surface of as-grown aligned MWNTs/AAO templates formed conductive paths and was utilized to construct resistive sensors, they are undesirable in capacitive sensor design due to the possibility of shorting the capacitive electrodes. As can be seen from the capacitive sensor design in Figure 3.7 (top view) and Figure 3.8 (cross-section view), the adjacent interdigitated capacitor (IDC) electrodes could be shorted in the presence of amorphous carbon. In order to remove the amorphous carbon prior to sensor fabrication, the surface of the as-grown MWNTs sample was etched in O_2 plasma for 6 min using a plasma etch system (Plasma-Preen 862 by Plasmatic System). Figure 3.9 shows the SEM images of MWNTs sample prior to

and after plasma etching. One can see from Figure 3.9 (B) that plasma etching removed amorphous carbon from the sample surface while at the same time kept the majority of CNTs remain intact. The surface of the plasma etched MWNT arrays was then confirmed to be insulating using four point probe measurement.

An IDC consists of two planar lumped electrodes (Figure 3.7) which can be manufactured by conventional thin film or thick film deposition technologies. Due to its simple structure and maximized three-phase interface between gas, electrodes and sensing material, IDC has been widely accepted as the basic electrode design for gas sensors. Here the capacitive sensor was fabricated by depositing 200 nm thick Ag planar IDC electrodes on top of aligned MWNTs/AAO template through a shadow mask using Kurt Lesker EPS-2000 thermal evaporator. The shadow mask with IDC pattern was also prepared by laser (Lambda Physik COMPex 102 excimer laser system) cutting through Al foil or transparency film. The width of IDC electrode is 0.5 mm with 2 mm line spacing and the total dimension of IDC is 18 mm by 14 mm. A photograph of a capacitive sensor based on plasma-etched MWNTs/AAO template is shown in Figure 3.10. The sensor response was evaluated by monitoring capacitance variation at room temperature in the presence of target gases.

3.2.4 Inductor-capacitor resonant sensor

The concept of inductor-capacitor resonant gas sensor, in which the sensing mechanism is based on the dielectric response of the sensing material, was reported by Ong and coworkers [69][76]. They fabricated the sensor by depositing a thin layer of MWNTs-SiO_2 composite on a planar LC (spiral inductor and IDC) resonant circuit sensor platform as shown in Figure 3.11. Upon exposure to target gases, the adsorption of gas molecules in the MWNTs-SiO_2 layer alters its complex permittivity and therefore changes the resonant frequency of the sensor. Sensor response can be determined by tracking the impedance spectrum of the LC resonant circuit. A typical impedance spectrum of a LC resonant circuit is shown in Figure 3.12, where the resonant frequency f_0 is defined as the frequency where the real part of the impedance reaches its maximum, and the zero-reactance frequency f_z is defined as the frequency at which the imaginary

part of the impedance goes to zero. The complex permittivity ($\varepsilon_r^* = \varepsilon_r' - j\varepsilon_r''$) of the gas sensing coating (MWNTs-SiO_2 composite) can be calculated from the measured f_0 and f_z by modeling the sensor as an RLC circuit (Figure 3.13) using standard circuit analysis techniques [69][77][78]:

$$\varepsilon_r' = \frac{1}{(2\pi f_0)^2 L\kappa\varepsilon_0} - \varepsilon_S \tag{3.1}$$

$$\varepsilon_r'' = \frac{\sqrt{f_0^2 - f_z^2}}{4\pi^2 f_0^3 L\kappa\varepsilon_0} \tag{3.2}$$

where ε_r' is the real part of the complex permittivity, ε_r'' is the imaginary part of the complex permittivity, κ is the cell constant of the IDC, and L is the inductance of the spiral inductor. Both κ and L can be calculated from the resonant circuit dimensions. The free space permittivity ε_0 and the relative permittivity of the electrically lossless substrate material ε_s are known parameters. As can be seen from Eq(3.1) and (3.2), the complex permittivity of the gas sensing material is directly proportional to the measured frequency f_0 and f_z. Therefore by measuring the impedance spectrum of the LC sensor, the dielectric response of the sensing materials can be determined. Furthermore, Ong and coworkers tracked the sensor response with a loop antenna, thus making the LC resonant sensor a possible candidate for wireless, remote query applications. The LC resonant sensor design was assembled and verified in this dissertation using the MWNTs/AAO based capacitive sensor and a commercially available capacitive humidity sensor.

3.2.5 Experiment setup

The sensor testing system is schematically depicted in Figure 3.14. The sensor is placed inside a sealed glass test chamber and the variation of its electrical signal is monitored by an instrument. Three electrical instruments have been used for sensor testing: Hewlett Packard 3478A digital multimeter for resistance measurement, Hewlett Packard 4192A impedance analyzer for capacitance measurement, or Hewlett Packard 8753E network analyzer for impedance spectrum (LC resonant sensor) measurement. Nitrogen (N_2) or compressed dry air is used as the carrier gas. The target gases are either pure (CO_2) or diluted by N_2 (NH_3, NO_2, etc.). A mass flow controller is used for mixing

the carrier and target gases and feed them into the test chamber at the desired concentrations and flow rates. The gas flow rates and concentrations are varied with a Sierra Instruments dual channel mass flow system, which is controlled by LabVIEW software through a National Instruments USB-6009 Data Acquisition device (DAQ). A computer was used for controlling the mass flow system and electrical instrument via a GPIB interface, as well as analyzing and processing the measurements. The sensors were tested either at room temperature or at moderate temperatures up to 100 ºC. A heater tape wrapped around the chamber and a power supply were applied to achieve the elevated temperature. The relative humidity (RH) inside the test chamber was maintained at 9% by the flow of carrier gas. Higher RH up to 90% can be achieved by a small portion of carrier gas bubbling through pure DI water, then feeding the water vapor into the test chamber. In order to maintain the constant baseline reading, prior to each experimental session, sensors were baked in vacuum at 100°C for at least 2 hours to desorb gas molecules.

3.3 Results and Discussion

3.3.1 Resistive response

Ammonia (NH_3) was selected as one of the target gases for the resistive sensor because ammonia is a reducing gas with a penetrating odor, and high concentrations are threat to human health. The allowed long term concentration limit is 50 ppm [4]. Immediate and severe irritation of nose and throat occurs at 500 ppm. Extremely high concentrations (above 5000 ppm) are lethal within a few minutes. Measuring NH_3 concentration is of great interest in four major areas, i.e., environmental gas analysis [79], automotive industry [80], chemical industry [81], and medical applications [81]. The most commonly used NH_3 sensors are WO_3 metal oxide semiconductor sensors, gas FETs with Pd catalytic gates, and conducting polymer sensors. A lower detection limit of 1 ppm has been demonstrated, however only the conducting polymer sensor can operate at room temperature [81].

The response of MWNTs/AAO resistive sensor to 1% NH_3 exposure is shown in Figure 3.15. The sensor was placed inside the test chamber in the flow of N_2 at the beginning of the experiment and the sensor resistance was monitored by a digital multimeter. After the sensor reached the equilibrium condition, i.e. constant resistance reading, NH_3 was introduced into the chamber and mixed as 1% in volume to the existing carrier gas N_2 for 1 hour at room temperature. The sensor was then allowed to recover in the flow of pure N_2. The result in Figure 3.15 shows that the sensor resistance increased over 7% in the presence of NH_3 and decreased immediately after turning NH_3 off. Here the sensitivity S is defined as:

$$S(\%) = \frac{R_{NH_3} - R_{N_2}}{R_{N_2}} \times 100 \tag{3.3}$$

where R_{NH3} is the sensor resistance in the presence of NH_3 gas, and R_{N2} is the sensor resistance in equilibrium condition.

The increase of the sensor resistance in the presence of NH_3 is believed to be the result of charge transfer between nanotubes and NH_3 molecules [65][68][69]. When MWNTs are exposed to NH_3 gas (reducing agent, i.e., electron donor), electrons are transferred from NH_3 to MWNTs. A space charge region is then formed at the surface of the semiconducting MWNTs and as a result, the conductivity is reduced. Making use of the existence of amorphous carbon and electrical contacts on the surface of MWNTs/AAO template, resistance changes of the nanotubes can be measured to determine sensor response. The resistance increase in the presence of a reducing agent is evidence that the MWNTs are p-type semiconducting [68]. One can see from Figure 3.15 that the recovery of the sensor is incomplete and the recovery rate is much slower than the response rate. This indicates that the adsorbed NH_3 molecules can not be completely removed by the flow of carrier gas due to the bonding between nanotubes and gas molecules.

Shown in Figure 3.16 is the measured sensor response to repeated 1% NH_3 exposure at room temperature. After the sensor reached equilibrium, the ambient inside the test chamber was cycled between 1% NH_3 and pure N_2 for a period of 10 minutes each. The

recorded resistance change was plotted in Figure 3.16. The data shows that the change of resistance followed the gas delivery pattern promptly. The sensor response is reversible and the sensitivity stabilized at approximately 8%.

As the concentration of NH_3 increased, the sensitivity of the sensor increased accordingly as expected. Figure 3.17 shows the measured sensor response to 5% NH_3 exposure. During the first exposure period, the sensitivity of the sensor increased from 6.1% to 16% when the NH_3 concentration increased from 1% to 5%. The data in Figure 3.17 indicated that the sensor recovery was also incomplete for 5% NH_3 exposure. It seems that the baseline drift was caused by the residual NH_3 gas molecules building up on the nanotubes. This further proved that the bonding between MWNTs and adsorbed NH_3 molecules is too strong to be completely removed by the kinetic energy of N_2 flux during the sensor recovery. Shown in Figure 3.18 is the sensor response to various concentrations of NH_3. The sensor sensitivity was plotted as a function of NH_3 concentration and the curve shows a linear fit. The response to various NH_3 concentrations shown in Figure 3.18 was measured on the same sample and this is a different sample from the one shown in Figure 3.15, Figure 3.16, and Figure 3.17. One can see that the sensitivities to same concentrations of NH_3 are different for the two sensors. It seems that this discrepancy in sensor response was caused by the uncontrolled coverage of amorphous carbon. As a result, the amount of nanotubes exposed to ambient environment and available to interact with gas molecules varies sample to sample, thus causing the difference in sensor response. The resistive sensor based on MWNTs/AAO template demonstrated a lower NH_3 detection limit of 100 ppm as shown in Figure 3.19. The sensitivity to 100 ppm NH_3 exposure is up to 0.75% at room temperature.

The resistive sensor is also found to be sensitive to carbon dioxide (CO_2). CO_2 sensors are important in air quality monitoring [82], food and medicine package spoilage detection [76], and industrial process control [83]. To date, electrochemical, optical and metal oxide semiconductor sensors have been used for CO_2 detection.

To test the CO_2 response, after the sensor reached equilibrium the ambient inside test chamber was cycled between CO_2 and N_2 for 10 minutes each. The measured sensor response to repeated CO_2 exposure at room temperature is plotted in Figure 3.20. The sensor shows reversible response and incomplete recovery. The CO_2 sensitivity (less than 4%) is much lower compared to the NH_3 sensitivity by the same sensor shown in Figure 3.16 and Figure 3.17. This indicates that MWNTs have a higher affinity for NH_3 which is in agreement with the fact that NH_3 is a much stronger reducing agent than CO_2. Figure 3.21 shows the room temperature humidity dependency of the sensor. One can see that as the relative humidity (RH) inside test chamber varies, the sensor resistance alters correspondingly. The result shown in Figure 3.21 indicates that the sensor performance could be highly affected by the ambient humidity levels.

In summary, the resistive sensors based on as-grown MWNTs/AAO template have demonstrated the ability to detect NH_3 and CO_2 at room temperature and strong humidity dependency. Being sensitive to reducing gases confirmed the p-type semiconductor characteristic. The lower detection limit of NH_3 is 100 ppm and the sensitivity shows a linear dependency on the concentration in the range of 1% to 5%. The sensitivity for NH_3 detection is much higher than that of CO_2 detection, which is consistent with the reports elsewhere [69] and indicates that the nanotubes adsorb NH_3 more easily than CO_2 molecules. The sensor response is reversible in the multiple-cycled testing and partially recovered by the flow of N_2. The sensing and recovery mechanisms can be explained as follows: the observed resistance change is due to the adsorption of reducing gas molecules (NH_3 and CO_2) into either the core or the surface of the MWNTs. The reducing agents inject electrons into p-type MWNTs and decrease the conductivity. To date, the gas-MWNT bonding mechanisms have not been fully understood yet. It is believed that gas molecules absorbed into MWNTs through a strong chemisorption and a weak physisorption. During the sensor recovery stage, the weak electrostatic bond between MWNTs and physisorbed gas molecules are easily overcome by the kinetic energy of the flowing N_2, therefore result in the release of the physisorbed gas molecules. On the other hand, the bond between MWNTs and chemisorbed gas molecules are too strong to be broken by the flow of N_2. As a result, there is a slow buildup of chemisorbed

gas molecules on MWNTs surface and therefore the sensor recovery is incomplete. Due to the strong humidity dependency and uncontrolled nature of amorphous carbon coverage on the surface of as-grown MWNTs/AAO template, currently the as-prepared aligned MWNTs samples are practical only for preliminary gas sensing investigation instead of sensor device prototyping.

3.3.2 Capacitive response

The measured response of plasma etched MWNTs/AAO capacitive sensor to 1% NH_3 exposure at room temperature is shown in Figure 3.22. After the sensor reached equilibrium in N_2, the ambient inside the test chamber was cycled between 1% NH_3 and pure N_2 for periods of 10 minutes. The variation of sensor capacitance was recorded by an impedance analyzer and plotted in Figure 3.22. The data shows that the dynamic response of capacitance followed the gas delivery pattern promptly, i.e., the capacitance is sensitive to NH_3 and allowed to recover in N_2 ambient. One can see that the sensor response is reversible and the sensor capacitance increased in the presence of NH_3 gas. The sensor recovery is incomplete but there is no evidence of NH_3 gas molecule gradually building-up inside MWNTs/AAO template as found in resistive sensor response. The sensitivity is in the range of 0.25% to 0.3%. Here the sensitivity S is defined as:

$$S(\%) = \frac{C_{NH_3} - C_{N_2}}{C_{N_2}} \times 100 \tag{3.4}$$

Where C_{NH3} is the sensor capacitance in the presence of NH_3 gas, and C_{N2} is the sensor capacitance in equilibrium condition. As the concentration of NH_3 was raised, the sensitivity increased accordingly as shown in Figure 3.23. The concentration of NH_3 was increased to 5% and as a result the sensitivity of the sensor increased to the range of 0.5% to 0.6%. Once again, the response followed the presence of gas inside test chamber closely with a response time less than 2 minutes. The sensor capacitance increased in the presence of 5% NH_3 and recovered in pure N_2 flux.

Similar to the resistive sensor, the MWNTs/AAO capacitive sensor is also sensitive to CO_2 as shown in Figure 3.24. First, an equilibrium condition was achieved by soaking

the sensor in N_2 ambient. Next the sensor was exposed to CO_2 and N_2 alternately for periods of 10 minutes at room temperature. The change of capacitance was monitored by an impedance analyzer and plotted in Figure 3.24. One can see that the capacitance increased as the sensor was subjected to CO_2 exposure and recovered in the ambient of pure N_2. The sensitivity of the first CO_2 exposure cycle is as high as 1.2% but gradually decreased through out the duration of the experiment. The data in Figure 3.24 also indicated that there was a gradual downward drift in the baseline capacitance. It is believed that the baseline drift associated with the CNT sensor is the result of electrical noise characteristic of nanotubes. As described by Collins and coworkers [84], carbon nanotubes generate a high level of 1/f noise. The noise power density is inversely proportional to the measurement frequency as well as the number of nanotubes.

In order to identify the active gas sensing materials of the capacitive sensor, the model of IDC and its building block - unit cell are investigated. Figure 3.25 depicted the schematic description of the IDC and a unit cell. By definition, the capacitance of an interdigitated capacitor is calculated by summing the 2-dimensional unit cell capacitances. The unit cell is shown in the highlighted area of Figure 3.25 A and in detail in Figure 3.25 B. Neglecting the edge effects, the total capacitance of the IDC is [85]:

$$C_{IDC} = C_{UC}(N-1)L \tag{3.5}$$

where N is the number of unit cells and L is the length of the electrodes. The capacitance C_{UC} of a unit cell is composed of three partial capacitances C_1, C_2 and C_3, as shown in Figure 3.25 B. The capacitance of a unit cell is defined as [85]:

$$C_{UC} = C_1 + C_2 + C_3 \tag{3.6}$$

where C_1, C_2 and C_3 are corresponding to permittivity ε_1, ε_2 and ε_3 as shown in Figure 3.25 B. According to the sensor design which consists of IDC electrodes deposited on the surface of MWNTs/AAO template, ε_1 and ε_2 are identical and equal to the ambient permittivity inside the test chamber. The permittivity ε_3 is the permittivity of the MWNTs/AAO template. Therefore C_1 and C_2 are determined by the ambient inside the test chamber and only C_3 is directly related to the MWNTs. In order to demonstrate that the MWNTs are the active sensing materials, first a control sensor was constructed by replacing the MWNTs/AAO template with a passive ceramic alumina substrate as shown

in Figure 3.26. Identical IDC electrodes were then deposited on the surface of alumina substrate. The unit cell of the control sensor is the same as the one shown in Figure 3.25 B except that the MWNTs/AAO template was replaced by a passive ceramic substrate. The control sensor was then placed inside the test chamber and subjected to NH_3 and CO_2 exposure as described earlier in this section. The capacitance of the control sensor did not show any response. The partial capacitances C_1 and C_2 are the same for both MWNTs sensor and the control sensor, and they are subjected to the same gas exposure. The only difference between these two sensors is C_3 (i.e., ε_3) therefore C_3 is the only contribution in the capacitance change of MWNTs sensor and C_1 and C_2 are non-factors. This is the evidence that the permittivity ε_3 is the only contribution for the variation of sensor capacitance upon exposure to target gases, thus confirming that the MWNTs/AAO template is the active sensing material.

Next, second control sensor was fabricated and tested to further prove that it is the nanotube not the AAO of the MWNTs/AAO template causing the sensor response in the presence of gases. The second control sensor is similar to the first one except that the passive ceramic substrate was replaced by a porous AAO template, which is the same as the one used for nanotube synthesis. Thus the second control sensor is composed of IDC electrodes deposited on the surface of porous AAO template (Figure 3.26). The only difference between the MWNTs sensor and the second control sensor is the presence of MWNTs. The control sensor was then subjected to target gas exposure as described previously and, as expected did not show any response. The experiment result with the second control sensor further demonstrated that the nanotubes inside the MWNTs/AAO template are indeed the active gas sensing materials and their interaction with the gas molecules alters the capacitance of the sensor during the experiments.

Once the MWNTs were identified as the active sensing material for the capacitive sensor, the sensing mechanism was examined. It has been demonstrated that the capacitance of the sensor increased in the presence of reducing agents such as NH_3 and CO_2. Oxygen was selected as target gas to investigate the sensor response to an oxidizing agent. After the sensor reached equilibrium in N_2, the ambient inside the test chamber

alternated between O_2 and N_2 for a period of 10 minutes each. The variation of sensor capacitance was recorded by an impedance analyzer and plotted in Figure 3.27. One can see from Figure 3.27 that the capacitance increased in the presence of O_2 and recovered in N_2. The initial sensitivity is approximately 0.26% and then gradually decreased during the experiment. The fact that sensor capacitance increased in the presence of both reducing and oxidizing agents indicated that the dielectric effect, instead of charge transfer, is the dominant factor in the sensing principles.

It is believed that the capacitance response of nanotubes to gas molecules is the combination of dielectric effect and charge transfer [67], i.e., it consists of contributions from both the dielectric and the charge effects of the adsorbed molecules:

$$\Delta C = \frac{\partial C}{\partial \varepsilon}\Delta\varepsilon + \frac{\partial C}{\partial Q}\Delta Q \tag{3.7}$$

Where the dielectric effect (the first term) is the result of the field-induced polarization of surface dipoles and the second term is the contribution of charge transfer between the nanotubes and adsorbed molecules. The complex permittivity ε^* of the gas sensing material MWNTs can be expressed as:

$$\varepsilon^* = \varepsilon' - j\varepsilon'' \tag{3.8}$$

Where the real part ε' is directly related to the dielectric effect and the imaginary part ε'' is directly proportional to the conductivity σ as:

$$\sigma = 2\pi f \varepsilon_0 \varepsilon'' \tag{3.9}$$

Where f is the measurement frequency and ε_0 is the free space permittivity. Thus the change in imaginary part ε'' is due to the charge transfer between the nanotubes and the adsorbed gas molecules.

Ong, *et al.* [69] applied the mixture of MWNTs and SiO_2 powder (mechanical binder) as active gas sensing material to construct an LC sensor which consists of a planar IDC and a spiral inductor. They analyzed the response of the complex permittivity of the nanotubes in the presence of reducing (NH_3 and CO_2) and oxidizing agents (O_2) respectively by monitoring the impedance spectrum. Their data shows that both the real and imaginary parts of the CNTs' complex permittivity are sensitive to the target gases

but the latter is much more sensitive. Therefore they claimed that the sensor response is mostly composed of the contribution from the charge transfer between nanotubes and gas molecules, i.e., charge transfer induced conductance change is the principle gas sensing mechanism for their MWNTs gas sensor. However, the in-depth investigation of our capacitive sensors based on MWNTs/AAO template revealed otherwise.

In order to investigate the effect of target gas exposure on the complex permittivity of the MWNTs capacitive sensor, the capacitance of the IDC is modeled as a pure capacitive, conventional parallel plate capacitor. The capacitance C is then expressed as:

$$C = \frac{\varepsilon_0 \varepsilon^* A}{d} \tag{3.10}$$

Where A is the surface area of the plate and d is the distance between the two parallel plates. Substitute Eq. 3.8 into Eq. 3.10, then capacitance can be expressed as:

$$C = \frac{\varepsilon_0 (\varepsilon' - j\varepsilon'') A}{d} \tag{3.11}$$

The impedance Z of a pure capacitor is defined as:

$$Z = \frac{1}{j\omega C} \tag{3.12}$$

where ω is angular frequency. Therefore the admittance Y of the capacitor can be expressed as:

$$Y = G + jB = \frac{1}{Z} = j\omega C \tag{3.13}$$

where G is conductance and B is susceptance of the capacitor. Substitute Eq. 3.11 into Eq. 3.13 then the admittance Y can be expressed as:

$$Y = G + jB = j\omega \left[\frac{\varepsilon_0 (\varepsilon' - j\varepsilon'') A}{d} \right] \tag{3.14}$$

As the result, conductance G is proportional to the imaginary part of complex permittivity ε`` as:

$$G = \frac{\omega \varepsilon_0 A}{d} \varepsilon'' \tag{3.15}$$

Susceptance B is proportional to the real part of complex permittivity ε` as:

$$B = \frac{\omega \varepsilon_0 A}{d} \varepsilon' \tag{3.16}$$

One can see from Eq. 3.13 to 3.16 that by measuring capacitance C, conductance G and susceptance B simultaneously, the in-depth investigation of complex permittivity gas response is possible. Thus the variation of susceptance B correlates with the dielectric effect and the change of conductance G is the direct reflection of charge transfer. Figure 3.28 and Figure 3.29 shows the measured C, B and G of the MWNTs/AAO capacitive sensor in the presence of NH_3 (5%) and O_2 respectively. One can see that for both reducing and oxidizing agents, the capacitance response is solely determined by the variation of susceptance B and the effect of conductance change is negligible. Therefore the experiment results shown in Figure 3.28 and Figure 3.29 indicate that the gas sensing mechanism of the MWNTs/AAO capacitive sensor is based on the dielectric effect, i.e. surface dipole polarization, instead of charge transfer. This surface capacitance effect is believed to be caused by electric field radiating from IDC electrodes when the device is under test. The electrical field produces a net polarization of the adsorbed gas molecules and the result can be detected as an increase in sensor capacitance in the presence of either reducing or oxidizing gas.

A model of MWNTs/AAO capacitive sensor is developed and partially adapted from the work of Endres, *et al* [85]. The cross section view of the MWNTs capacitive sensor is shown in Figure 3.30. The capacitance of an IDC is commonly calculated by summing all the unit cell capacitance C_{UC}. Neglecting edge effects, the IDC capacitance is:

$$C = C_{UC}(N-1)L \tag{3.17}$$

Where N is the number and L is the length of the electrodes. The capacitance C_{UC} of a unit cell is the summation of three partial capacitances C_1, C_2, and C_3 corresponding to the permittivity ε_1, ε_2 and ε_3 as shown in Figure 3.30. Thus:

$$C_{UC} = C_1 + C_2 + C_3 \tag{3.18}$$

Capacitance C_1 and C_3 can be calculated by conformal mapping of two semi-planes with permittivity ε_1 and ε_3 into two parallel plate capacitors. C_1 and C_3 can be expressed by using a complete elliptic integral of the first kind K[x] as the transformation [85]:

$$C_1 + C_3 = \varepsilon_0 \frac{\varepsilon_1 + \varepsilon_3}{2} \frac{K\left[\left(1 - \left(\frac{d_{sep}}{d_{cell}}\right)^2\right)^{1/2}\right]}{K\left[\left(\frac{d_{sep}}{d_{cell}}\right)\right]} \quad (3.19)$$

Where d_{sep} is the electrode separation and d_{cell} is the width of a unit cell. ε_1 is the relative permittivity of the ambient gas encompass partial capacitance C_1. ε_3 is the relative permittivity of the MWNTs/AAO template which depends on the pore structure of the porous AAO and ε_{CNT}. The relative permittivity of the composite can be modeled as a linear combination of the individual relative permittivity weighted by respective volume fractions f [86], i.e.,

$$\varepsilon_3 = \varepsilon_{CNT/AAO} = f_{CNT} \times \varepsilon_{CNT} + f_{AAO} \times \varepsilon_{AAO} + f_{air} \times \varepsilon_{air} \quad (3.20)$$

The volume between the electrodes is treated as a parallel plate capacitor C_2:

$$C_2 = \varepsilon_0 \varepsilon_2 \frac{h}{d_{sep}} \quad (3.21)$$

Where h is the thickness of the electrodes and ε_2 is the same as ε_1.

The model of the capacitance sensor indicated that the reduction of the electrode spacing d_{sep} will increase the capacitance, reduce the signal-to-noise ratio, and hence increase the sensitivity of the sensor. Currently, the IDC electrodes are patterned by physical metal deposition through a shadow mask. However, the resolution limit of the shadow mask prohibited d_{sep} to be less than 1 mm. Therefore in order to reduce the IDC dimension, the technique of photolithography with much higher resolution is desired for the future improvement of the capacitive sensor performance.

3.3.3 LC resonant sensor impedance response

In order to verify the design of LC resonant sensor, a Vishay BCComponants capacitive humidity sensor was purchased from Digi-Key Corporation. First the sensor was characterized in response to the change of relative humidity using the sensor testing system. The result showed in Figure 3.31 A indicated that the capacitance of the sensor precisely followed the variation of relative humidity inside the test chamber. The

measured characteristic of the sensor, i.e. capacitance as a function of relative humidity, is almost identical as claimed in its datasheet. Next the capacitive humidity sensor was incorporated into a planar spiral inductor platform to form a pseudo LC resonant sensor. The structure of the spiral inductor is similar to the one shown in Figure 3.11 with a dimension of 40 mm in outer diameter, 25 mm in inner diameter, and 1 mm in electrode width. The sensor platform was based on a passive ceramic substrate and the inductor electrodes were patterned using Heraeus C5729 gold conductor paste through an Accu-coat 3230 screen printer (AREMCO Products). The capacitive humidity sensor was then connected with the planar inductor to form a pseudo LC resonant humidity sensor and subjected to humidity test. Since the inductance of the spiral inductor can be calculated by its geometry and the characteristic of capacitive humidity sensor is known, therefore the impedance spectrum and the resonant frequency of the pseudo LC resonant circuit can be calculated and predicted. Figure 3.31 B shows the predicted and measured resonant frequency of pseudo LC resonant sensor in response to the relative humidity change. The data indicated that the sensing behaviors of theoretical and measured LC sensor are in agreement with a difference in magnitude of the sensitivity. The results verified the operating principles of the LC resonant sensor, however future investigation is needed to understand the cause of magnitude discrepancy in resonant frequency.

A planar LC resonant sensor was constructed by replacing the component capacitive sensor with the MWNTs/AAO based capacitive sensor and in connection with the spiral inductor. The impedance spectrum of this nanotube based LC sensor was monitored in the presence of target gases, however no response was observed. It is believed that the response of MWNTs/AAO capacitor is not high enough for the resonant circuit to generate measurable impedance response. Therefore the key to improve the LC sensor performance is to increase the sensitivity of the MWNTs based capacitive sensor.

3.4 Conclusion

The synthesis method of MWNTs/AAO template was briefly discussed and the multi-walled structure was confirmed by material characterization techniques. Amorphous carbon was present on the surface of the as-prepared MWNT template and it was

believed to be the by-product of the nanotube growth process. The as-prepared MWNT sample was incorporated into resistive sensor structure for conductance-based room temperature gas sensing test and its resistance is in response to the exposure of reducing agents NH_3 and CO_2. The change of nanotube conductance is the contribution from charge transfer between nanotubes and the adsorbed gas molecules. The demonstrated increased resistance of MWNTs/AAO material to reducing gas molecules served as the evidence of p-type semiconductor.

Capacitive sensors were designed and fabricated by depositing interdigitated electrodes on the surface of plasma etched MWNTs/AAO templates. The sensors showed response to both reducing and oxidizing agents. The in-depth investigation revealed that the capacitive sensing mechanism is mainly based on the field-induced surface dipole polarization instead of charge transfer reported elsewhere. The magnitude of the capacitive sensitivity is restrained by the IDC dimension, which is explained by a capacitive sensor model. Advanced patterning techniques are desired to achieve finer IDC dimension, therefore to increase capacitance and to improve sensor performance.

The inductor-capacitor resonant sensor design was verified by constructing and testing a pseudo LC sensor, which consists of a component capacitive humidity sensor and a thick film planar spiral inductor. This pseudo LC sensor was then subjected to humidity variation and the sensor response is consistent with the calculated prediction, only with a discrepancy of magnitude in sensitivity. The MWNTs based LC sensor did not show observable response upon exposure to target gas due to the relatively low capacitive sensitivity demonstrated by MWNT/AAO materials.

In summary, the MWNTs/AAO templates have demonstrated promising aspect for potential room temperature gas sensing applications. However, some major technical challenges have to be addressed, such as reproducibility, structural robustness and batch productivity, before further sensor prototyping investigations are undertaken.

Table 3.1: The list of AAO pore diameter, MWNT inner core diameter, and MWNT wall thickness for a series of samples prepared for gas sensing experiment. Data was provided by Dr. Vijay Singh's group.

AAO pore diameter (nm)	MWNT inner core diameter (nm)	MWNT wall thickness (nm)
50	40	10
35	25	10
25	15	10
12	2	10

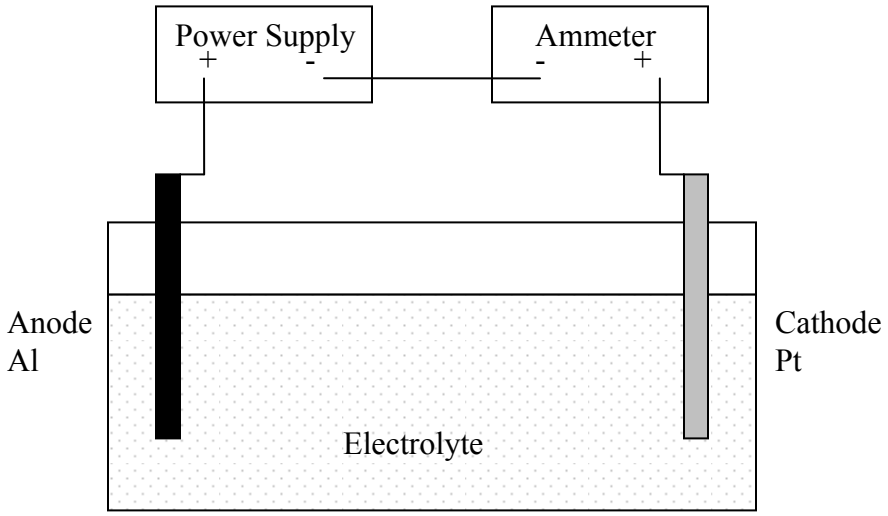

Figure 3.1: Schematic diagram of the setup for Al anodization, adapted from [72].

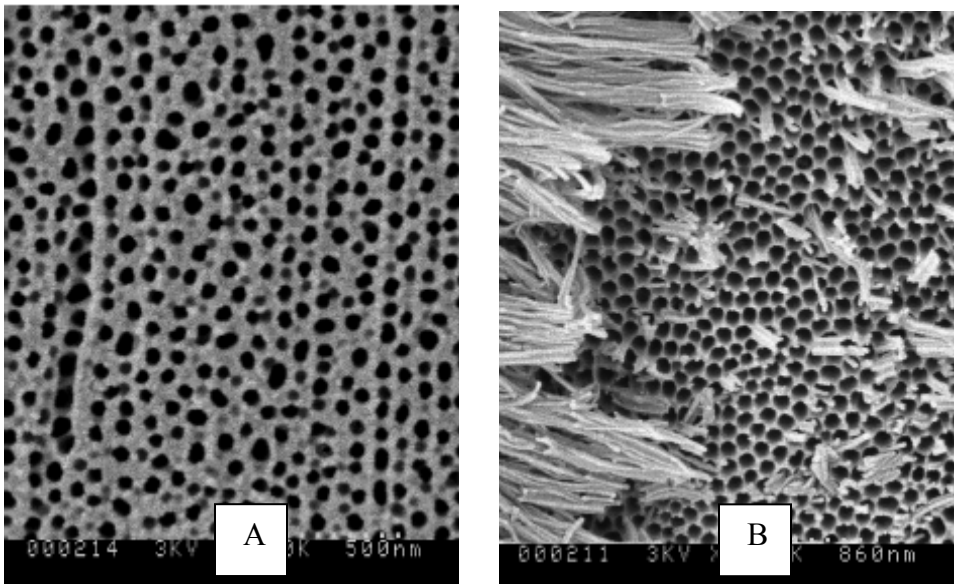

Figure 3.2: SEM images of the top view of anodized porous alumina (AAO) template with different pore size. A of 45 nm and B of 75 nm.

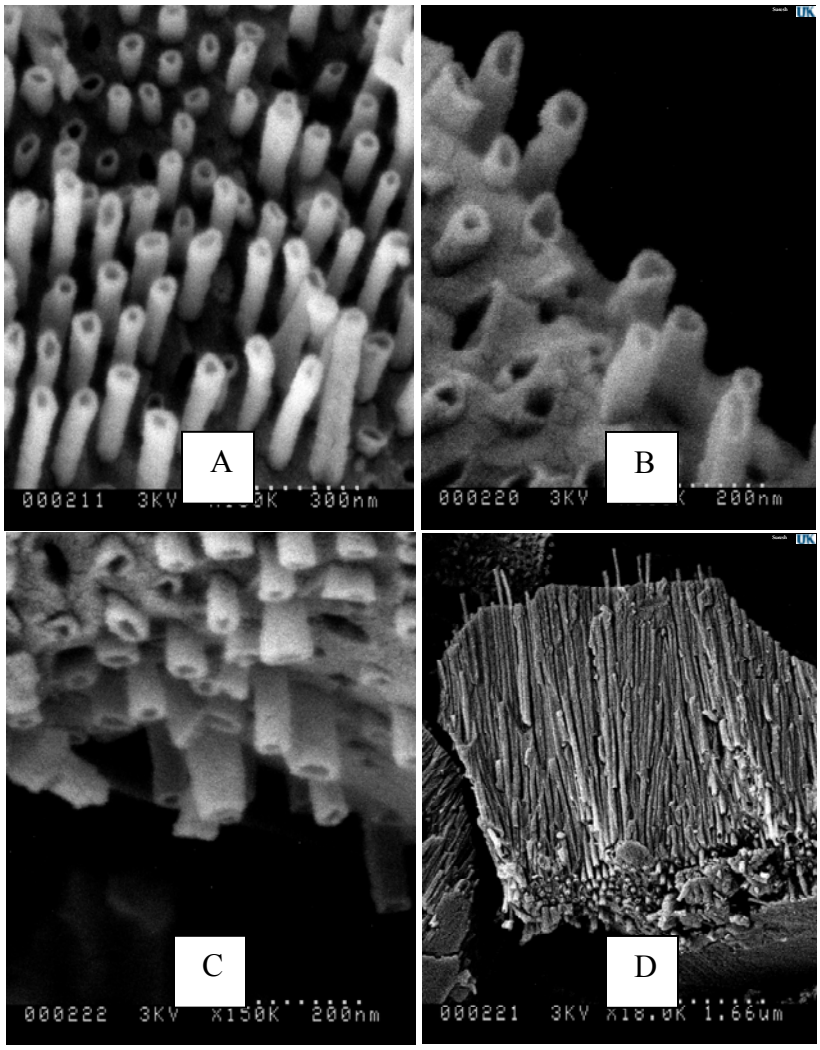

Figure 3.3: SEM images of spatially well separated, aligned nanotube arrays growth within porous AAO template. Where A shows the spatially well separated CNTs protrude through the surface of porous AAO template. B and C shows the nanotubes are open-ended on both sides. D shows the cross section of the CNTs containing AAO template.

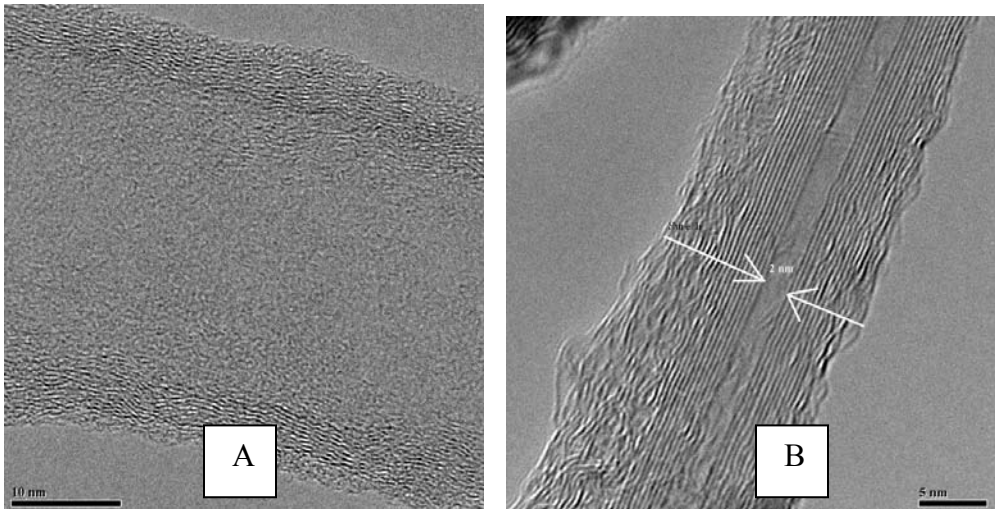

Figure 3.4: TEM images show MWNTs with 25 nm (A) and 2 nm (B) inner core diameters in addition to 5 nm wall thickness.

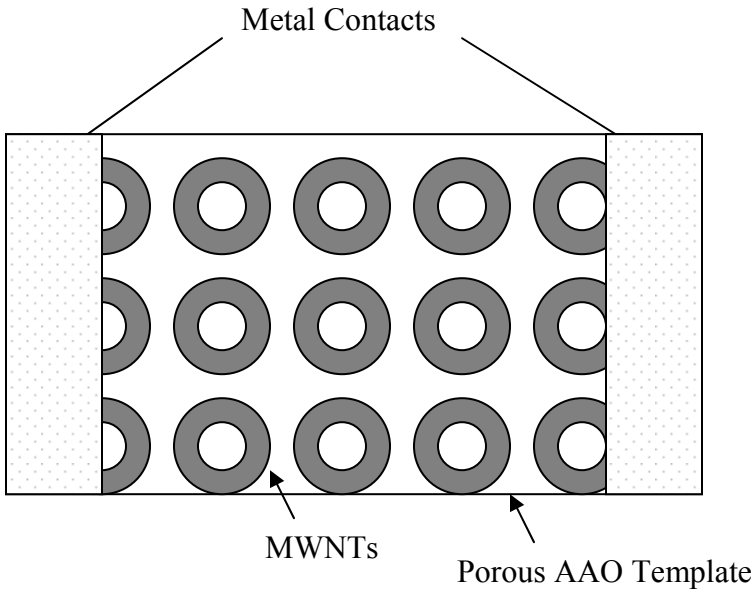

Figure 3.5: Schematic diagram of the as-grown MWNTs based resistive gas sensor (top view). The device was constructed by depositing metal contacts on the surface of the as-prepared aligned MWNTs/AAO template. Amorphous carbon is not shown.

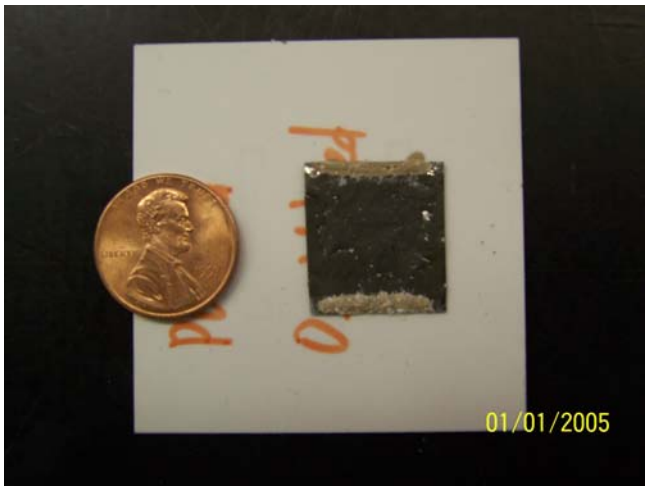

Figure 3.6: The photograph of a resistive gas sensor based on as-grown, aligned MWNTs/AAO template.

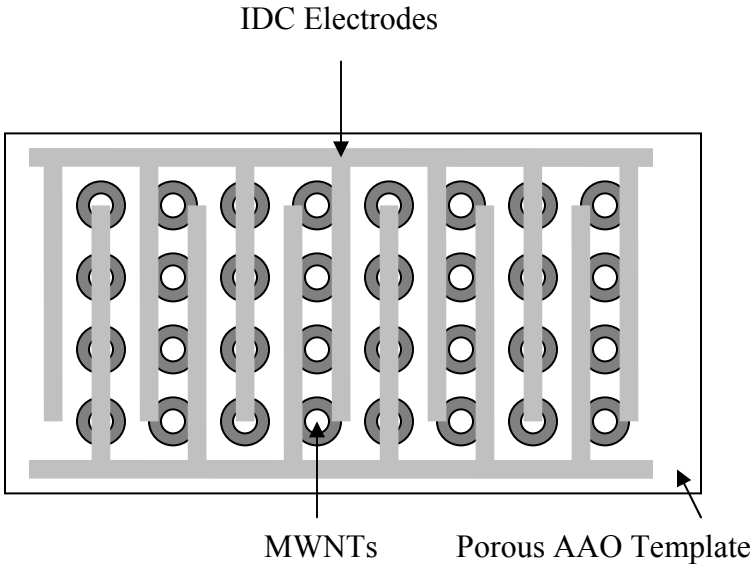

Figure 3.7: Schematic diagram of the MWNTs capacitive gas sensor (top view). The sensor was constructed by depositing IDC metal electrodes on the surface of plasma-etched, aligned MWNTs/AAO template.

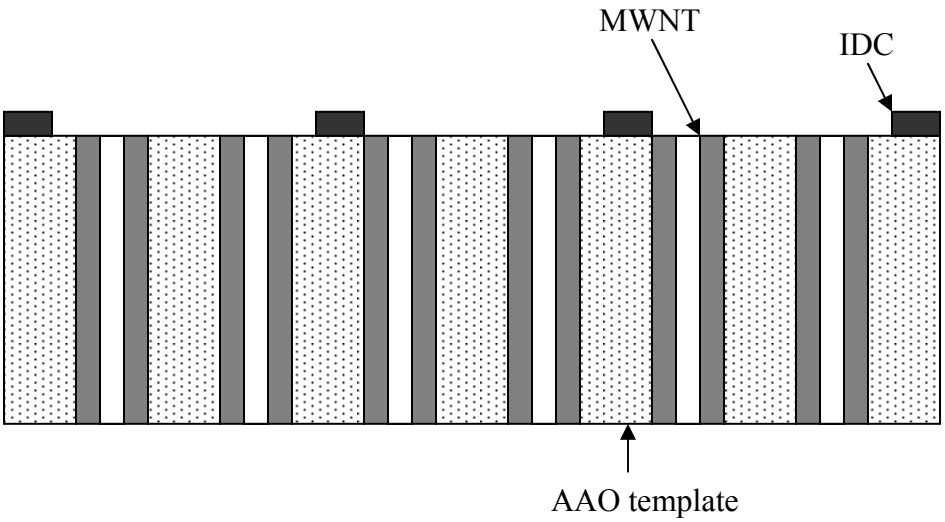

Figure 3.8: Schematic diagram of the MWNTs capacitive gas sensor (cross-section view).

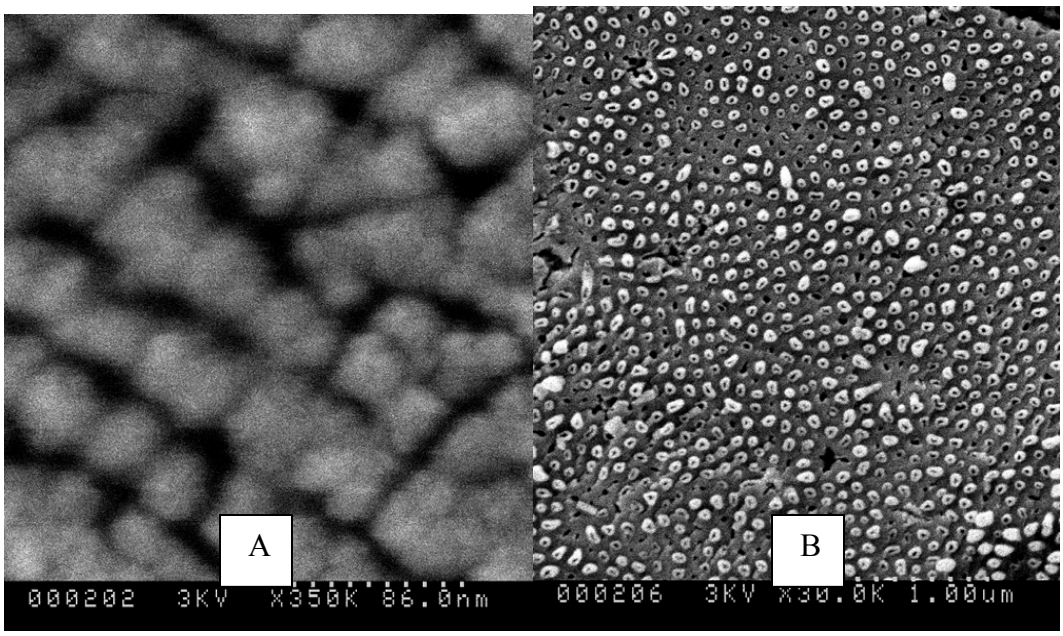

Figure 3.9: The SEM images of the as-grown (A) and plasma-etched (B) MWNTs/AAO template. It can be seen that the plasma etching removed the amorphous carbon from sample surface while kept the majority of the CNTs remain intact.

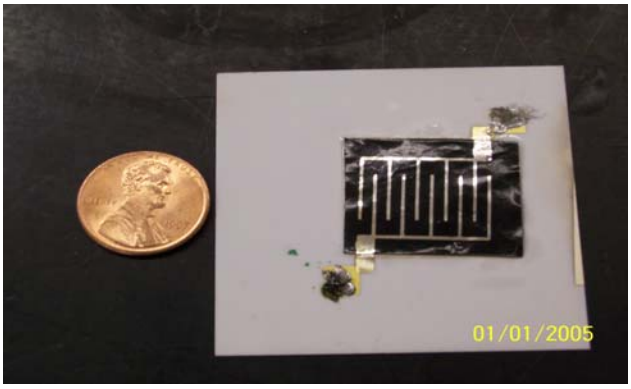

Figure 3.10: The photograph of a capacitive gas sensor based on the plasma-etched, aligned MWNTs/AAO template.

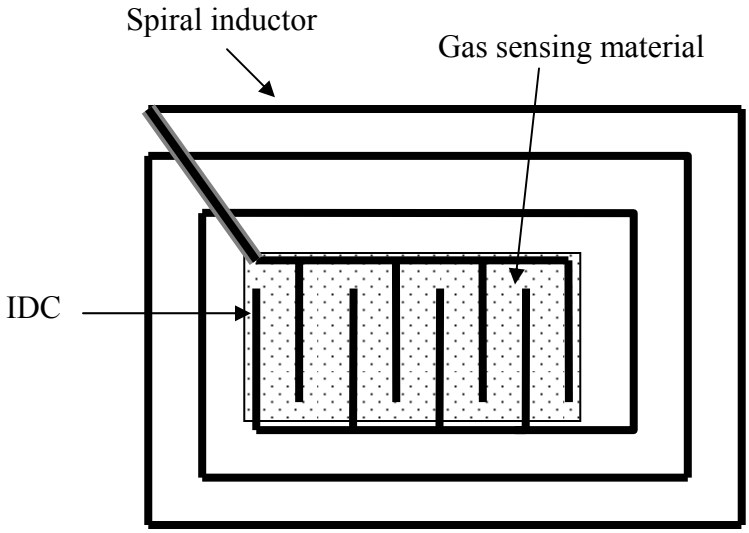

Figure 3.11: Schematic diagram of the LC resonant sensor (top view). It consists of an IDC in connection with a spiral inductor. The IDC is coated with the gas sensing material.

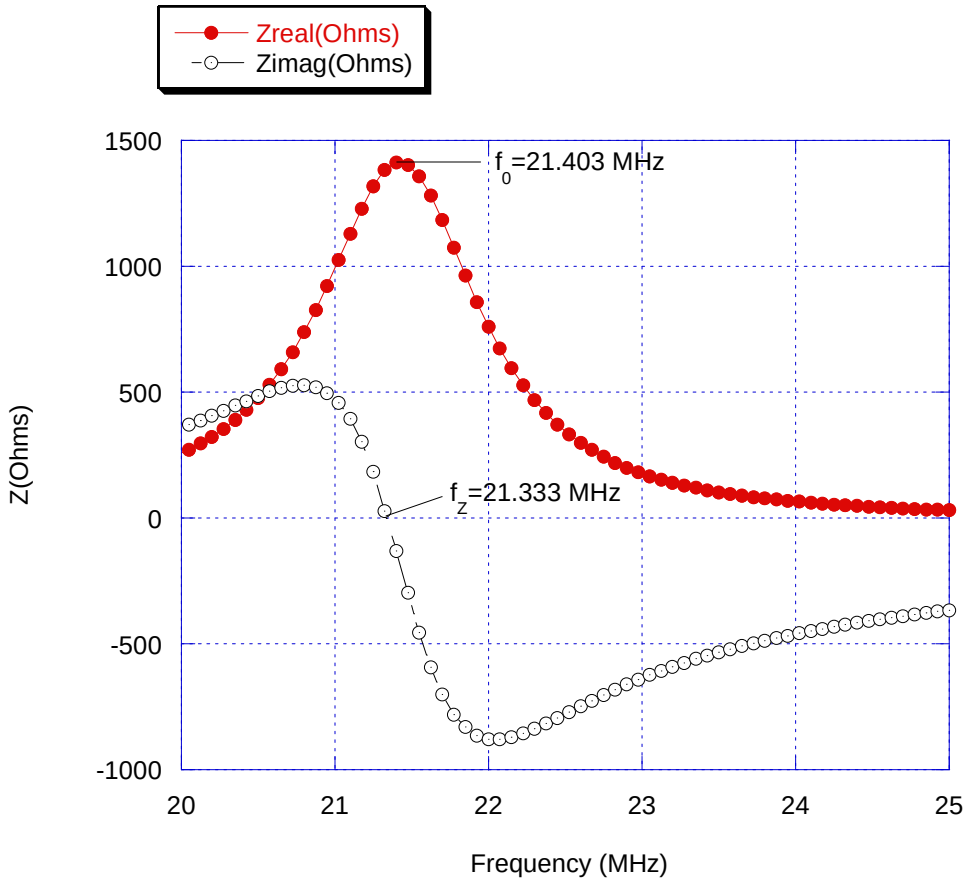

Figure 3.12: An illustrative measured impedance spectrum of LC resonant circuit. The resonant frequency f_0 is defined as the frequency where the real part of the impedance reaches its maximum, and the zero-reactance frequency f_Z is the frequency where the imaginary part of the impedance crosses zero.

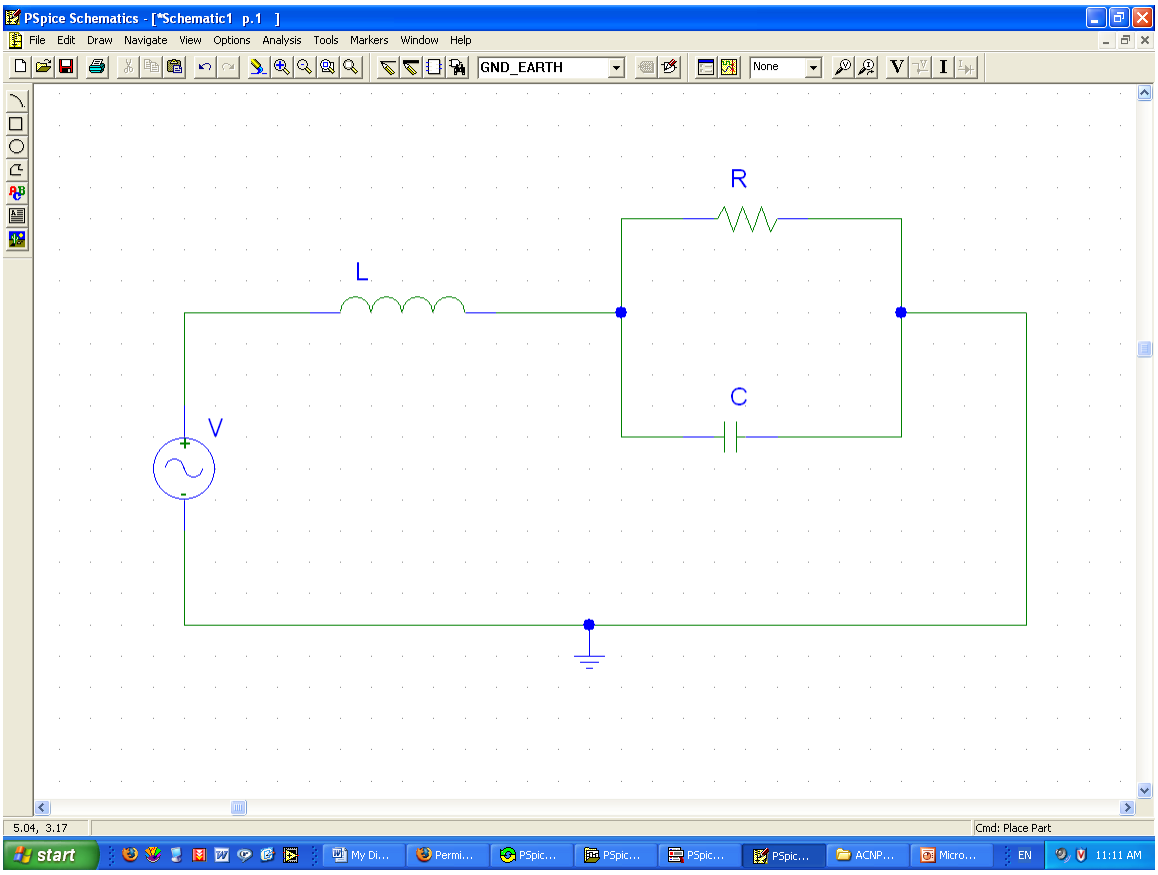

Figure 3.13: Equivalent circuit model of the LC resonant sensor. The sensor is modeled as an RLC circuit.

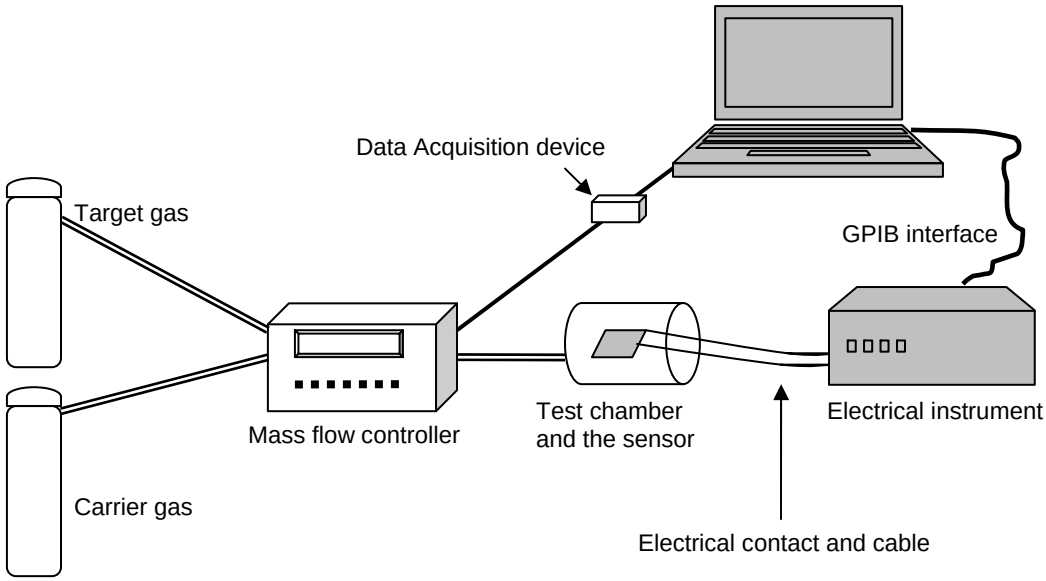

Figure 3.14: Schematic description of the gas sensor testing system. The sensor is placed inside a sealed glass chamber. Nitrogen (N_2) or compressed dry air is used as the carrier gas. The target gases are either pure (CO_2) or diluted by N_2 (NH_3, NO_2, etc.). A mass flow controller is used to mix the carrier and target gases and feed them into the test chamber at various proportions and flow rates. The electrical instruments included a digital multimeter, impedance analyzer, or network analyzer depending on the types of electrical signal to be measured.

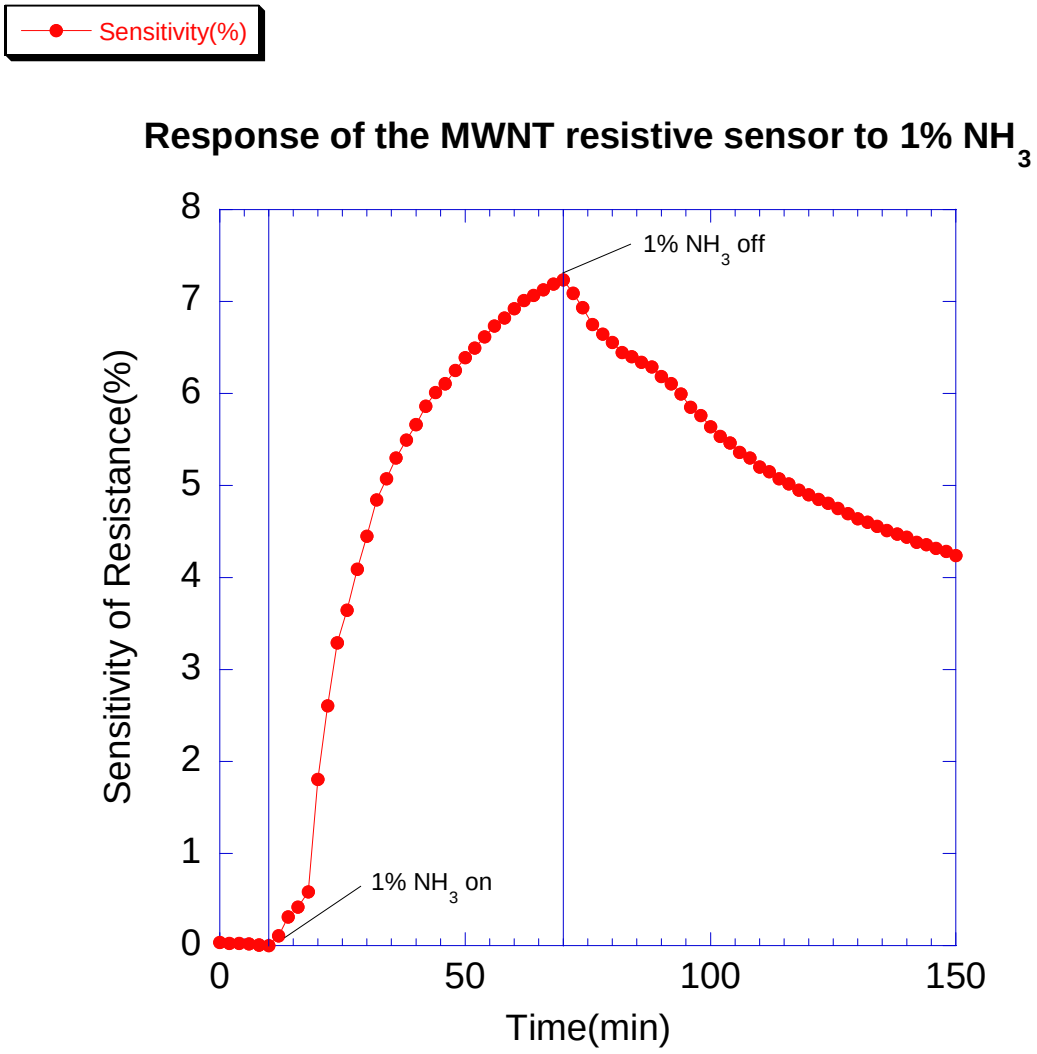

Figure 3.15: Measured resistance response when the MWNTs/AAO sensor is exposed to 1% NH_3 (in the flow of N_2) for 1 hour at room temperature.

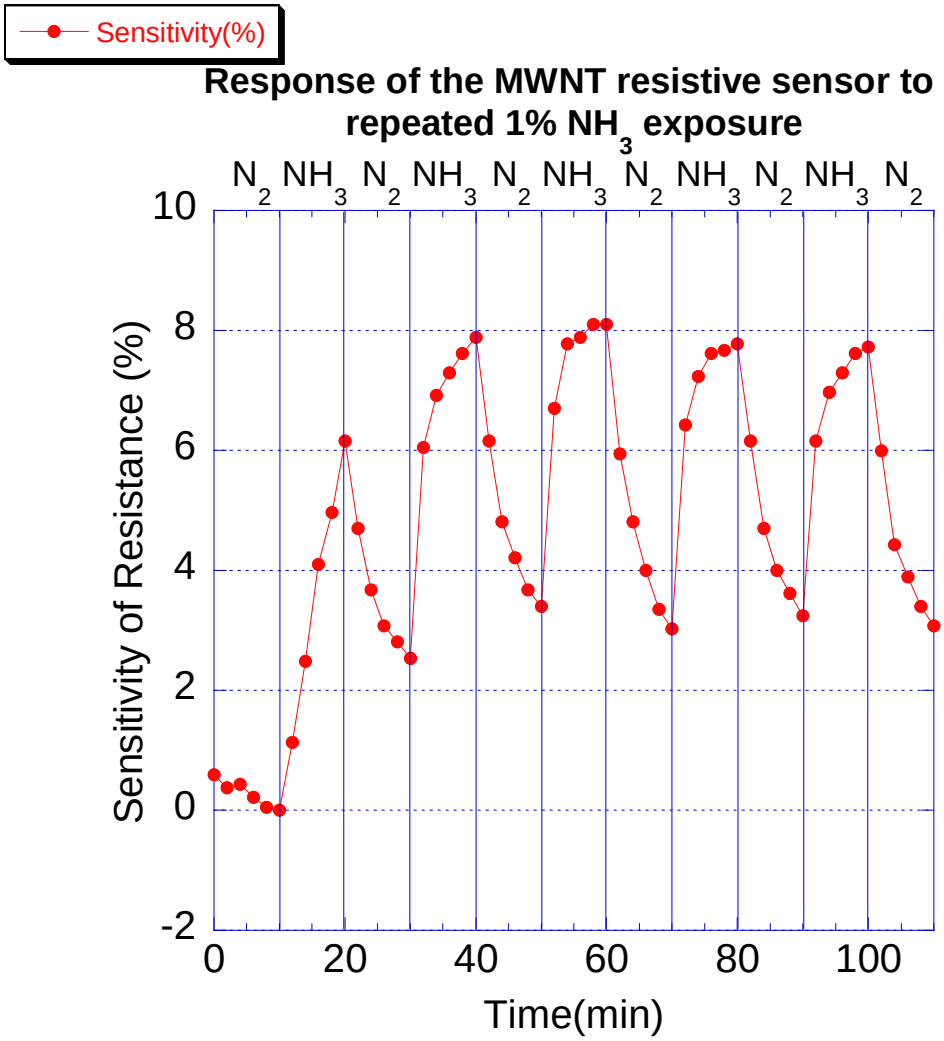

Figure 3.16: Measured resistance response when the MWNTs/AAO sensor is exposed to 1% NH_3 and pure N_2 alternately for periods of 10 minutes at room temperature. The sensor shows reversible response and incomplete recovery.

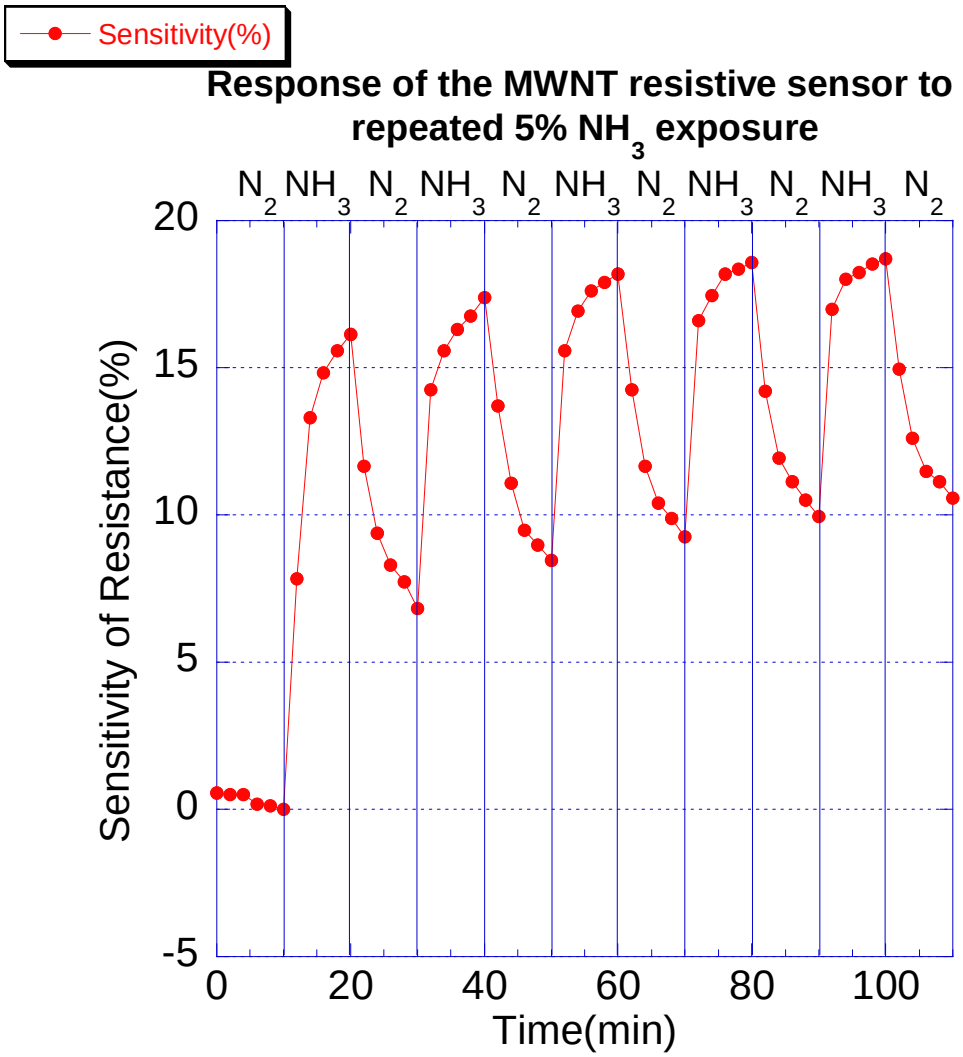

Figure 3.17: Measured resistance response as the MWNTs/AAO sensor is exposed to 5% NH_3 and pure N_2 alternately for periods of 10 minutes at room temperature. The sensitivity has increased as expected. The response is reversible and the sensor recovery is incomplete.

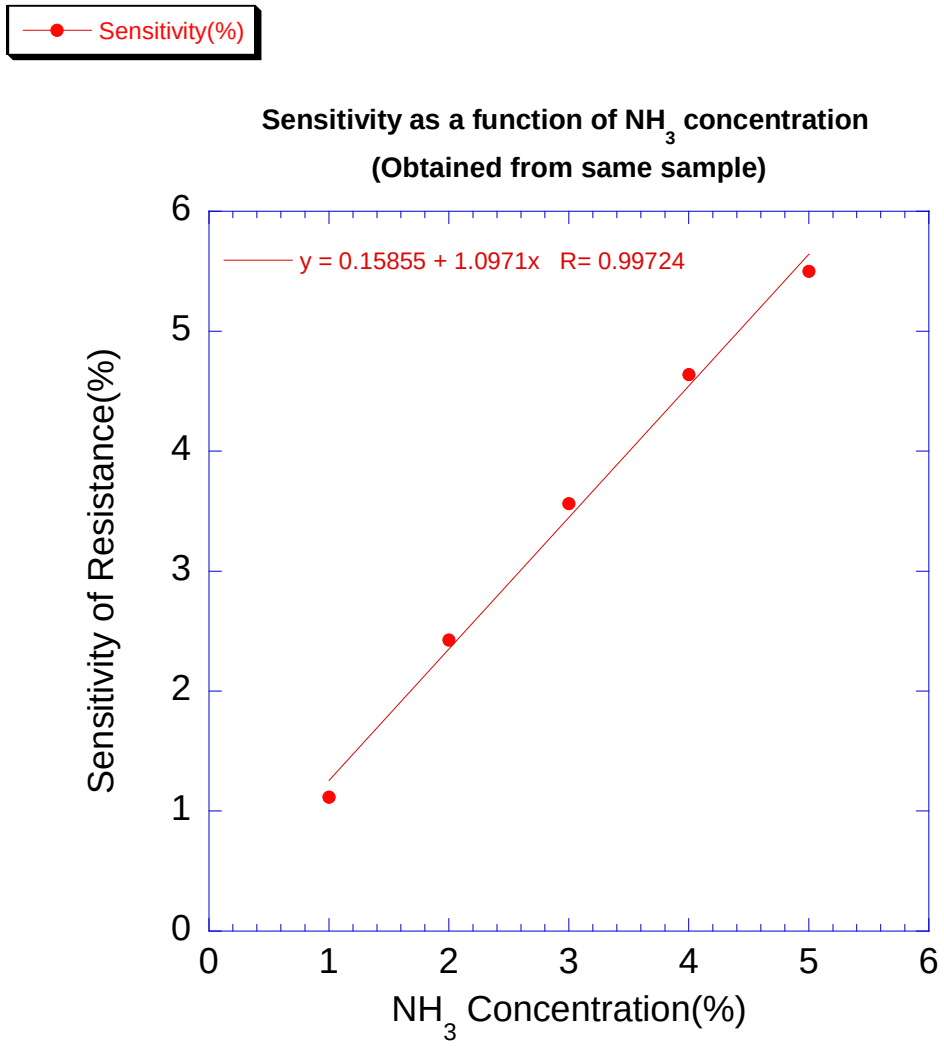

Figure 3.18: Measured response of the resistive sensor to various NH_3 concentrations at room temperature. The change in resistance with respect to the baseline was plotted versus the NH_3 concentration. The curve shows a linear fit.

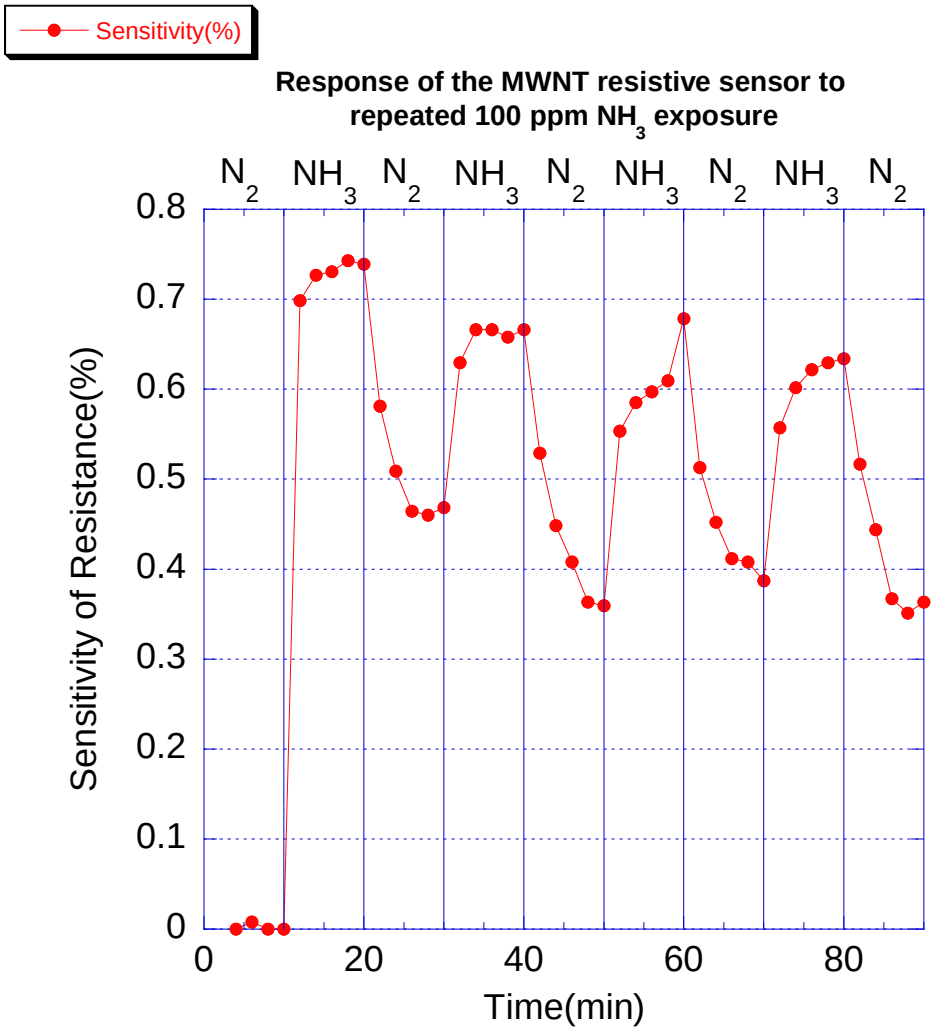

Figure 3.19: Measured resistance response when the sensor is exposed to 100 ppm NH_3 and pure N_2 alternately for periods of 10 minutes at room temperature. Despite the relatively low sensitivity, the sensor shows reversible response and incomplete recovery.

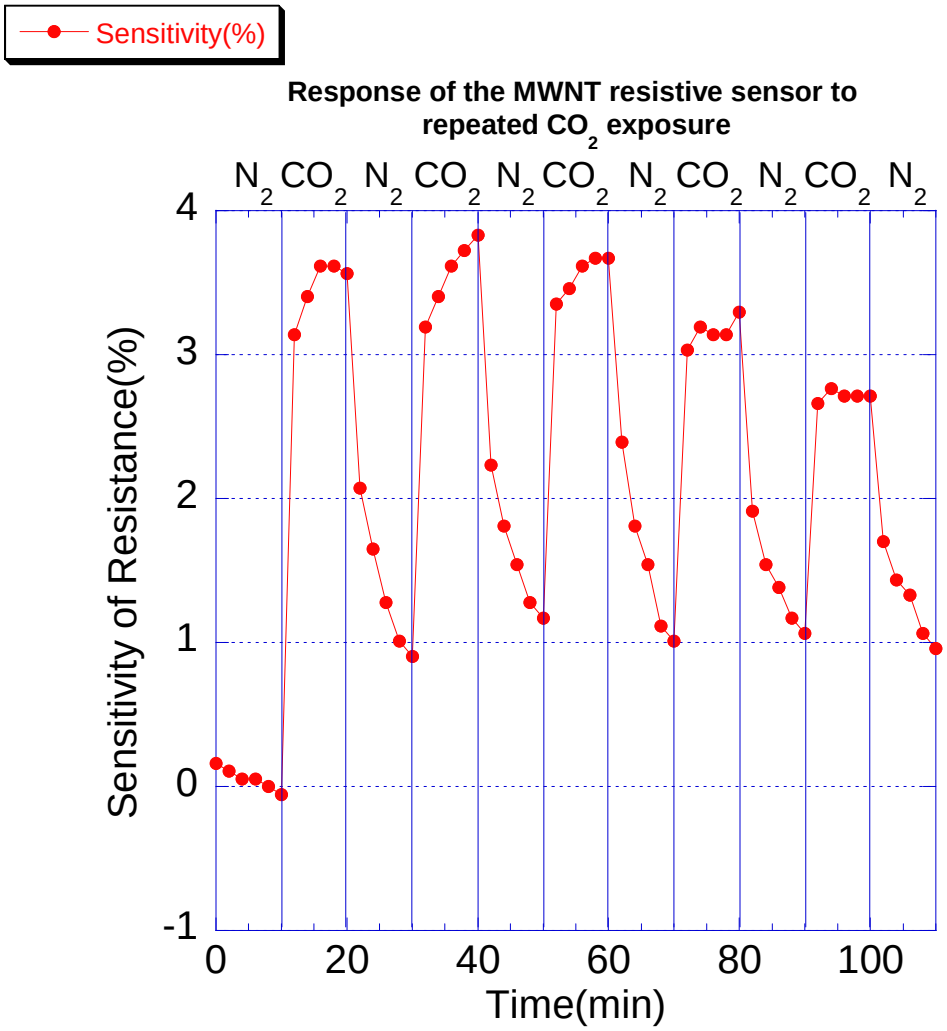

Figure 3.20: Measured resistance response when the MWNTs/AAO sensor is cycled between CO_2 and N_2 for 10 minutes respectively at room temperature. The sensor shows reversible response and incomplete recovery.

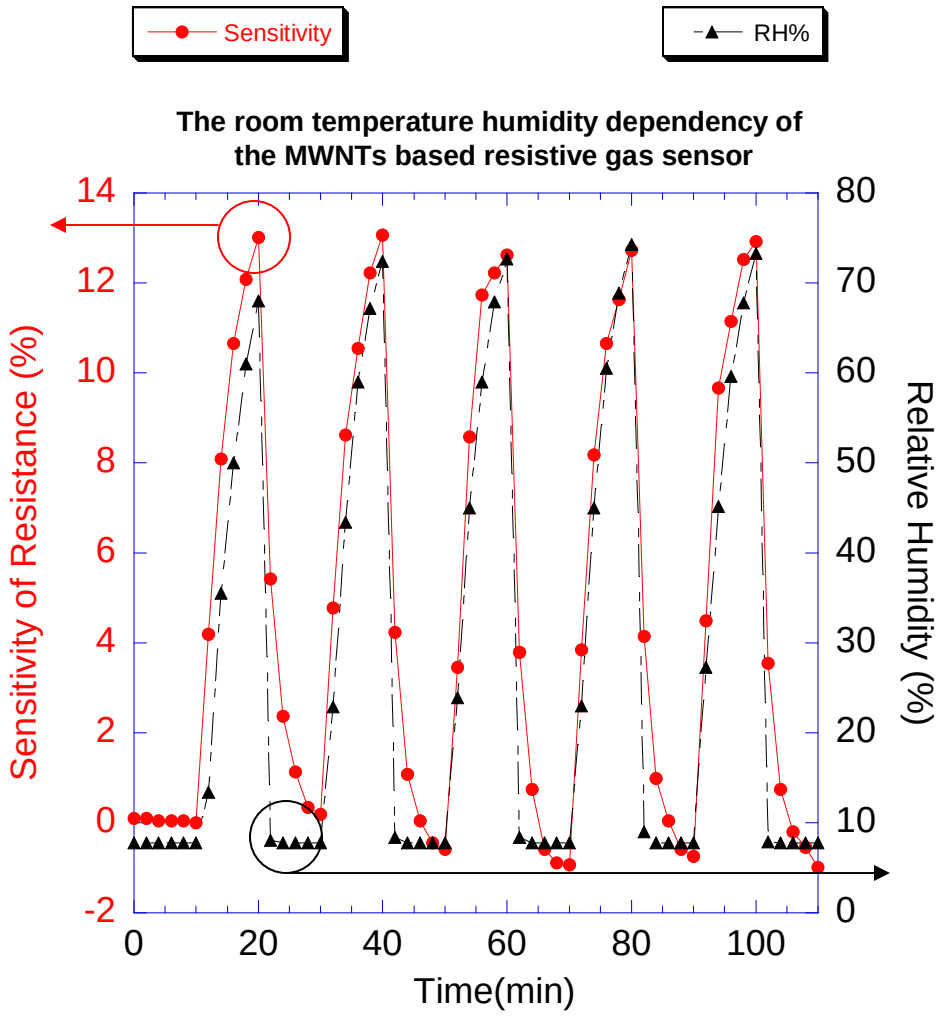

Figure 3.21: Measured resistance response as the MWNTs/AAO sensor was subjected to relative humidity (RH) variation at room temperature. A strong humidity dependency was observed.

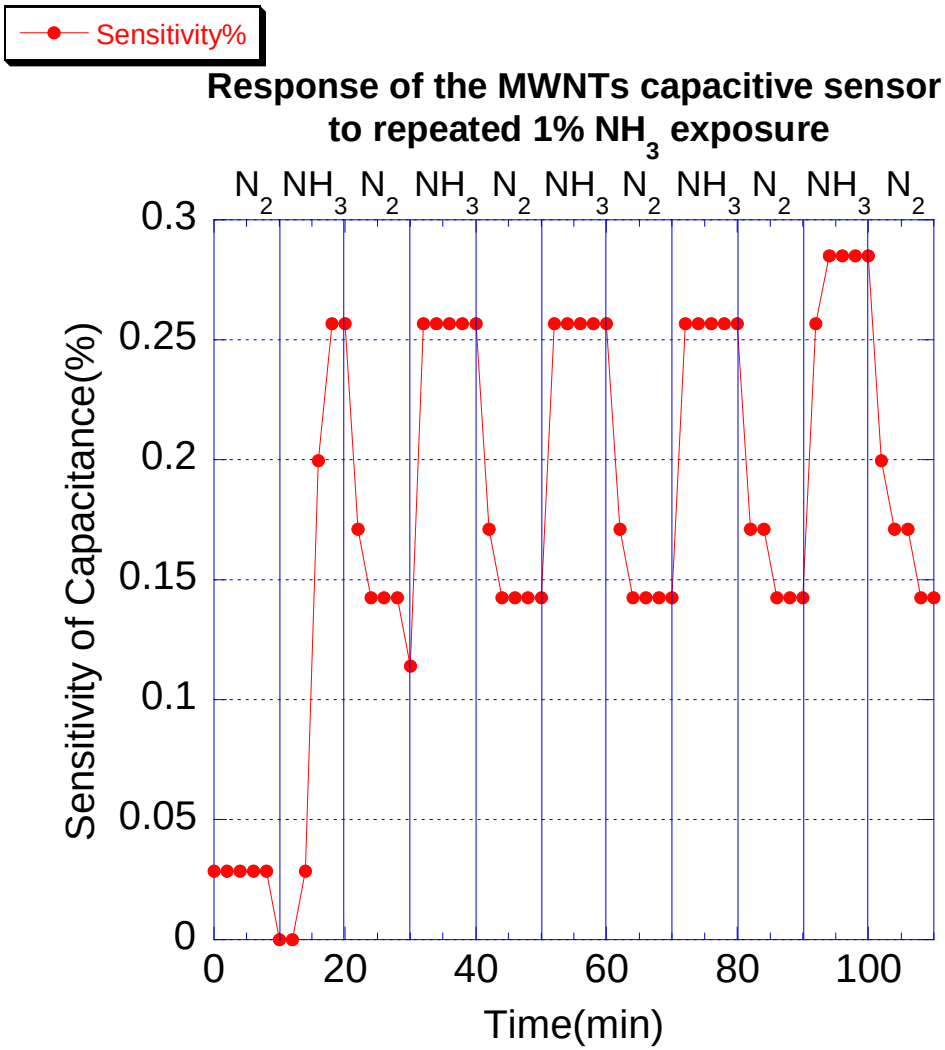

Figure 3.22: Measured capacitance response as the MWNTs/AAO sensor is exposed to 1% NH_3 and pure N_2 alternately for 10 minutes periods at room temperature. The response is reversible and the sensitivity is in the range of 0.25% to 0.3%.

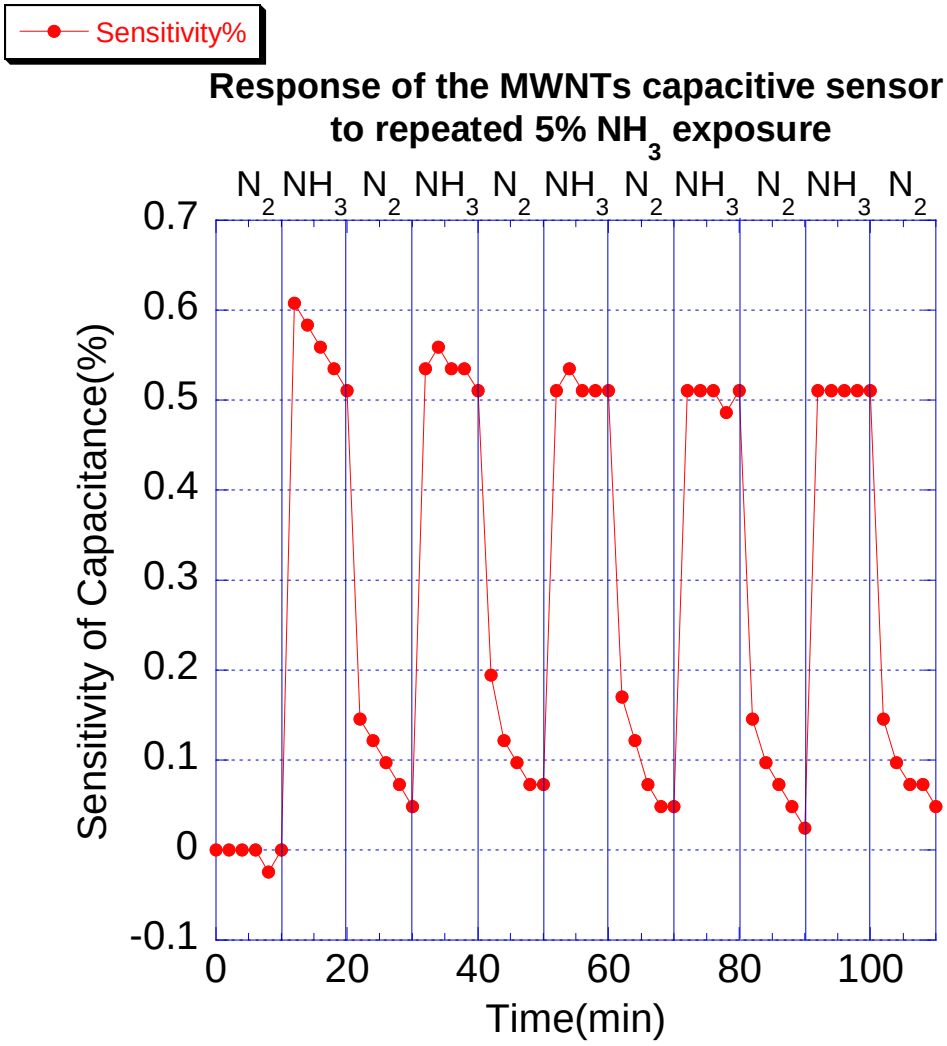

Figure 3.23: Measured capacitance response as the MWNTs/AAO sensor is exposed to 5% NH_3 and pure N_2 alternately for 10 minutes periods at room temperature. The response is reversible and the sensitivity is correspondingly increased to the range of 0.5% to 0.6%.

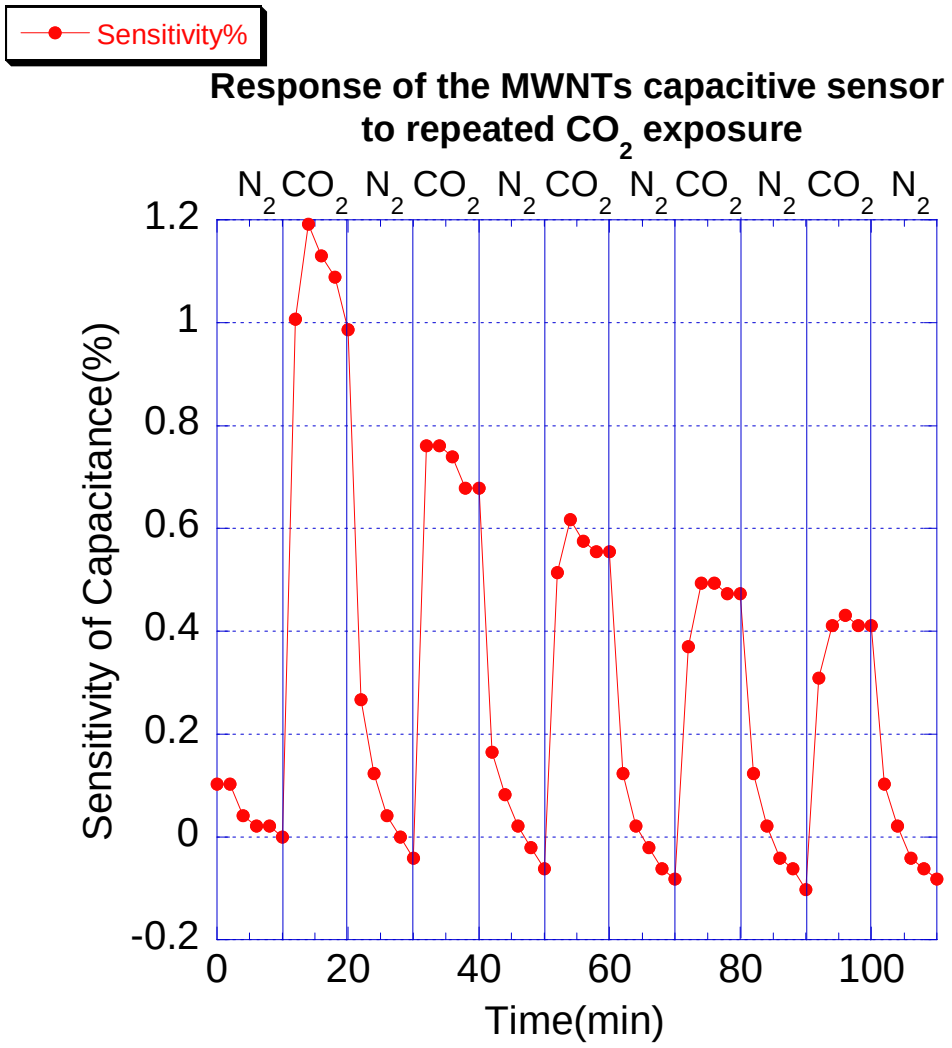

Figure 3.24: Measured capacitance response as the MWNTs/AAO sensor is exposed to CO_2 and N_2 alternately for 10 minutes periods at room temperature. The response is reversible but the baseline is drifting down continuously.

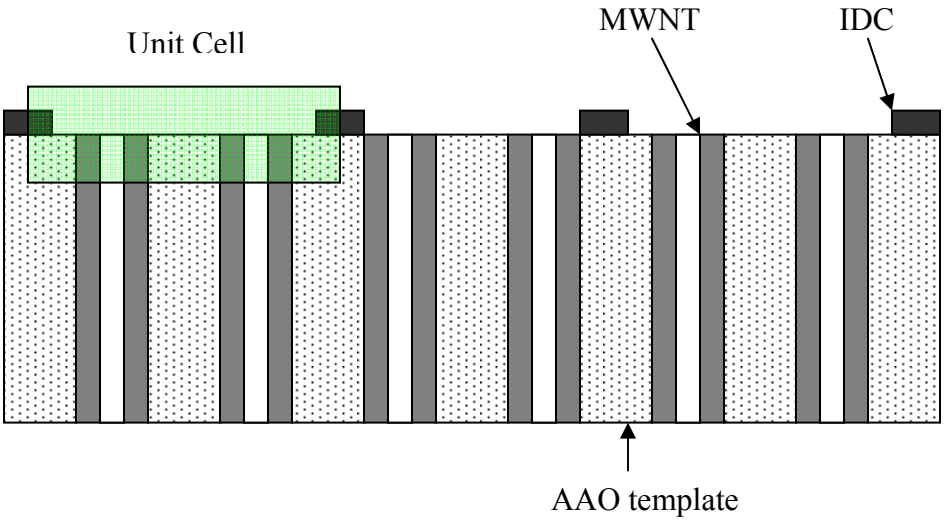

(A)

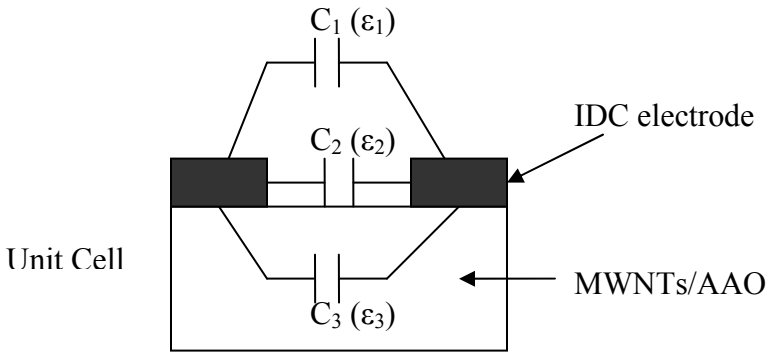

(B)

Figure 3.25: Schematic description of the unit cell within a capacitive MWNTs sensor. Where A shows the simplified cross-section of the sensor and the highlighted unit cell is shown in detail in B. The capacitance of a unit cell is composed of three partial capacitances, corresponding to permittivities ε_1, ε_2, and ε_3.

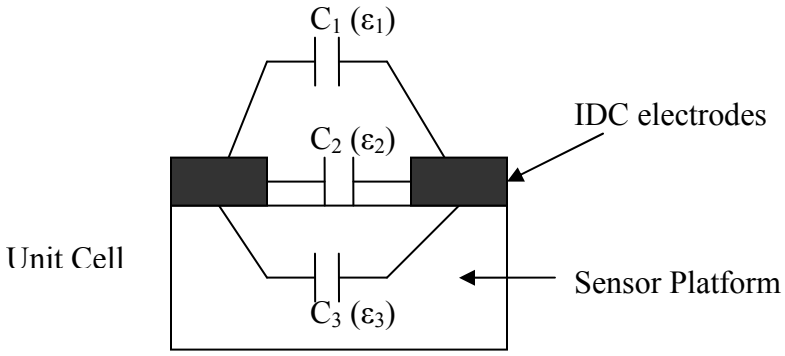

Figure 3.26: Schematic diagram of the unit cell for MWNTs capacitive sensor and control sensors. The choice of sensor platform material is MWNTs/AAO template for nanotube capacitive sensor, passive ceramic substrate for control sensor one and porous AAO template without MWNTs for control sensor two.

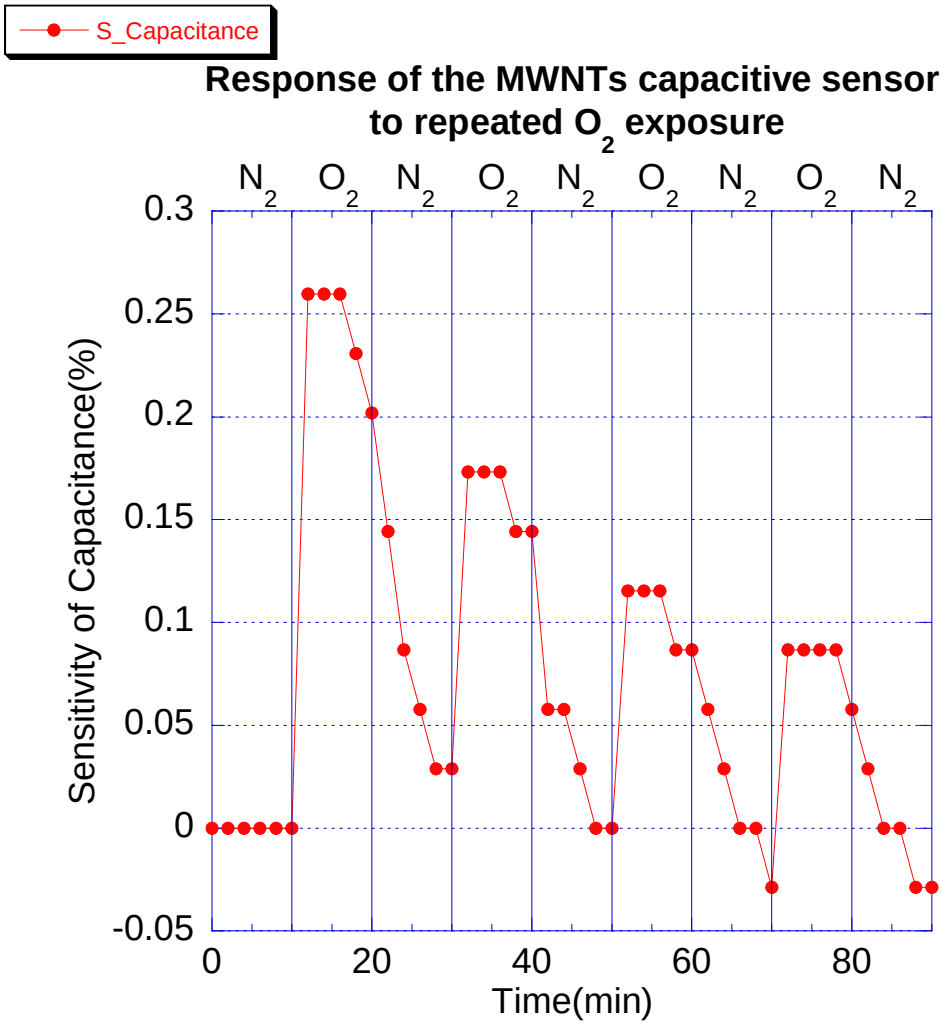

Figure 3.27: Measured capacitance response as the MWNTs/AAO sensor is exposed to O_2 and N_2 alternately for 10 minutes periods at room temperature. The sensor response is reversible. The data indicates that the sensor responses to oxidizing agent and reducing agent in the similar way, which implies that the sensing mechanism is dielectric based rather than conductance based.

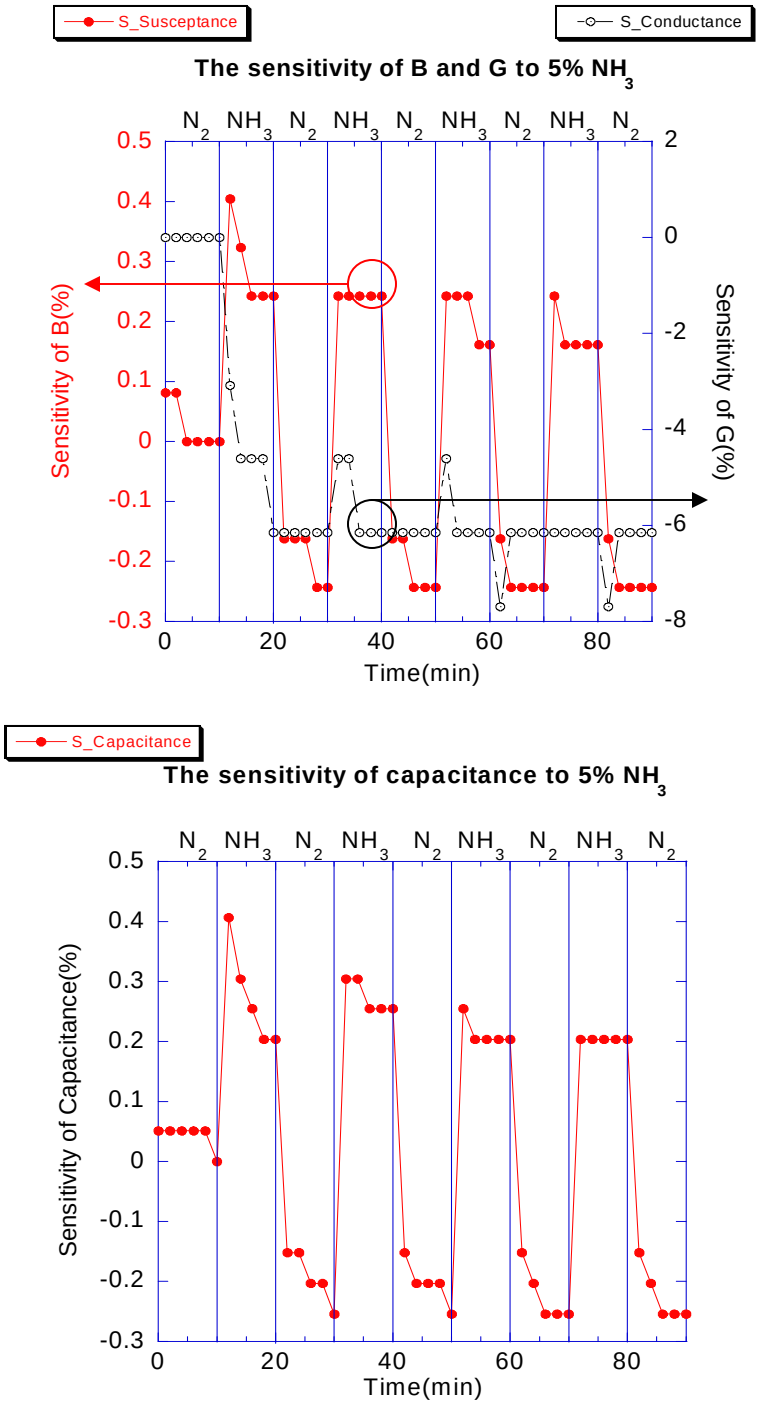

Figure 3.28: Measured response of capacitance C, susceptance B, and conductance G in the presence of 5% NH_3 gas. The data indicates that the response of C is determined by susceptance B instead of conductance G.

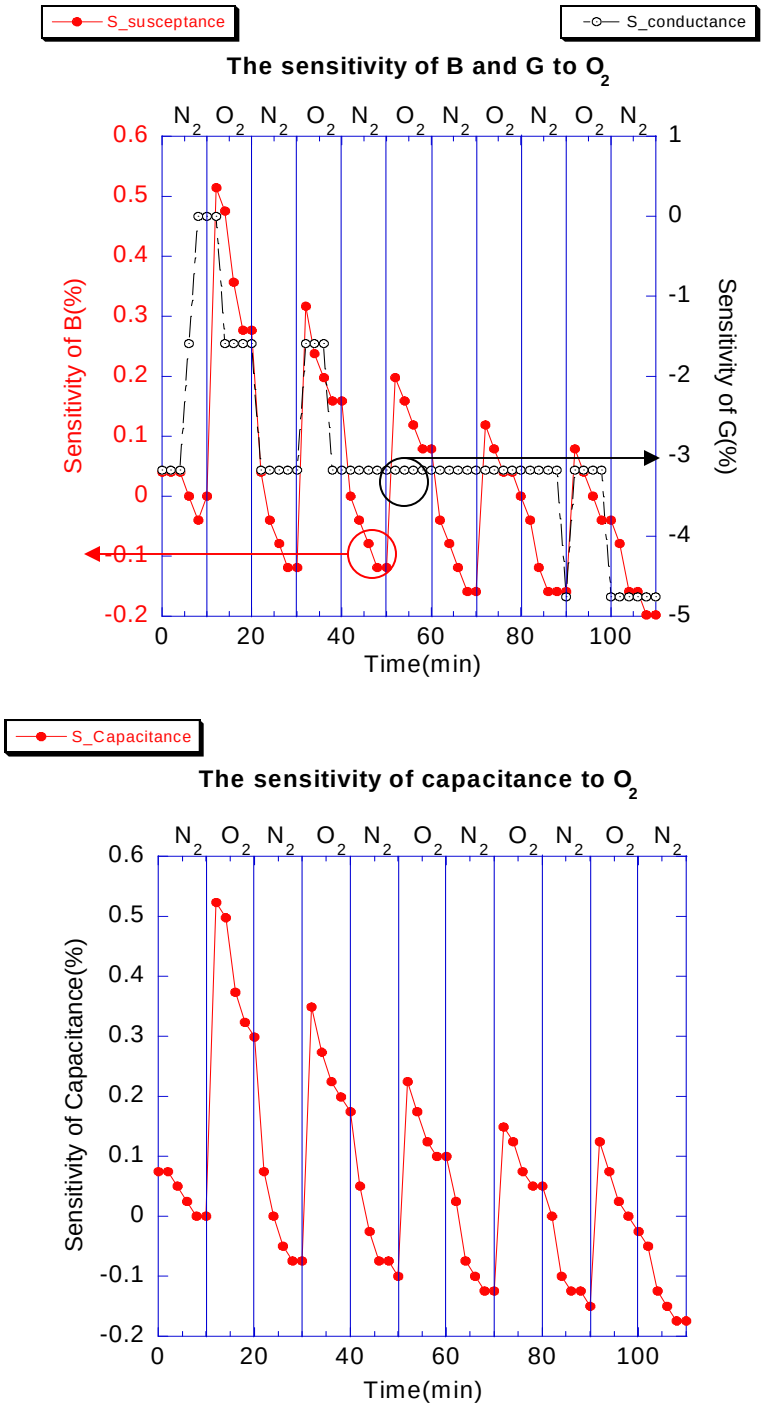

Figure 3.29: Measured response of capacitance C, susceptance B, and conductance G in the presence of O_2. The data indicates that the response of C is determined by susceptance B instead of conductance G.

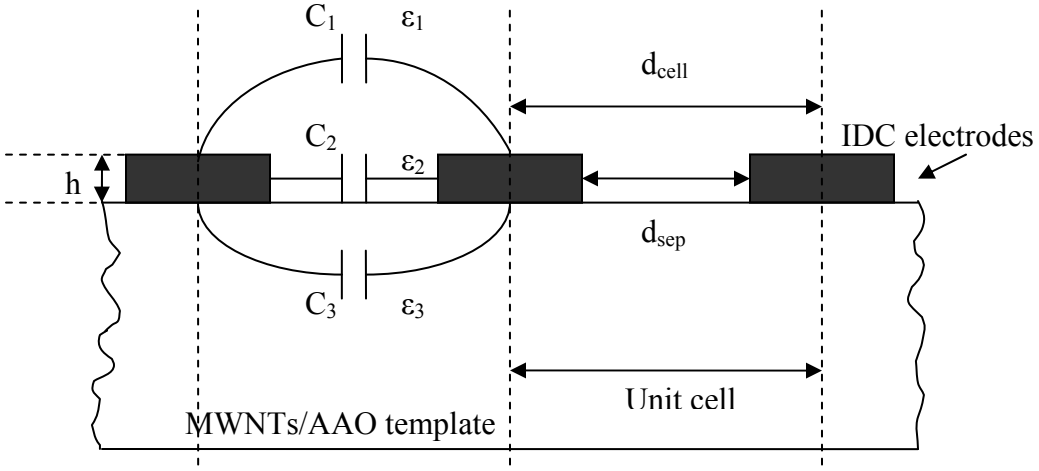

Figure 3.30: Schematic description of the model for the MWNTs/AAO based capacitive gas sensor. Shown is the cross sectional view and some of the key parameters. The length of IDC electrode L is not shown.

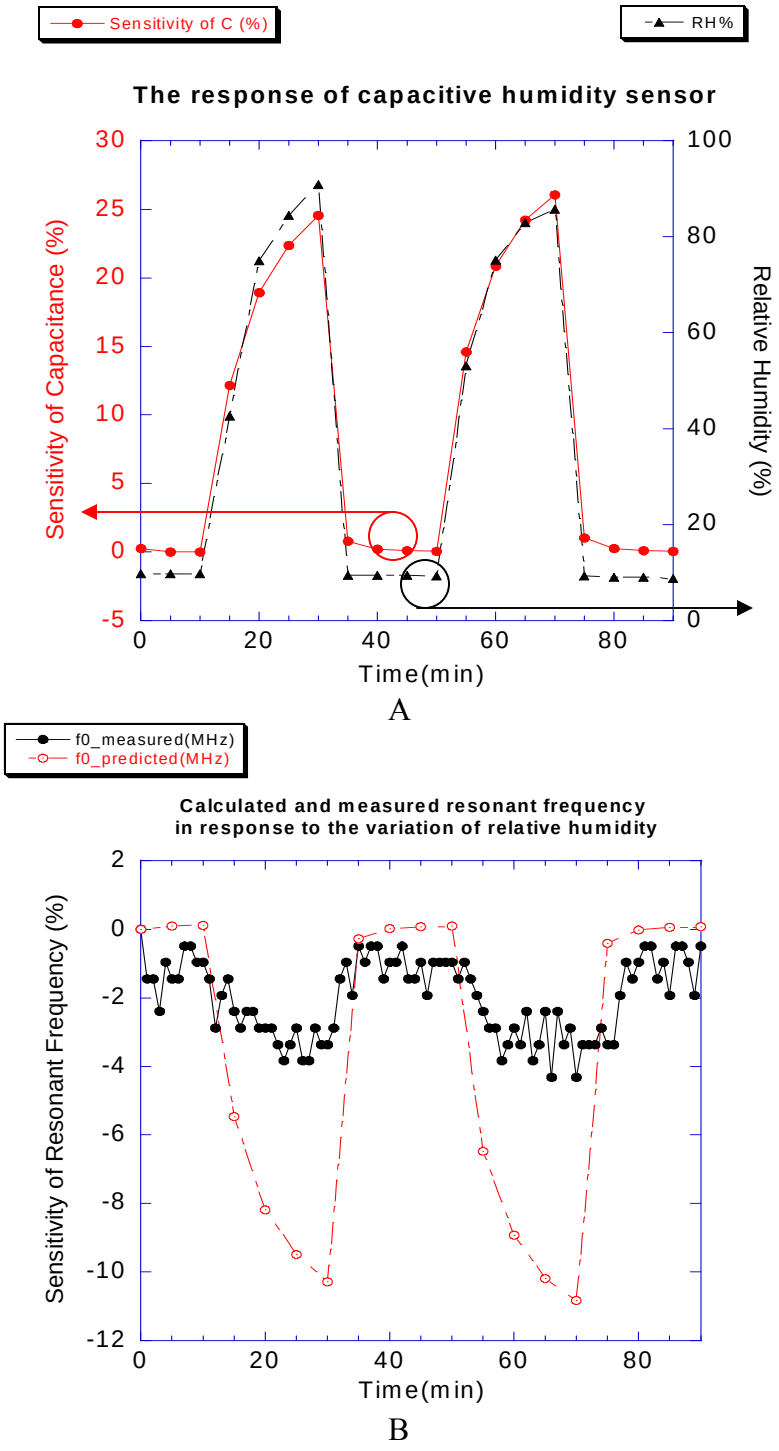

Figure 3.31: Measured response of the capacitive humidity sensor (A) and the calculated and measured resonant frequency of an LC humidity sensor in response to the change of relative humidity (B).

CHAPTER4: GAS SENSORS BASED ON SWNTS

4.1 Introduction

Both single-walled and multi-walled carbon nanotubes for gas sensing at room temperature have attracted great interest because most of the commercially available gas sensors operate at elevated (at least 200°C) temperatures. Gas sensors based on MWNTs are discussed in chapter 3. A low cost resistive gas sensor based on SWNTs for the room temperature detection of NO_2 and NH_3 is presented in chapter 4. The sensor was fabricated by coating the interdigitated electrodes with the mixture of SWNTs and organic binder, thus SWNT networks covering the IDC electrodes. The resistance of the sensor was monitored in the presence of various concentrations of NO_2 and NH_3 (balanced by N_2) at room temperature.

The resistance of SWNTs sensor was found to be sensitive to both NO_2 and NH_3. The sensor demonstrated lower detection limits of 1 ppm for NO_2 and 10 ppm for NH_3 with reversible and reproducible response. At room temperature, sensor recovery was found to be slow and incomplete, therefore possible solutions were investigated to facilitate the recovery process. The gas molecule adsorption and desorption mechanisms are discussed. Sensor performance in the background of air instead of N_2 is also investigated and discussed in preparation for the future device prototyping.

4.2 Experimental

4.2.1 Sensor fabrication

The sensor electrodes were prepared by the technique of thick film screen printing. Au (C5729 lead free gold conductor paste, Heraeus) interdigitated electrodes were patterned on ceramic substrate (ADS-96R, CoorsTek) using an Aremco Accu-coat 3230 screen printer. Once patterned, the conductor paste was dried to evaporate the solvent at 150ºC and then fired for 60 minutes with a peak temperature of 850ºC using an Intex TF76 infrared thick film firing furnace.

The SWNTs were purchased from Cheap Tubes Inc., USA [87]. These 90 wt% purified SWNTs have 1-2 nm outer diameter and 0.8-1.6 nm inner diameter with the length of 5-30 μm. To prepare the low cost gas sensing material, 1 wt% SWNTs (lowest reported loading for this type of sensor) were dispersed in an organic binder α-terpineol ($C_{10}H_{17}OH$, Alfa Aesar) by 1 hour ultrasonic vibration. A Thinky AR-250 planetary mixer was then used to obtain the well dispersed SWNT mixture by mixing for 10 minutes at 800 rpm. In order to obtain uniformly distributed gas sensing material on the sensor platform, spin-coating was chosen instead of screen-printing to apply the SWNT mixture. The mixture of well-dispersed SWNTs and α-terpineol was then coated on the sensor platform by spin-coating for 30 seconds at 3500 rpm. Next, the sample was kept in the infrared thick film firing furnace at 350ºC for 2 hours to burn off the residual organic binder [88][89]. Figure 4.1 shows the schematic description of the SWNTs based resistive sensor (top view). Figure 4.2 shows that uniformly distributed SWNT network was achieved by spin-coating instead of screen-printing.

4.2.2 Resistive gas sensing and sensor recovery

A total of 9 SWNT sensors were prepared, of which 5 were used for NO_2 detection and 4 for NH_3 detection. Both NO_2 and NH_3 are foul smelling toxic gases, where NO_2 is one of the most prominent sources of air pollution. The immediately dangerous to life or health concentration of NO_2 is 20 ppm and the OSHA permissible exposure limits is 5 ppm [4]. The detection of NO_2 and NH_3 are of great importance for environmental protection, industrial control and medical applications.

The sensor was kept in vacuum at 100ºC for 2 hours prior to each experiment session for the purpose of gas molecule desorption. The SWNT sensor was then placed inside the test chamber in the flow of N_2 gas until the equilibrium condition was obtained, i.e. the resistance measurement stabilized. The response of sensor resistance to both reducing agent NH_3 and oxidizing agent NO_2 at various concentrations was monitored. Typical baseline resistance for the SWNT sensor ranged from 10 to 15 Ω. Multiple-cycled testing was also performed for each sample during which the ambient inside the

test chamber was alternated between pure N_2 and the target gases with desired concentrations for periods of 10 minutes each. The sensor response was evaluated by sensitivity S, which was defined as:

$$S(\%) = \frac{R_{gas} - R_{N_2}}{R_{N_2}} \times 100 \quad (4.1)$$

where R_{N2} is the resistance in the presence of carrier gas N_2, and R_{gas} is the resistance in the presence of the target gas. The sensor recovery was incomplete after the removal of the target gases. In order to evaluate the methods to improve the sensor recovery, the effects of ultraviolet illumination and heating on sensor response were investigated. In order to prepare for the future device prototyping work, the carrier gas N_2 was replaced by the compressed air and the sensor performance in the background of air instead of N_2 was evaluated. In this case, the sensitivity S was defined as:

$$S(\%) = \frac{R_{gas} - R_{air}}{R_{air}} \times 100 \quad (4.2)$$

where R_{air} is the sensor resistance in the presence of carrier gas air. The dependency of the SWNT sensor to temperature and humidity in the ambient of air was also investigated. The experiment setup was previously described in detail in section 3.2.5.

4.3 Results and Discussion

4.3.1 NO_2 detection

The response of a SWNT resistive sensor to 10 ppm NO_2 exposure is shown in Figure 4.3. The sensor was placed inside the test chamber in the flow of N_2 at the beginning of the experiment. The sensor resistance was monitored by a digital multimeter (Hewlett Packard 3478A). After the sensor reached the equilibrium condition (constant resistance), NO_2 was introduced into the chamber at a concentration of 10 ppm in addition to the existing carrier gas N_2. The sensor was exposed to NO_2 for 30 minutes at room temperature and then allowed to recover in the flow of pure N_2. The result in Figure 4.3 shows that the sensor resistance responded promptly to the presence of NO_2. The resistance was reduced by 11% in response to NO_2 exposure and increased immediately upon the removal of NO_2.

Shown in Figure 4.4 is the measured sensor response to repeated 10 ppm NO_2 exposure at room temperature. After the sensor reached equilibrium, the ambient inside the test chamber was cycled between 10 ppm NO_2 and pure N_2 for periods of 10 minutes each. The recorded resistance change is plotted in Figure 4.4. The data shows that the change of resistance followed the gas delivery pattern promptly. The dynamic sensor response is reversible and the sensor recovery in the flow of N_2 is incomplete. The incomplete recovery is attributed to the built-up of NO_2 molecules on the surface of SWNTs. As a result, the sensor shows an irreversible decrease in resistance throughout the duration of the experiment.

Five SWNTs sensors were employed for the NO_2 detection. The response of all five sensors to various concentrations of NO_2 gas is depicted in Figure 4.5. The concentrations of NO_2 varied from 1 ppm to 50 ppm and the data was based on the experiment results of 10 minutes NO_2 exposure. Shown in the plot is the average sensitivity of all five samples (with one standard deviation) as a function of NO_2 concentration. One can see that the sensitivity of SWNTs sensors increases with an increase in the concentration of NO_2 gas and demonstrated a lower detection limit of 1 ppm. Figure 4.5 indicated that the sensitivity was nearly a linear function of the NO_2 concentration.

The response of the SWNTs sensor to NO_2 is in agreement with trends reported elsewhere [55][57] and the sensing mechanism can be explained as follows. Heat treatment (350ºC) applied during the sensor preparation to burn off organic residual have formed SWNT bundles of open-ended tubes, as described by Nguyen and coworkers [89]. The possible adsorption sites for gas molecules in the bundles are, therefore, the inner channels of tubes, the external walls, the interstitial channel between the tubes within the bundles, and the grooves between two outer tubes of neighboring bundles [90][91][92][93][94]. Upon exposure, NO_2 gas molecules are present at these adsorption sites and charge transfer from SWNTs to NO_2 occurs. Known as a strong oxidizer, NO_2 has an unpaired electron [55] and this strong electron-withdrawing ability

results an increased conducting holes carrier concentration within SWNT bundles. As can be seen from Figure 4.3, Figure 4.4 and Figure 4.5, the resistance of the SWNT sensor decreased in the presence of oxidizing agent NO_2, which indicates that conducing holes are the majority carriers for these SWNTs. Therefore SWNTs employed in this work demonstrate p-type semiconducting characteristic.

As can be seen from Figure 4.4, room temperature sensor recovery in the flow of N_2 was incomplete as evidenced by an irreversible decrease in sensor electrical resistance. The incomplete recovery compromises the long term performance of the sensor. In order to improve the sensor recovery, it is necessary to investigate the mechanism of gas molecule adsorption on SWNT in detail. Although the exact binding mechanism between gas molecules and SWNTs is not yet fully understood, it is generally believed that it involves weak physisorption and strong chemisorption [69][95][96]. The reversible and irreversible responses observed with the SWNT sensors are consistent with adsorption of gas molecules present on SWNTs through both physisorption, i.e. non-covalent Van der Waals force, and chemisorption, i.e. chemical bond through defect sites on SWNT surface. The kinetic energy of flowing N_2 breaks the weak electrostatic bonds between SWNTs and the physisorbed gas molecules during the sensor recovery (switching from target gas to pure N_2). The desorption of the physisorbed gas molecules causes the reversible SWNT resistance change. At the same time, the stronger bonds between the chemisorbed gas molecules and SWNTs can not be overcome by the flow of N_2, as a result the chemisorbed gas molecules build up through multiple-cycled test, and therefore an overall incomplete sensor recovery featuring irreversible resistance change is observed.

4.3.2 NH_3 detection

The dynamic room temperature responses of SWNT sensor to NH_3 exposure are shown in Figure 4.6 and Figure 4.7. Shown in Figure 4.6 is the sensor response to 100 NH_3 for 30 minutes in the flow of N_2. The sensor was allowed to reach equilibrium condition first. N_2 diluted NH_3 was then introduced into the test chamber and mixed with N_2 at a concentration of 100 ppm. The sensor was exposed to NH_3 for 30 minutes and

then recovered in the flow of pure N_2. The change of sensor resistance was recorded and plotted in Figure 4.6. One can see that the sensor responded promptly to the presence of NH_3 and its resistance increased by approximately 2% in a period of 30 minutes. The data of Figure 4.6 also shows that the resistance of SWNT sensor starts to decrease immediately upon removal of NH_3, however the recovery is at a much slower rate compared to its response rate. We have observed that even after several days keeping in air at room temperature, the SWNT sensors are still unable to fully recover from the detection of NH_3 and NO_2.

The measured sensor response to repeated 100 ppm NH_3 exposure at room temperature is shown in Figure 4.7. After the sensor reached equilibrium, the ambient inside the test chamber was cycled between 100 ppm NH_3 and pure N_2 for periods of 10 minutes each. The recorded resistance change was plotted in Figure 4.7. The data shows that the change of resistance followed the gas delivery pattern promptly. The sensor response is reversible and the sensor recovery in the flow of N_2 is incomplete. Similar to the NO_2 detection, there exists an irreversible drift in the sensor resistance which can be attributed to the built-up of NH_3 molecules on the surface of SWNTs.

Figure 4.8 shows the response of SWNT sensors to various concentrations of NH_3 at room temperature. The data was based on the experiment results of four sensors for 10 minutes NH_3 exposure. The NH_3 concentration varied from 10 ppm to 100 ppm. Shown in the plot is the average sensitivity of all four sensors (with one standard deviation) as a function of NH_3 concentration. The sensor sensitivity increased with an increase in the concentration of NH_3 and the lower detection limit is 10 ppm. At lower concentrations (less that 50 ppm) the sensitivity slowly follows the increase of gas concentration whereas a rapid resistance increase is observed above 80 ppm.

Given the possible p-type semiconducting nature of the SWNTs and the fact that NH_3 is a reducing agent (electron donor), sensor resistance increases in the presence of NH_3 as expected. The NH_3 sensing mechanism is similar to the case of NO_2 except that electron charges transfer from NH_3 molecules to SWNTs. The charge transfer caused a decrease

of the majority carrier (holes) concentration inside SWNTs and therefore an increase in resistance. The increase of SWNT resistance in the presence of NH_3 gas observed in this dissertation is consistent with the reports by other researchers [55][62][88][89]. The fact that its resistance increases in the presence of reducing agent NH_3 (electron donor) and decreases in the presence of oxidizing agent NO_2 (electron acceptor) serves as solid evidence of p-type semiconductor. The demonstrated capability to alter its electrical resistance in the presence of target gases at room temperature make the SWNT employed in this work a promising gas sensing material.

4.3.3 Effect of UV illumination on sensor recovery

The resistive gas sensors based on SWNTs have been proved to be sensitive to low concentration NO_2 and NH_3 exposure as described in section 4.3.1 and 4.3.2. However, the inability of SWNTs sensor to fully recover in time from gas detection has to be addressed before further investigation towards practical gas sensing application. As stated previously, the incomplete sensor recovery is the evidence of partial gas molecules desorption from the active sensing materials SWNTs. Degassing by the flux of pure N_2 does not entirely remove the adsorbed gas molecules from the SWNT sites; therefore the residual molecules caused the sensor resistance drift as shown in Figure 4.4 and Figure 4.7.

To improve the sensor recovery, extra energy source must be supplied to the chemisorbed gas molecules for them to overcome desorption energy barrier from SWNTs. Both photo-energy [58] and thermal-energy [88] are investigated to improve gas desorption and the effects of both treatments on SWNTs gas sensors are discussed in this dissertation.

A Blak-Ray B-100AP ultraviolet (UV) lamp with a 365 nm wavelength was chosen as the photo-energy source to enhance the sensor recovery. The SWNT sensor was once again subjected to 10 ppm NO_2 exposure for 30 minutes at room temperature after reaching equilibrium in the flow of N_2. The UV illumination is applied immediately following the removal of NO_2 therefore the sensor is allowed to recover under UV

illumination in addition to the flow of carrier gas N_2. The additional photo-energy is expected to break chemical bonds, therefore to cause more adsorbed NO_2 molecules to gain enough energy degassing from SWNT sites and to enhance the sensor ability to recovery. Figure 4.9 demonstrates that the UV illumination drastically improved the sensor recovery as expected. One can see from Figure 4.9 that the addition of UV illumination results a ninefold improve in sensor recovery during a period of 20 minutes. The improved sensor recovery is the result of more adsorbed oxidizing agent molecules desorption from SWNT sites by gaining extra photo-energy.

The data shown in Figure 4.10 is the evidence that UV illumination improves sensor performance during multiple-cycled NO_2 exposure. Similarly, the UV illumination was only applied during sensor recovery cycles, in addition to the flow of N_2. It is clearly that the sensor recovery was enhanced by the photo-induced gas molecule desorptions from SWNT sites as evidenced by a great amount of reduction in undesired resistance drift and an average of 2.59 times improvement of recovery. One can see from Figure 4.10 that the sensor response was also improved by the addition of UV illumination. The average relative sensitivity to 10 ppm NO_2 exposure is increase by approximately 3 times by the introduction of UV illumination during sensor recovery. The enhanced sensor response can be attributed to the "cleaning effect" of UV illumination during the each preceding recovery cycles. More specifically, the photo-induced molecule desorptions during recovery create additional SWNT sites available for NO_2 molecule adsorption for each following detection cycles, and as a result, an improved overall sensor performance.

An important factor needs to be considered is the oxygen molecules adsorbed by the SWNTs whenever the sensor is exposed to air. It has been reported that under ambient conditions, oxygen molecules adsorb by SWNTs with a binding energy of approximately 0.25 eV [56][97]. The adsorbed oxygen molecules oxidize SWNTs by withdrawing one tenth of an electron per molecule [97]. These oxygen molecules can not be completely removed from SWNT sites at the beginning of the experiment simply by N_2 flushing; therefore some of the SWNT adsorption sites are occupied by the oxygen molecules. As UV illumination was introduced at the sensor recovery stage, both NO_2 and oxygen

molecules gained the additional photo-energy to overcome the desorption energy barrier. As an oxidizing agent, the desorbing oxygen reduced the conducting hole carrier concentration of the p-type semiconducting SWNTs and caused an increase in the resistance of the sensor. Eventually, oxygen molecule desorption enhanced the effect of NO_2 gas molecules desorption and we believe the improved sensor recovery shown in Figure 4.9 and Figure 4.10 are the contributions of photo-induced molecular desorptions of both NO_2 and O_2.

In an effort to minimize the effect of adsorbed oxygen on sensor response, a UV pre-depletion procedure was applied at the beginning of the experiment. The sensor was exposed to UV illumination in N_2 ambient for at least 30 minutes until an equilibrium condition was achieved, followed by 30 minutes NO_2 exposure, and finally UV illumination as well as the N_2 flush for recovery. The result is shown in Figure 4.11 (green curve) and the previous data from Figure 4.9 is re-plotted for comparison. As can be seen from Figure 4.11, the UV pre-depletion induced oxygen desorption caused a 35% increase in sensor sensitivity, which indicates that more adsorption sites in SWNTs are available for NO_2 molecules due to the "cleaning effect" of UV at the beginning of the experiment. Similarly, the addition of UV illumination enhanced the sensor recovery and one can see from Figure 4.11 that the recovery has been improved by 5 times at the duration of 20 minutes.

Figure 4.12 shows the effect of UV illumination on sensor recovery from NH_3 detection. The result shows that the SWNT sensor slowly recovers from 30 minutes of 100 ppm NH_3 exposure in the flow of pure N_2. However, sensor resistance started to increase rather than decrease as soon as the UV lamp was turned on. The unexpected resistance increase is again attributed to absorbed oxygen molecules desorption from SWNT sites under the influence of UV illumination. The hole carrier concentration of semiconducting SWNTs was reduced by the photo-desorption of oxygen in competition with the increased hole concentration resulting from the desorption of reducing agent NH_3 molecules. The unexpected resistance increase shown in Figure 4.12 indicates that the effect of oxygen desorption dominates that of NH_3 desorption, and as a net result UV

illumination has no positive impact on sensor recovery in the case of NH_3 detection. Techniques other than UV illumination must be explored to enhance the sensor recovery from NH_3 detection in consideration for future practical applications.

4.3.4 Effect of heating on sensor performance

Thermal energy is another viable energy source to enhance the gas molecule desorptions from SWNT adsorption sites. The SWNT sensors are heated in the presence of NO_2 and NH_3 gases and the sensor performance was monitored. Since this dissertation is focused on the room temperature gas sensitivity of CNT materials, therefore the heating is limited to moderate temperature, i.e. 100ºC. To heat the sensor, a heater tape was wrapped around the test chamber and a power supply was applied for the temperature control. A thermocouple was connected into the test chamber to monitor the temperature of the sensor under test. Constant temperature at 100ºC was maintained throughout the entire experiment procedure so its effects on sensor recovery as well as response were investigated.

Figure 4.13 shows the effect of heating on sensor response and recovery in the presence of 10 ppm NO_2. One can see that after 30 minutes of NO_2 exposure, the sensitivity was increased from ~ 12% to ~ 20% by heating the sensor, i.e. 66.7% increase in sensitivity. The sensor recovery at 100ºC was improved by 3.5 times within 30 minutes compared to the same sensor recovered at room temperature. The data shown in Figure 4.13 are based on one of the SWNT sensors and similar results were found for all the other sensors. It is obvious that the elevated temperature enhances the sensor response as well as recovery during NO_2 detection. The effect of heating on sensor performance upon repeated NO_2 exposure is shown in Figure 4.14. The temperature of the sensor was maintained at 100ºC constantly while the sensor was subjected to multiple-cycled 10 ppm NO_2 exposure along with pure N_2 for recovery. One can see from Figure 4.14 that the heating has improved the sensor response by an average factor of 1.9 and the recovery by an average factor of 3.4 for all the individual cycles. As the results, the sensor demonstrated an increased sensitivity and a reduced cumulative drift effect, which are important for long term sensor performance.

The improved sensor response can be attributed to the additional adsorption sites on SWNTs created by heating the sensor. The addition of thermal energy induces more gas molecules to overcome the energy barrier and desorb from SWNT sites at the beginning of the experiment. Consequently, more adsorption sites on SWNTs are created and available for the following NO_2 detection cycle. The sensitivity of the sensor is increased accordingly. Next, the elevated temperature again caused more oxidizing gas molecules to desorb from SWNT site under the flow of N_2. As a result, the sensor resistance increases further toward its original value, thus an enhanced recovery. The sensor response to various concentrations of NO_2 at 100ºC is shown in Figure 4.15. One can see that in comparison to the response at room temperature, heating caused a less linear correspondence between the sensitivity and the NO_2 concentration beyond 20 ppm.

Figure 4.16, Figure 4.17 and Figure 4.18 show the effects of heating on NH_3 detection and recovery. One can see from Figure 4.16 and Figure 4.17 that the sensitivity to 100 ppm NH_3 has been significantly increased by heating the sensor to 100ºC. Based on the data in Figure 4.17, the sensor response and recovery has been increased by an average factor of 2.57 and 2.96, respectively, compared to the room temperature detection. This reveals that more SWNT adsorption sites were created for adsorbing NH_3 molecules by heating the sensor. At the same time, the sensor recovery has also been improved; however the problem of sensor resistance drift still exists. It seems that the enhancement of heating on sensor recovery from NH_3 detection is not as effective as NO_2 detection. This is believed due to the adsorption of oxygen molecules in the room ambient between vacuum baking and loading into the test chamber. As described in section 4.3.3, SWNTs are oxidized immediately as soon as they exposed to air. During the experiment, these oxygen molecules can not be completely released from adsorption sites by the flow of N_2 at room temperature. With the help of thermal energy, more oxygen molecules desorbed from SWNTs during sensor recovery stage along with NH_3 molecules. However, the contribution of NH_3 (reducing agent) desorption to the sensor will be neutralized by the contribution of oxygen (oxidizing agent) desorption. Accordingly, the improvement of heating on sensor recovery from NH_3 detection is not effective as NO_2 detection. Figure

4.18 shows the effect of heating on sensor response to various concentrations of NH_3. The NH_3 concentration varied from 10 ppm to 100 ppm. It indicates that heating caused the NH_3 sensitivity to increase more uniformly at various concentrations than the NO_2 dependence in Figure 4.15.

4.3.5 Sensor performance in air

In order to explore the possibility of device prototyping for practical applications, the characteristics of SWNT sensor in ambient condition were investigated by replacing the carrier gas N_2 with compressed air. Ultra low concentration of NO_2 and NH_3 detection was conducted at room temperature. The effects of UV illumination and heating on sensor recovery in air, instead of N_2 were studied. Furthermore, the temperature and humidity dependency of the SWNT sensors were monitored and discussed.

Figure 4.19 shows the sensor response to 10 ppm NO_2 at room temperature in air instead of N_2. One can see that the resistance decreases in the presence of NO_2 and partially recovered in the flow of air. The variation of the sensor resistance promptly reflects the gas delivery pattern, i.e. alternating between 10 ppm NO_2 and air. The sensing characteristic under ambient condition shown in Figure 4.19 is in agreement with the sensor response with N_2 background, which was demonstrated in Figure 4.4. Similar result was found for NH_3 detection as well. Shown in Figure 4.20 is the measured resistance response when the SWNT sensor is exposed to 100 ppm NH_3 and compressed air alternately for periods of 10 minutes each at room temperature. The presence and removal of NH_3 gas caused the sensor resistance to increase and decrease correspondingly. Thus the NH_3 sensing characteristic in air is consistent with its response in N_2 background as discussed in section 4.3.2. The demonstrated gas sensing capability in ambient condition makes the development of SWNT sensor one step closer towards a "working device" for practical applications.

The gas detection results (Figure 4.19 and Figure 4.20) of SWNT sensors under ambient condition indicate that the sensor recovery is incomplete and the cumulative residual gas molecules caused undesired resistance drift on sensor response. In order to

improve the sensor performance, the cumulative effect needs to be minimized. Section 4.3.3 and 4.3.4 discussed the investigation of UV illumination and moderate heating as the potential solutions to enhance sensor recovery. The same procedures were applied to the SWNT sensors for the NO_2 and NH_3 detections under ambient condition. Figure 4.21 shows the effect of UV illumination on sensor recovery from 10 ppm NO_2 exposure in air. The UV illumination was applied during each recovery cycles in addition to the flow of air. One can see that upon exposure, the sensor resistance has been increased by an average of 2% from its initial value, which seems caused by the "cleaning effect" of the UV illumination during the first recovery cycle, i.e. 0 to 10 minutes in Figure 4.21. The addition of UV illumination created more vacancy of adsorption site on SWNTs available for NO_2 molecules hence increased sensor sensitivity. However, there is no evidence that the UV illumination drastically improves the sensor recovery under ambient condition, which is inconsistent with the experiment result based on N_2 background, as described by section 4.3.3 and shown in Figure 4.10. By replacing the carrier gas N_2 with compressed air, the SWNTs are undergoing oxidization and cleaning at the same time during each recovery cycles. Thus the extra cleaning effect caused by the addition of UV illumination most probably was offset by the adsorption of interfering gas molecules (for instance oxygen) on SWNTs, and as a result there is no net improvement in sensor recovery. Hence the enhancement of SWNT sensor recovery in air by the addition of UV illumination is not as effective as in N_2 background.

The NO_2 and NH_3 detection in air by the SWNT sensor was also conducted at the elevated temperature. The sensor was heated to and maintained at 100ºC throughout the experiments. The effects of heating on sensor response and recovery for 10 ppm NO_2 and 100 ppm NH_3 detection are depicted in Figure 4.22 and Figure 4.23 respectively. One can see that the heating has dramatically improved the response and recovery of the SWNT sensor under ambient condition. For 10 ppm NO_2 detection, heating caused an average increase by a factor of 2.6 for all the detection cycles, and an average increase by a factor of 6.7 for all the recovery cycles. Similarly for the 100 ppm NH_3 detection, there is an average 2.6 times increase in sensor response and fourfold improvement in recovery by heating the sensor at 100ºC. The heating-induced enhancement in sensor response and

recovery demonstrated in Figure 4.22 and Figure 4.23 indicated that a built-in heater is a necessary element to achieve better sensor performance in future device prototyping work.

The temperature and humidity dependency of the SWNT sensor was investigated under ambient condition. Within 60 minutes, sensors were subjected to the variation of either temperature (25ºC to 100ºC) or relative humidity (10% to 95%), and the changes in their baseline resistances were monitored. Based on the data obtained from all the SWNT sensors, we found that the baseline resistance has an average 5% variation due to the increase in temperature. The dependency of SWNT resistance on ambient temperature has been demonstrated by Nguyen and coworkers [89]. They observed a slightly decrease in electrical resistance as the temperature increased from room temperature to 100ºC. The decrease of the sensor resistance with an increase in temperature demonstrates semiconducting behavior of the SWNTs. However, we witness both decrease and increase in the sensor resistance for our sensors. This inconsistency in the variation of SWNTs resistance in response with the heat treatment needs further investigation in the future. On the other hand, the increase in relative humidity causes an average 0.8% change in sensor resistance. Hence the short term influence of humidity variation on the SWNT sensor is negligible.

4.4 Conclusion

A SWNTs based resistive gas sensor was fabricated and tested for the detection of NO_2 and NH_3 at room temperature. The lowest reported 1 wt% loading of SWNTs were mixed with organic binder to form active sensing material and then coated on the interdigitated sensor electrodes. After annealing, the sensors were subjected to low concentration of NO_2 and NH_3 exposure while the variation of sensor resistance was monitored as the evidence of response. The SWNT sensors demonstrated lower detection limit of 1 ppm for NO_2 and 10 ppm for NH_3. In order to demonstrate the gas sensing functionality of SWNTs, a control sensor was prepared by spin-coated α-terpineol on IDC sensor platform, i.e., without nanotubes. After annealing treatment, the electrical characteristic of the sensor appears to be an open circuit. The observation based on the

control sensor proved that for SWNTs resistive sensors, the functionality was the result of nanotubes bridging adjacent interdigitated electrodes. Therefore SWNTs are indeed the active gas sensing material.

The decrease of resistance in the presence of oxidizing agent NO_2 and the increase of resistance in the presence of reducing agent NH_3 describe a p-type semiconducting behavior of the SWNTs employed in this work. However, the sensor recovery at room temperature is incomplete, therefore causes undesirable resistance drift for the repeated gas detection. The mechanism of sensing and recovery are discussed. UV illumination and moderate heating are examined as potential solutions to improve sensor recovery performance. The effects of UV and heating on sensor performance are described and explained. The influence of oxidized SWNTs on the sensor performance is also presented and discussed.

In preparation of future work of device prototyping, the performance of the SWNT sensor under ambient condition was investigated. Carrier gas N_2 was replaced by compressed air during the gas detection experiments. The NO_2 and NH_3 detection of the SWNTs sensor in the air produced similar sensing characteristic as that in N_2. Once again, The UV and heating are applied to improve sensor performance and the mechanisms are discussed. Furthermore, the temperature and humidity dependency of the sensor was investigated.

In summary, the resistive gas sensor based on SWNTs demonstrated great potential for detecting NO_2 and NH_3 at room or moderate temperatures. The advantages of the design include simple structure, very low nanotube loading, easy to measure and monitor, demonstrated functionality in air, and low humidity dependency. On the other hand, the issue with the sensor recovery needs to be continuously addressed to improve the long term sensor performance. The undesired resistance drift must be minimized in order for the sensor to function properly during the multiple-cycled gas detection applications.

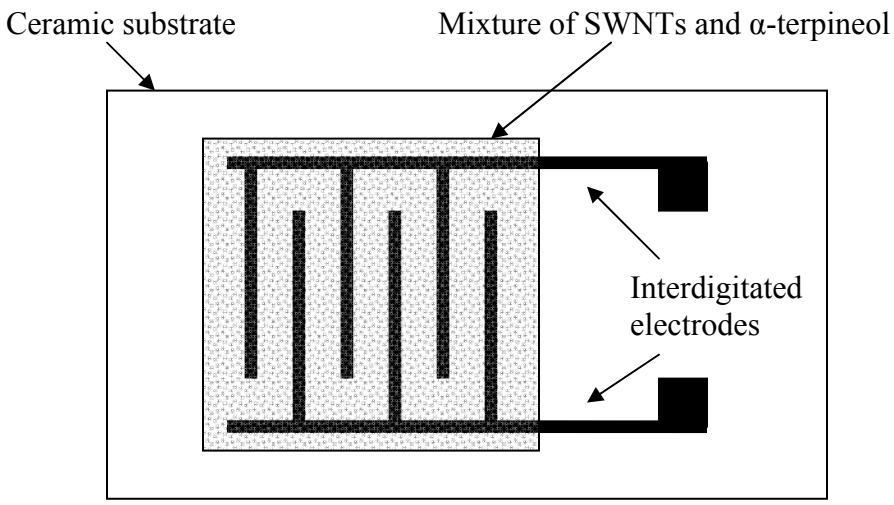

Figure 4.1: Schematic description of SWNTs based resistive gas sensor (top view).

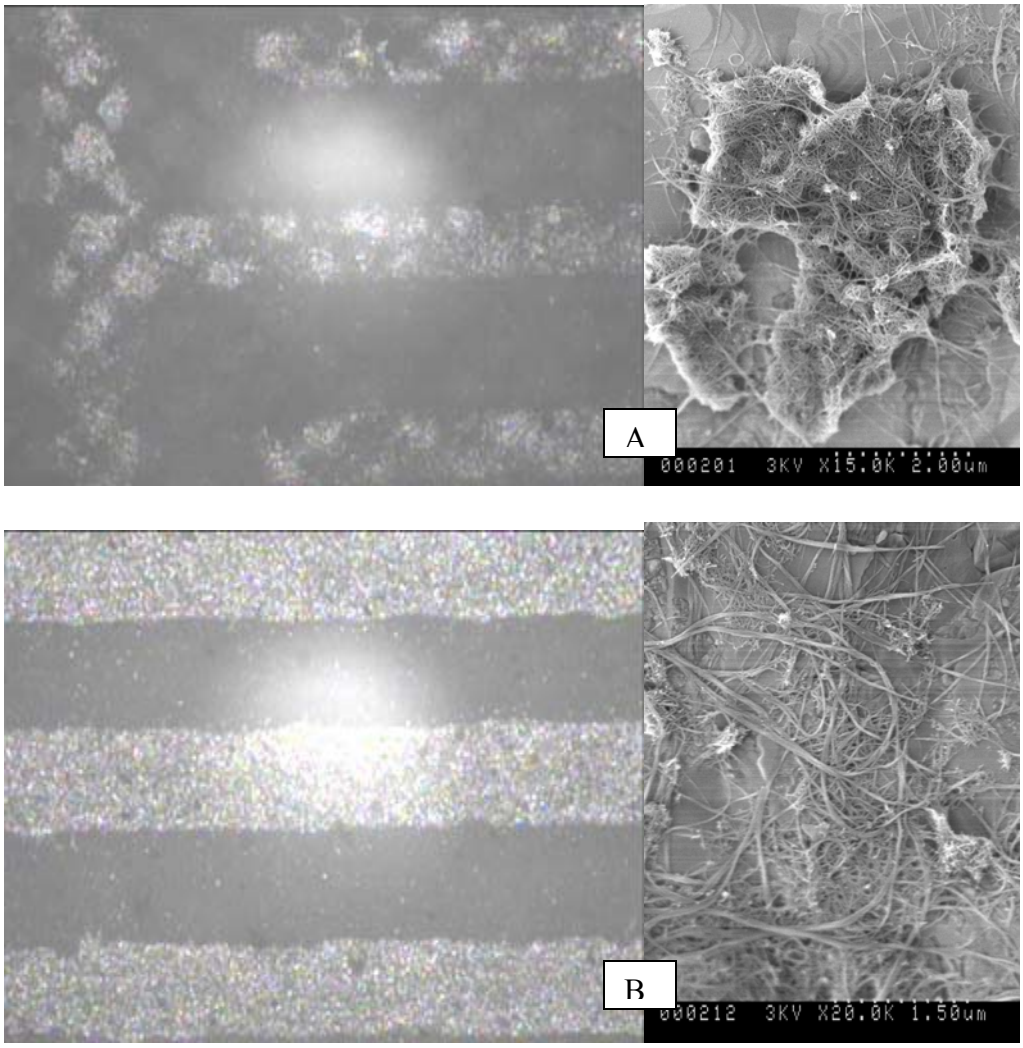

Figure 4.2: Microscopic views and SEM images indicated that uniformly distributed SWNTs network was achieved by spin-coating (B) instead of screen-printing (A).

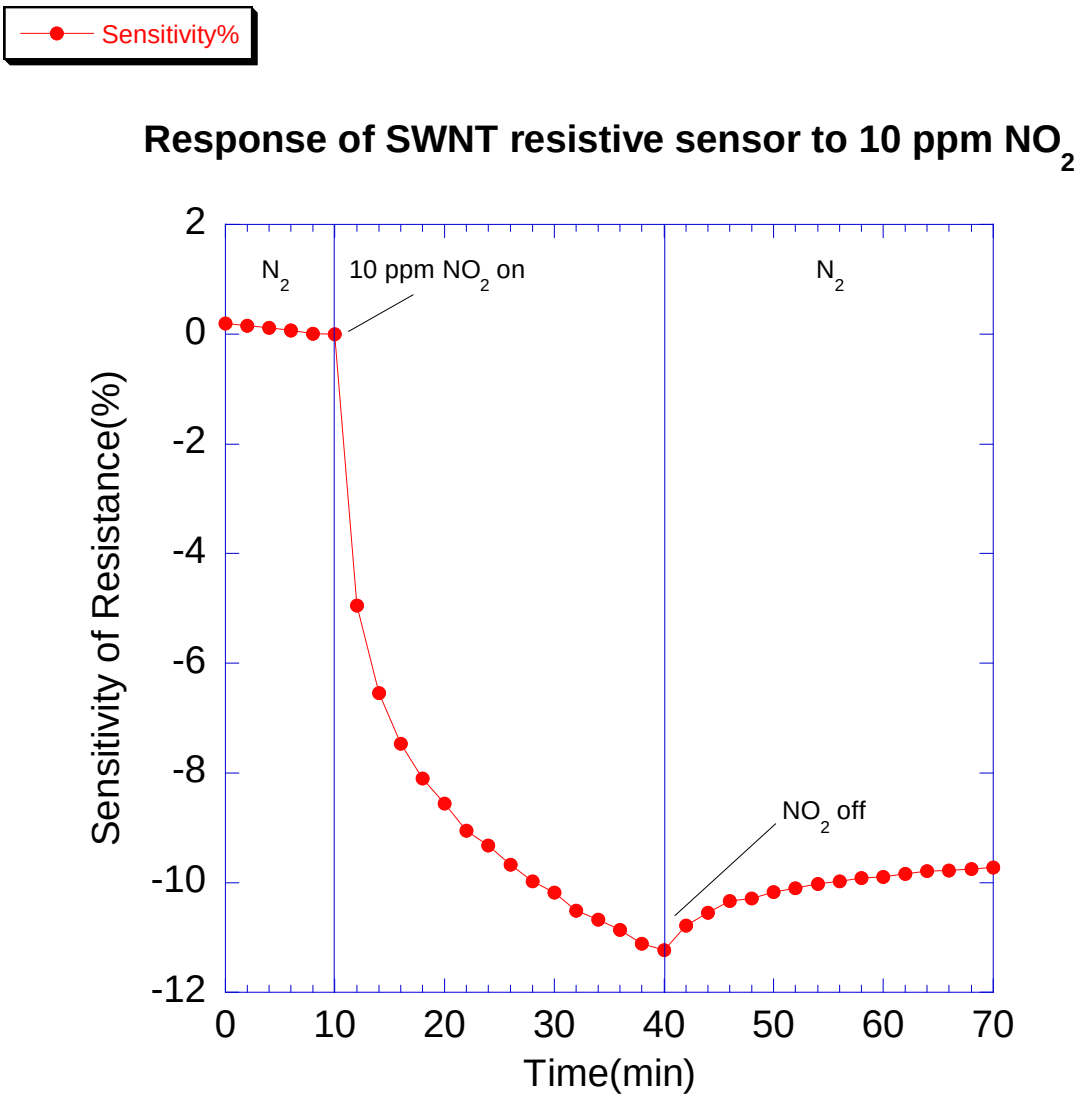

Figure 4.3: Measured resistance response as SWNT gas sensor is exposed to 10 ppm NO_2 (in the flow of N_2) for 30 minutes at room temperature.

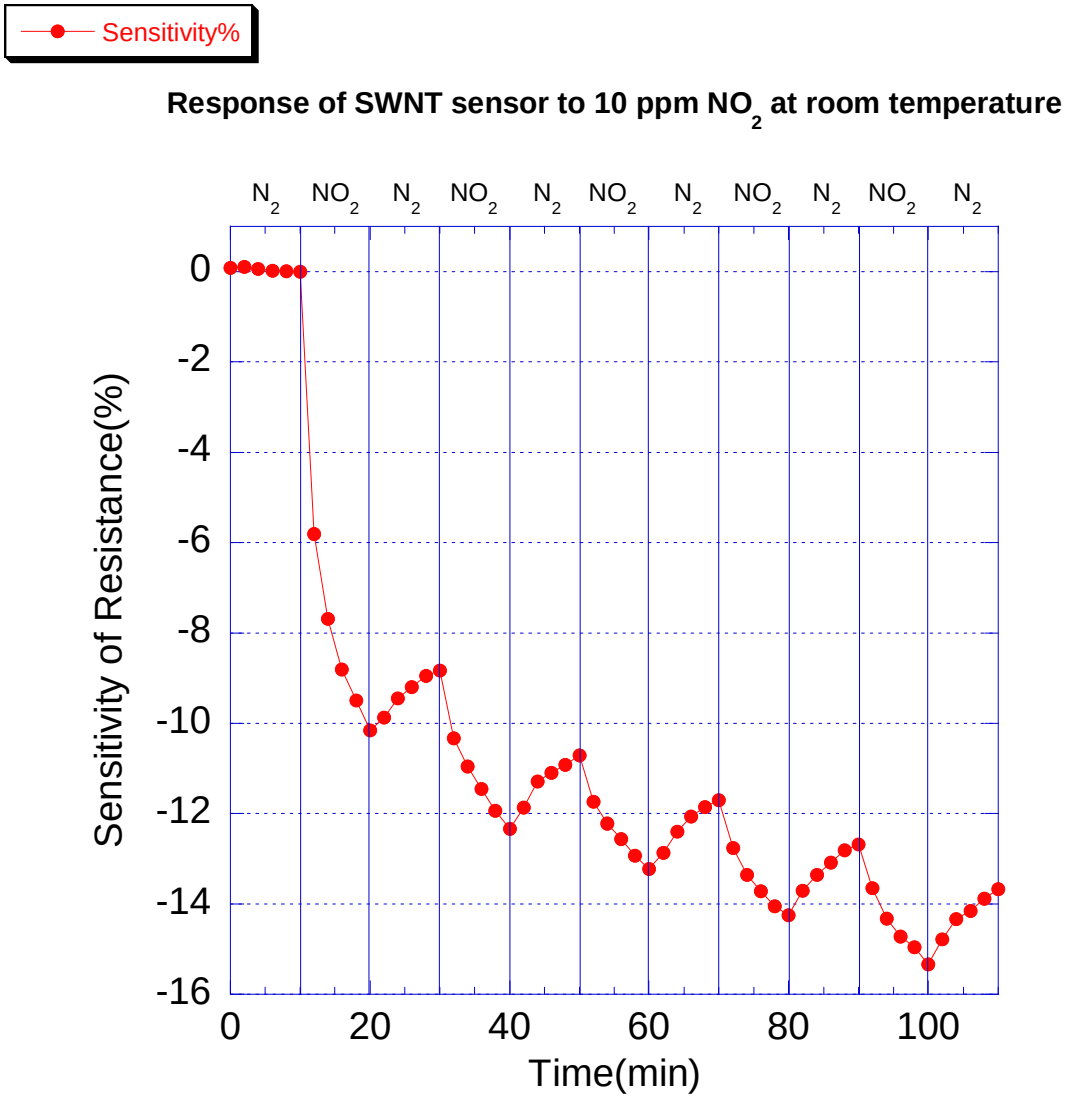

Figure 4.4: Measured resistance response as SWNT gas sensor is exposed to 10 ppm NO_2 and pure N_2 alternately for periods of 10 minutes each at room temperature. The sensor shows reversible response and incomplete recovery.

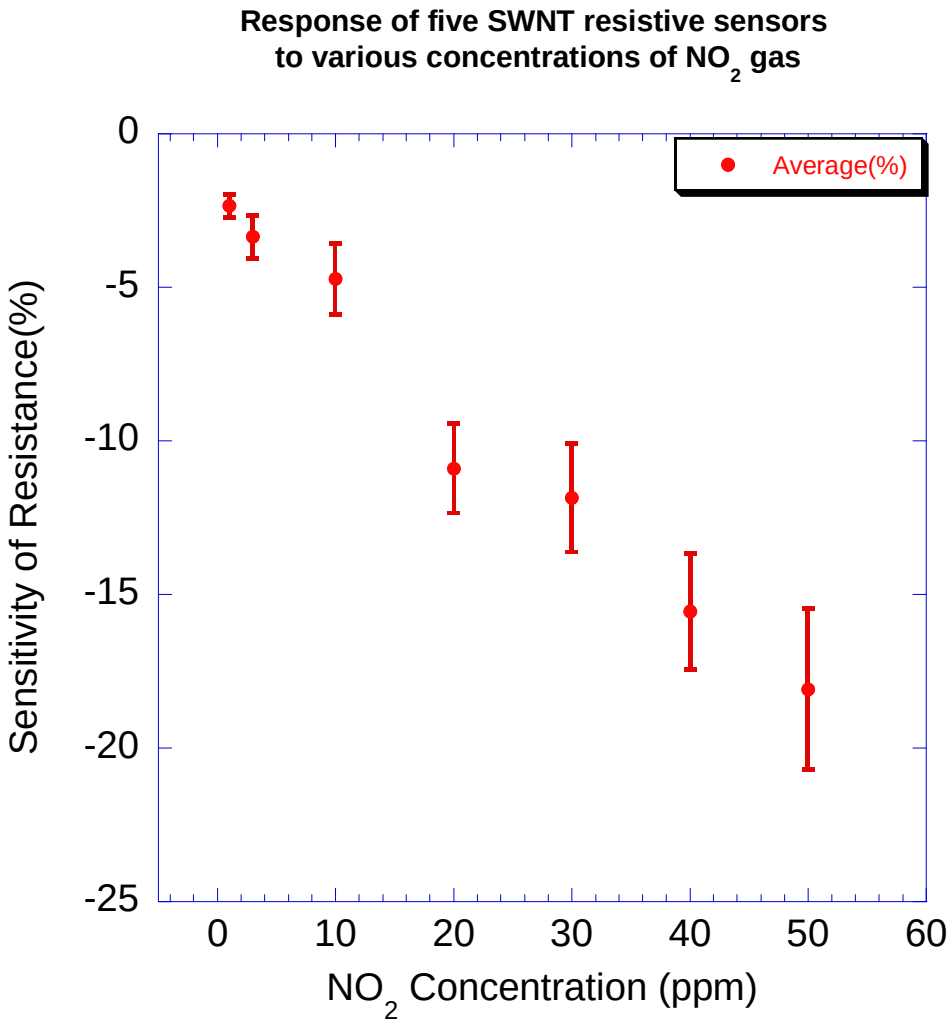

Figure 4.5: Measured response of SWNT gas sensors to various concentrations of NO_2 at room temperature. The data was based on the experiment results of 5 sensors for 10 minutes NO_2 exposure. The NO_2 concentration varied from 1 ppm to 50 ppm. Shown in the plot are the average sensitivity of all 5 samples and 1 standard deviation.

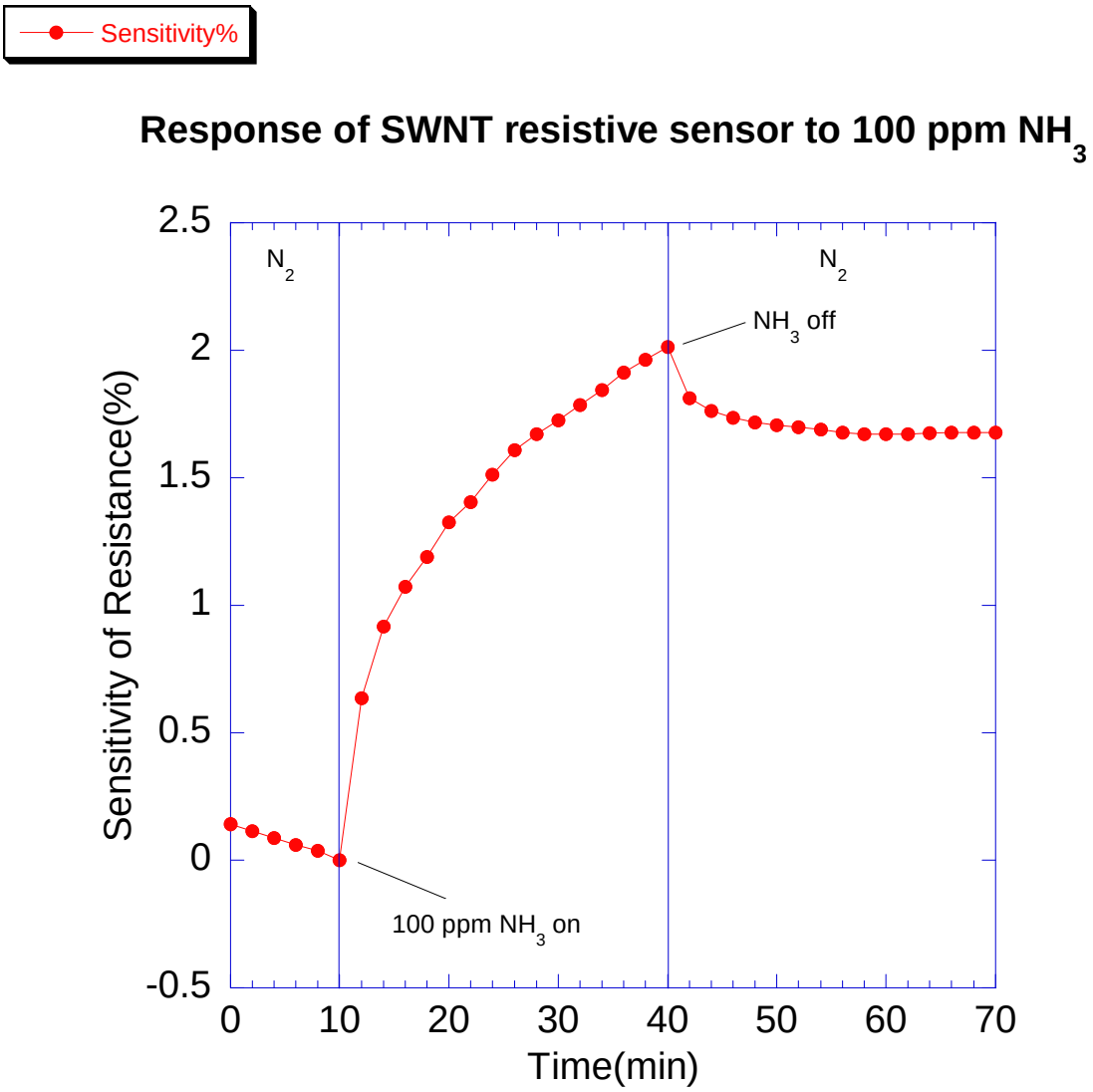

Figure 4.6: Measured resistance response as SWNT gas sensor is exposed to 100 ppm NH_3 (in the flow of N_2) for 30 minutes at room temperature.

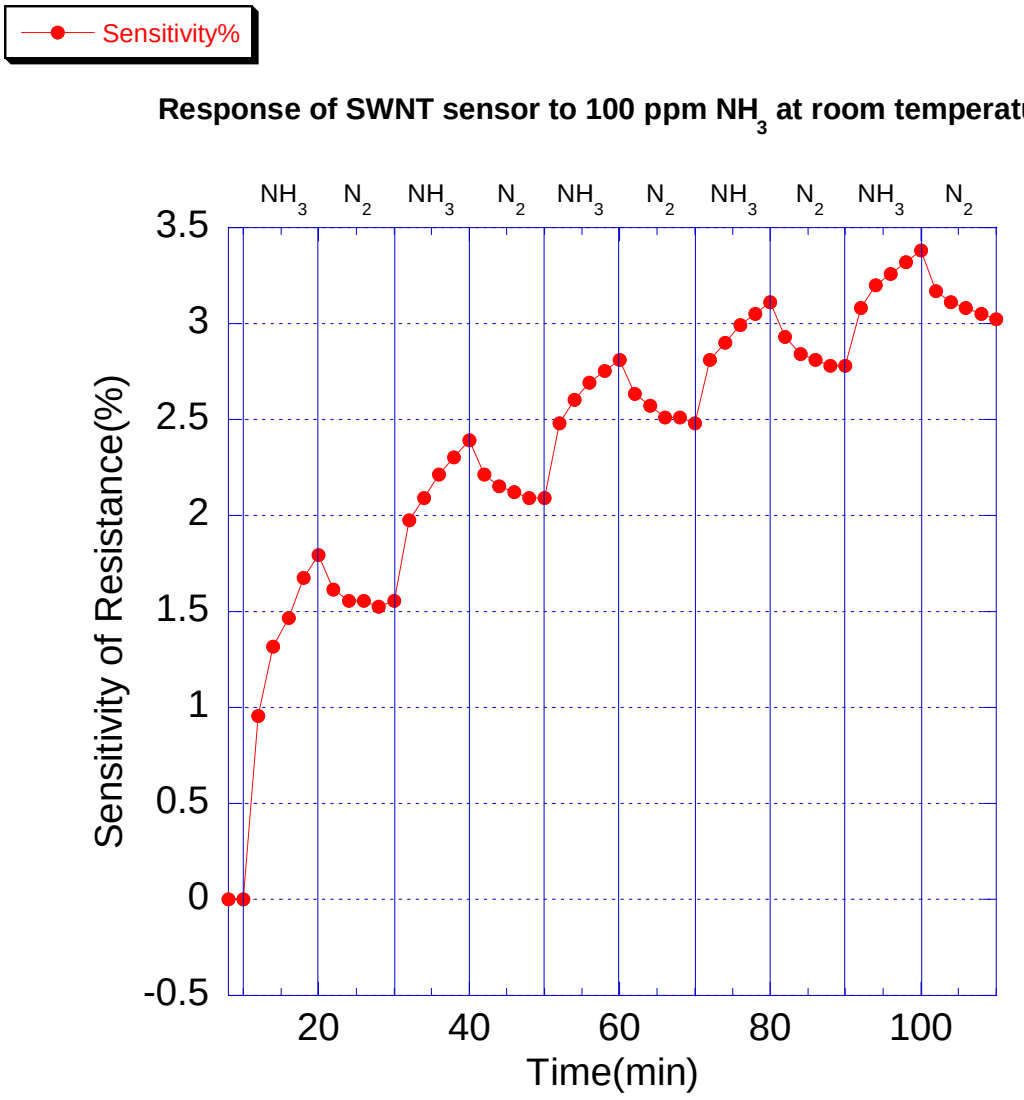

Figure 4.7: Measured resistance response as SWNT gas sensor is exposed to 100 ppm NH_3 and pure N_2 alternately for periods of 10 minutes each at room temperature. The sensor shows reversible response and incomplete recovery.

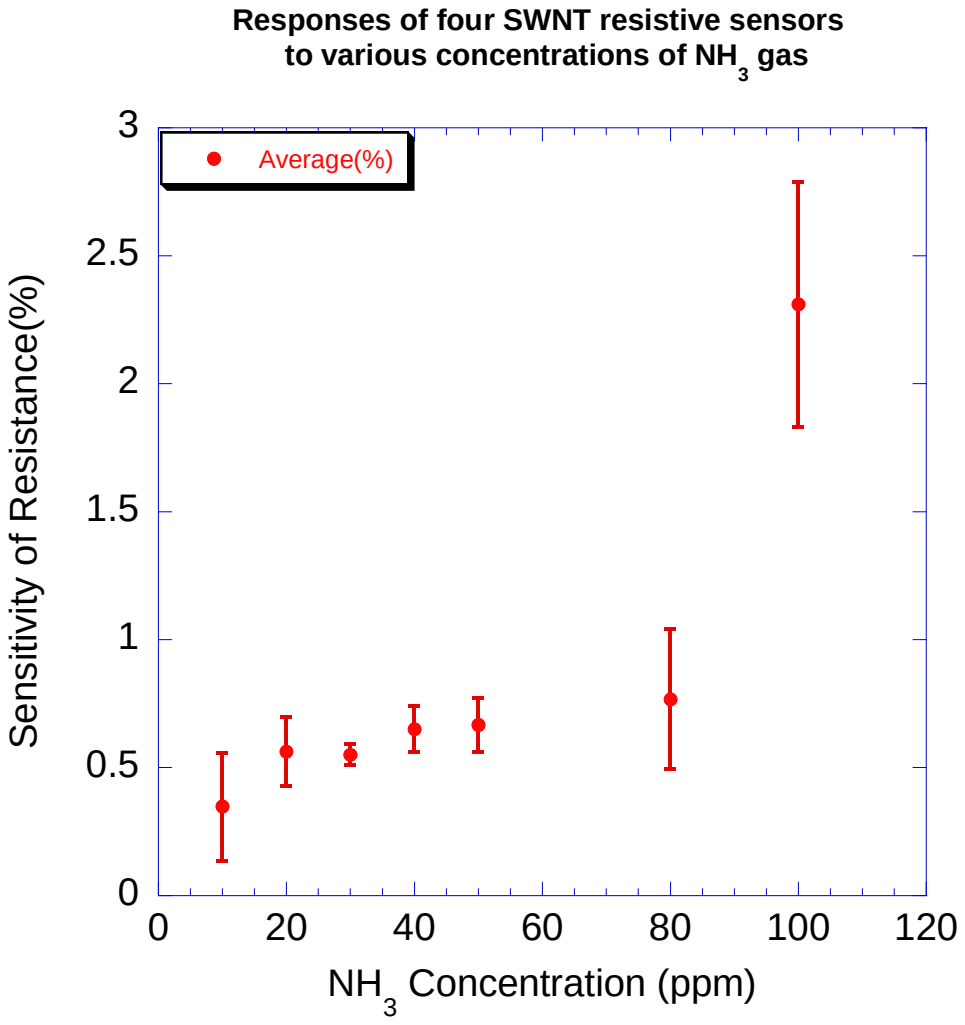

Figure 4.8: Measured response of SWNT gas sensors to various concentrations of NH_3 at room temperature. The data was based on the experiment results of 4 sensors for 10 minutes NH_3 exposure. The NH_3 concentration varied from 10 ppm to 100 ppm. Shown in the plot are the average sensitivity of all 4 samples and 1 standard deviation.

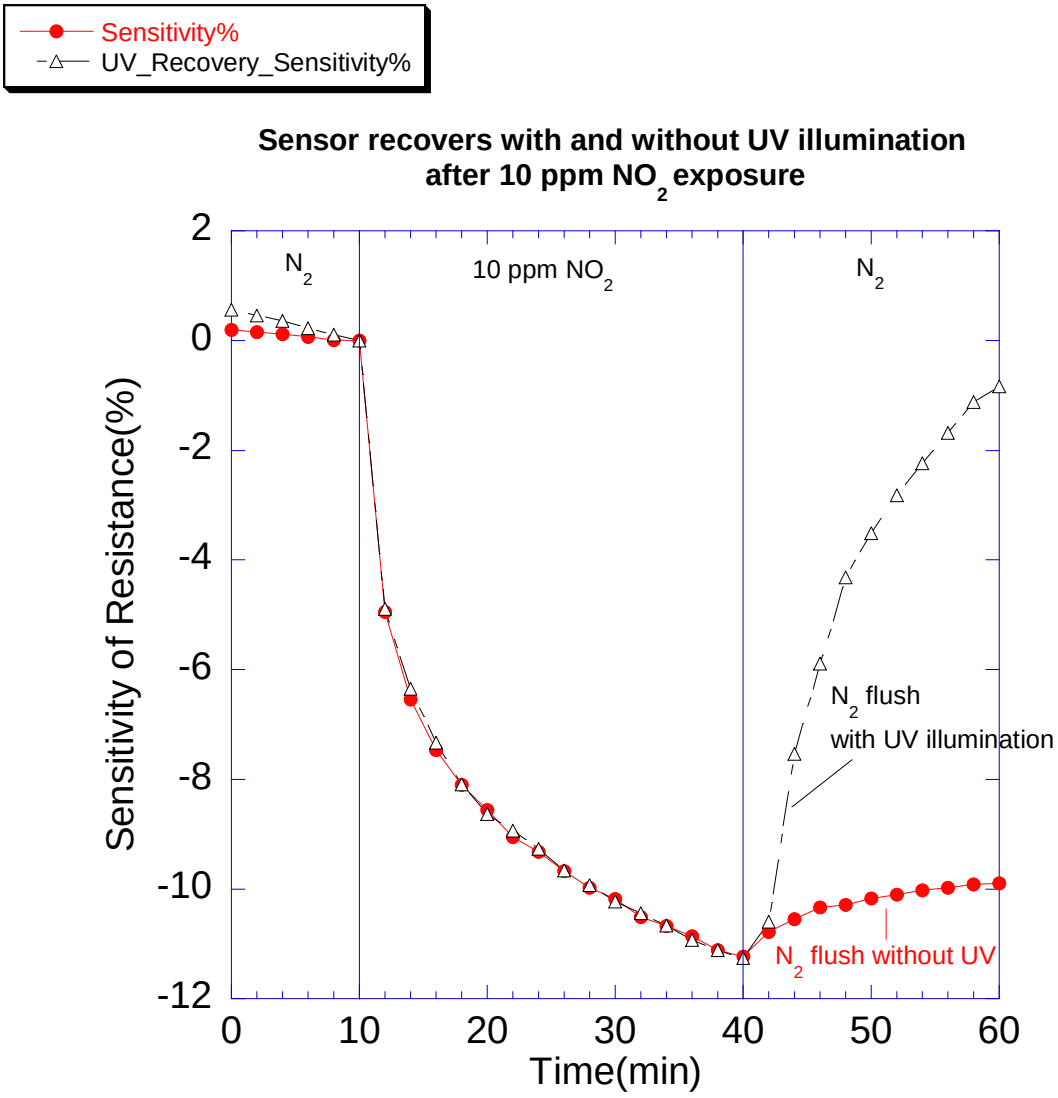

Figure 4.9: The effect of UV illumination on SWNT gas sensor recovery from 10 ppm NO_2 exposure. The red curve represents the sensor recovery in the flow of N_2 only, i.e., without UV illumination. The black curve represents the sensor response with UV illumination applied in addition to N_2 purge during its recovery stage.

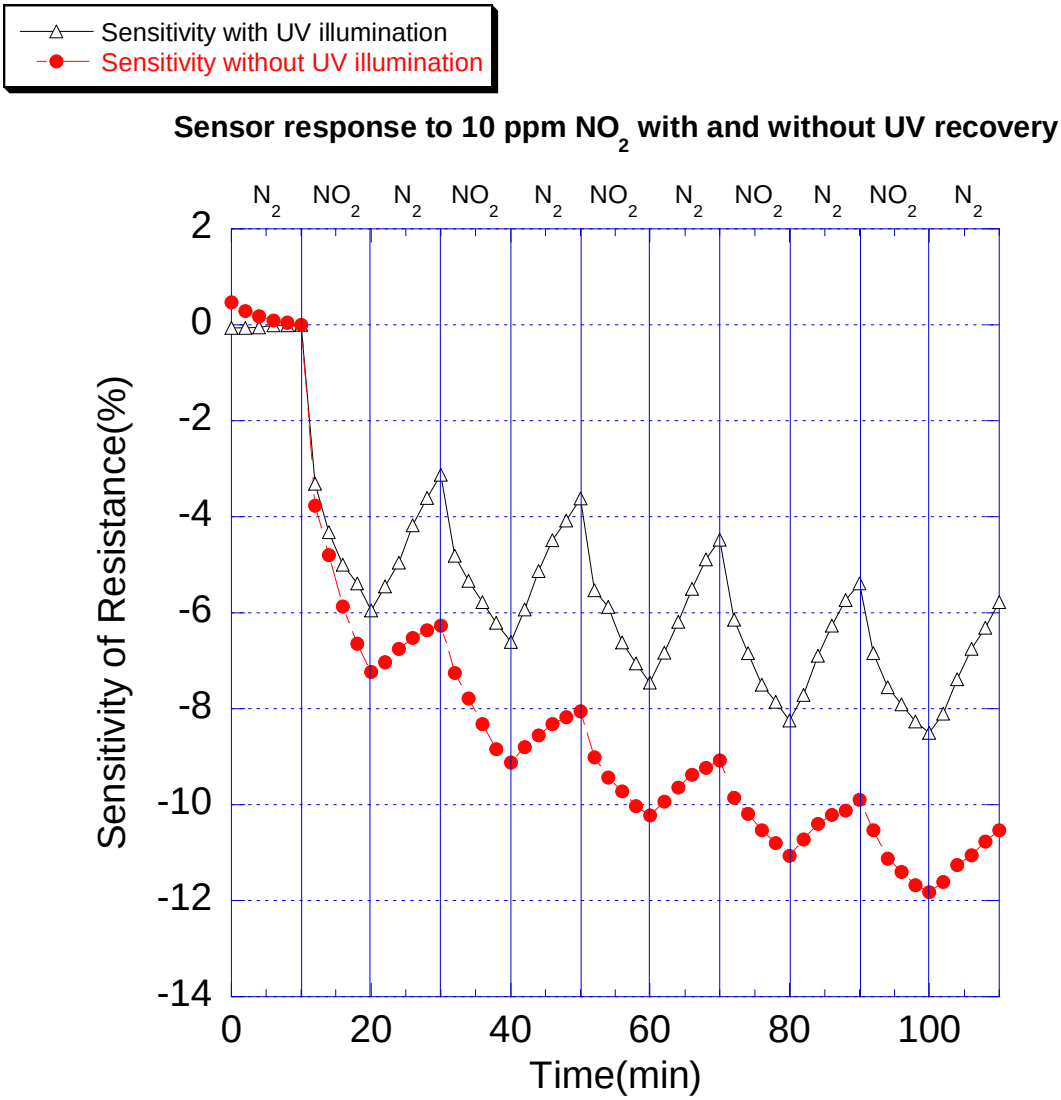

Figure 4.10: The effect of UV illumination on SWNT gas sensor recovery from 10 ppm NO_2 exposure. The red curve represents the sensor recovery in the flow of N_2 only. The black curve represents sensor recovery in the flow of N_2 with UV illumination.

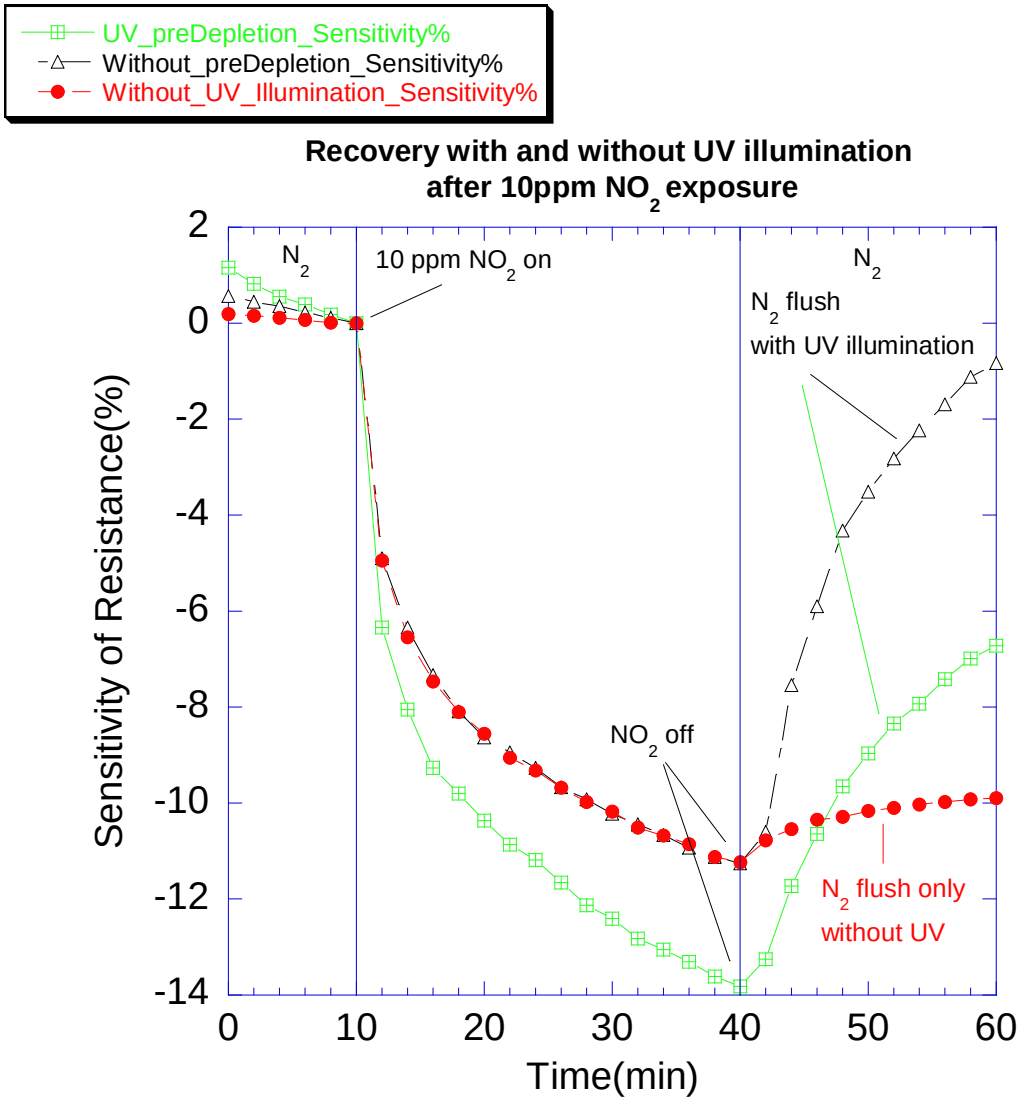

Figure 4.11: The effect of pre-experiment UV illumination on SWNT gas sensor response and recovery to NO_2 exposure. The red curve represents the sensor recovery in the flow of N_2 only. The black curve represents sensor recovery in the flow of N_2 with UV illumination. The green curve depicts the effect of pre-experiment oxygen desorption by UV illumination.

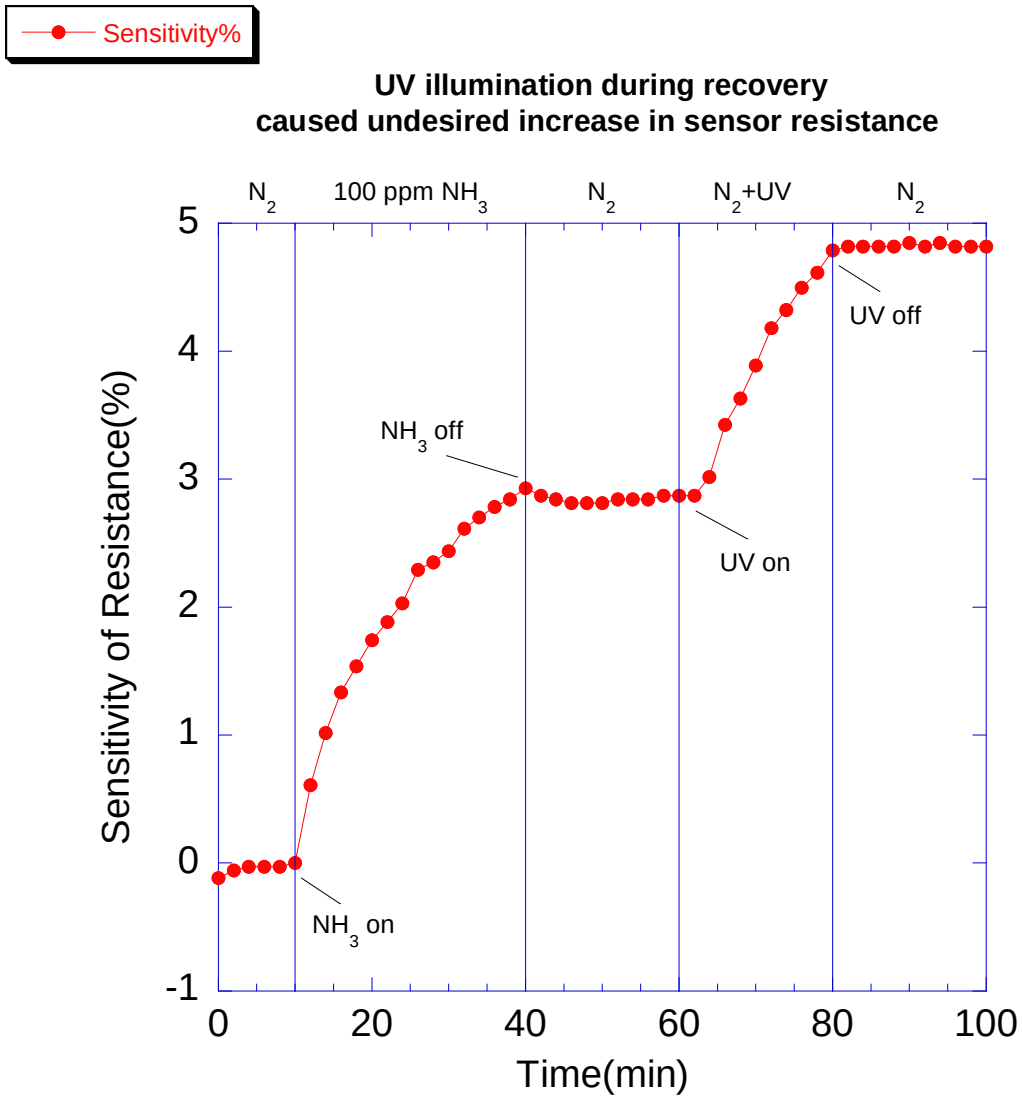

Figure 4.12: The effect of UV illumination on SWNT gas sensor recovery from 100 ppm NH_3 exposure.

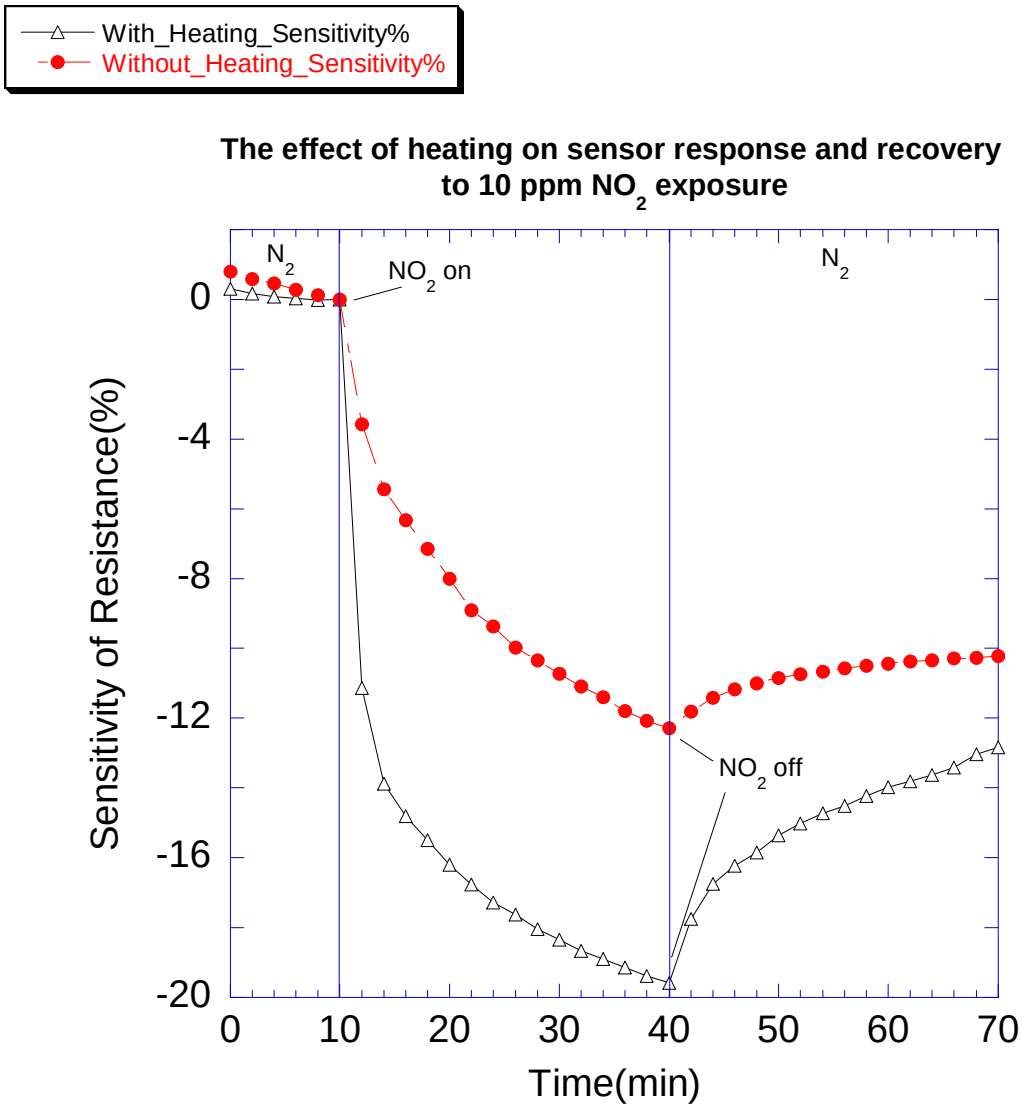

Figure 4.13: The effect of heating at 100ºC on SWNT gas sensor response and recovery in the presence of 10 ppm NO_2 for 30 minutes. The red curve represents the sensor response at room temperature. The black curve represents the sensor response at 100ºC.

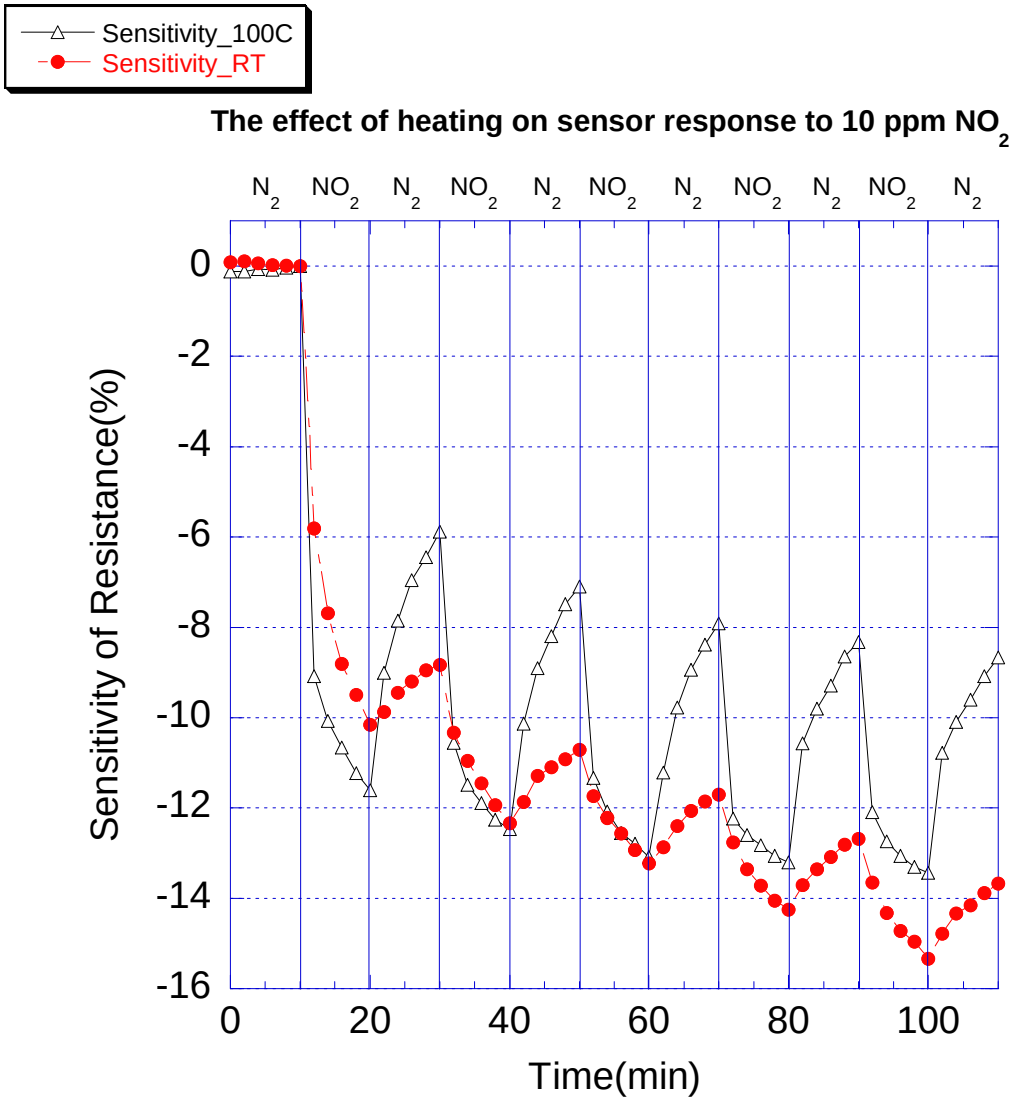

Figure 4.14: The effect of heating at 100ºC on SWNT gas sensor performance upon repeated 10 ppm NO_2 exposure. The red curve represents the sensor response at room temperature. The black curve represents the sensor response at 100ºC.

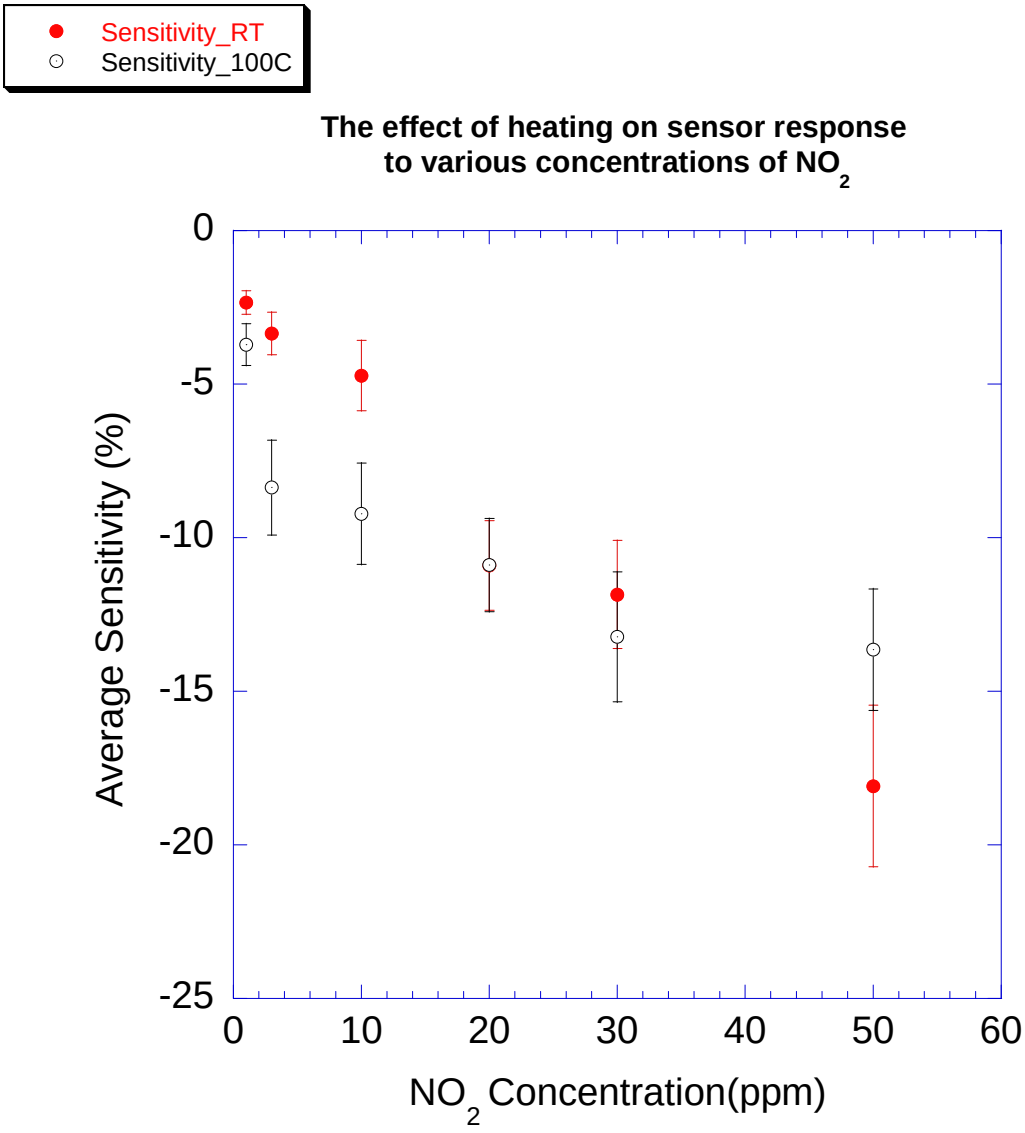

Figure 4.15: The effect of heating on SWNT gas sensor response to various concentrations of NO_2. The red data is the result at room temperature and the black one is the result at 100ºC. The NO_2 concentration varied from 1 ppm to 50 ppm. Shown in the plot is the average sensitivity of all 5 samples and 1 standard deviation.

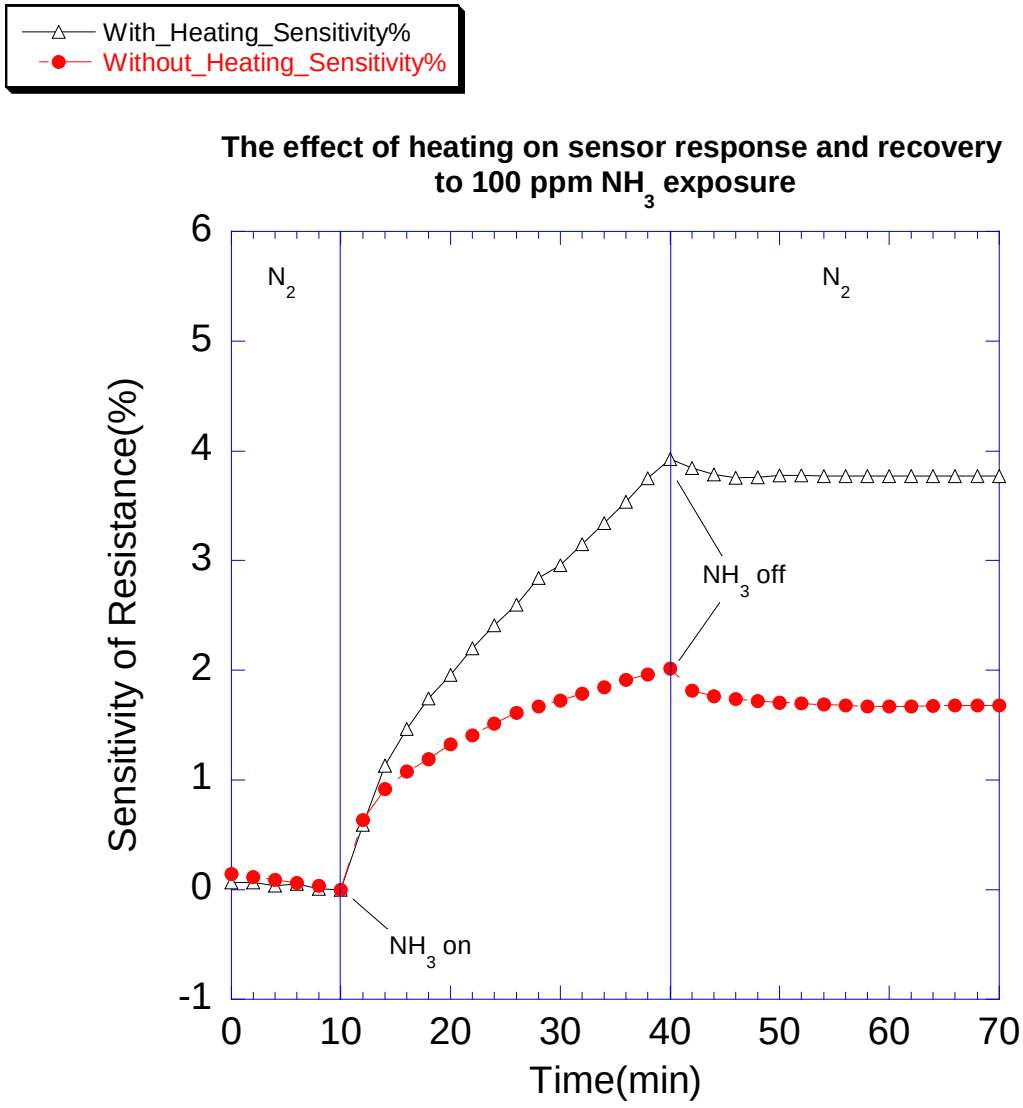

Figure 4.16: The effect of heating at 100ºC on SWNT gas sensor response and recovery in the presence of 100 ppm NH_3 for 30 minutes. The red curve represents the sensor response at room temperature. The black curve represents the sensor response at 100ºC.

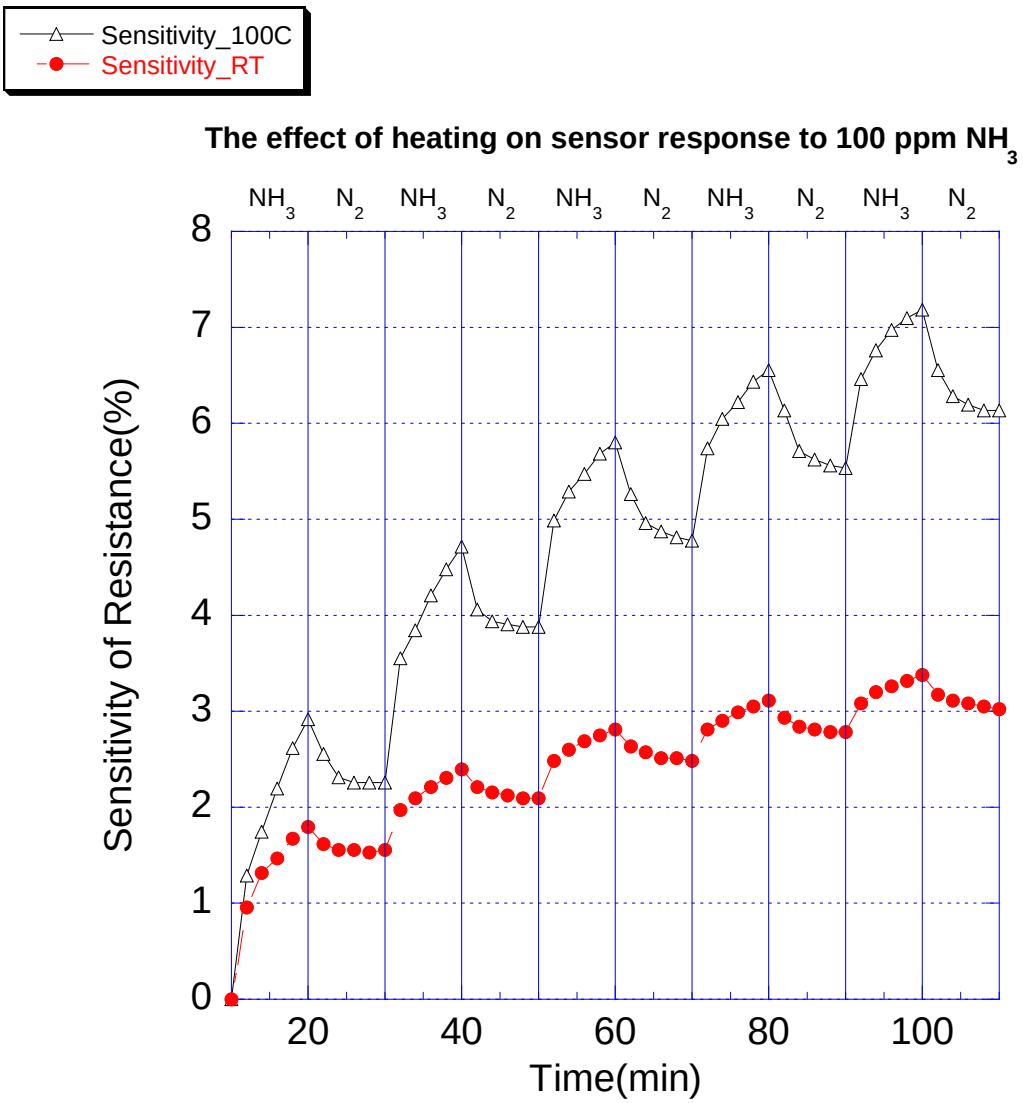

Figure 4.17: The effect of heating at 100ºC on SWNT gas sensor performance upon repeated 100 ppm NH_3 exposure. The red curve represents the sensor response at room temperature. The black curve represents the sensor response at 100ºC.

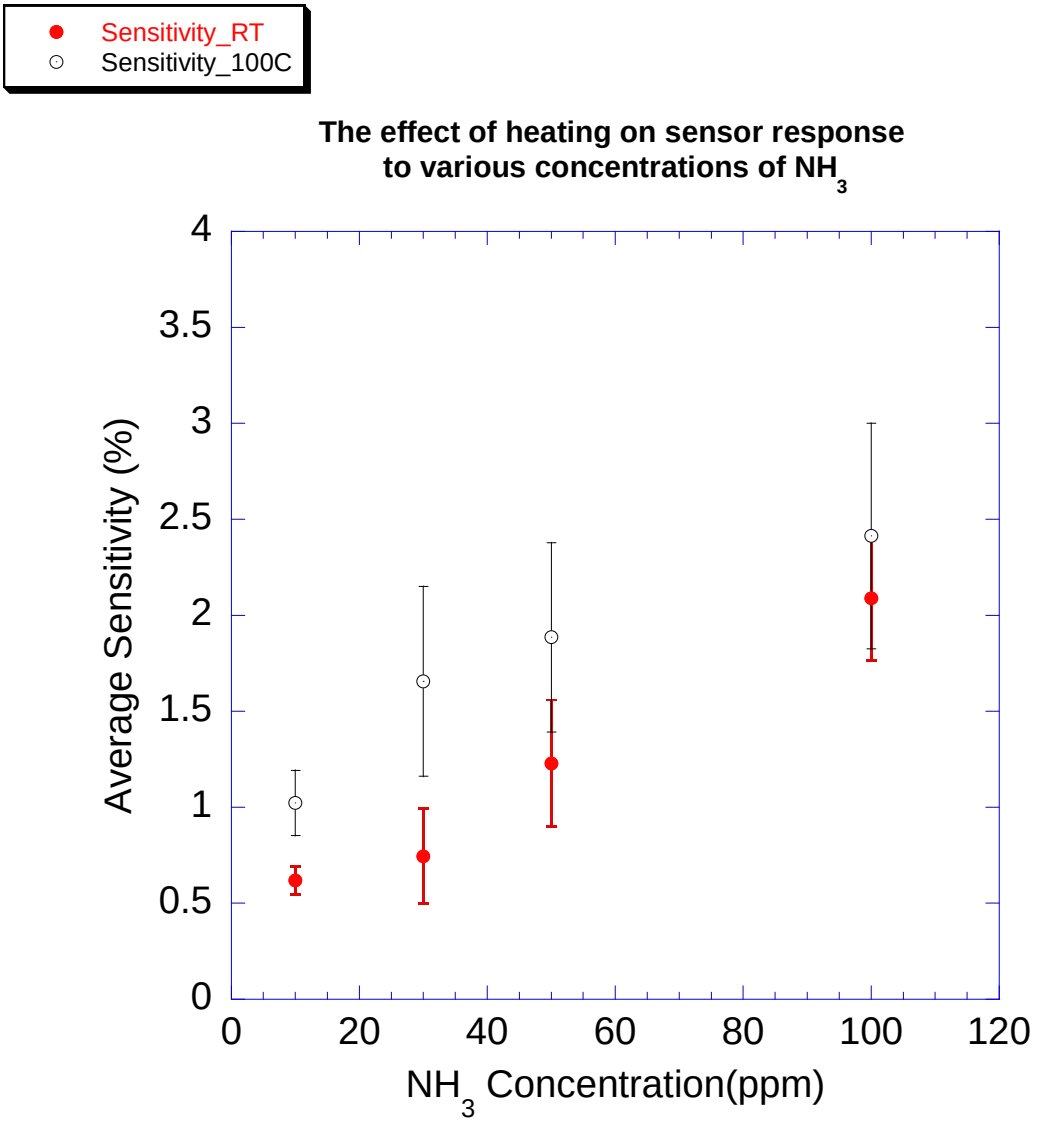

Figure 4.18: The effect of heating on SWNT gas sensor response to various concentrations of NH_3. The red data is the result at room temperature and the black one is the result at 100ºC. The NH_3 concentration varied from 10 ppm to 100 ppm. Shown in the plot is the average sensitivity of all 4 samples and 1 standard deviation.

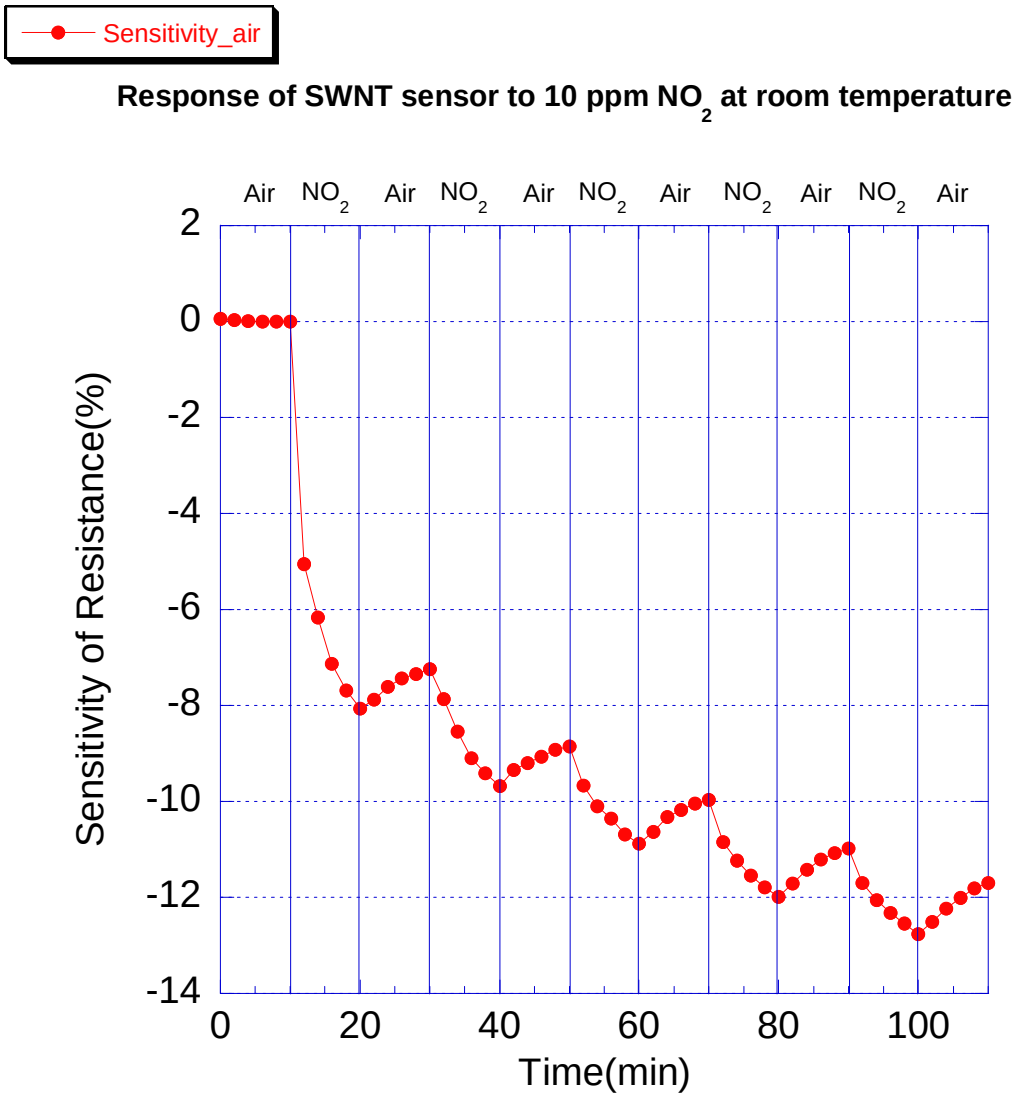

Figure 4.19: Measured resistance response as SWNT gas sensor is exposed to 10 ppm NO_2 and compressed air alternately for periods of 10 minutes each at room temperature. The sensor shows reversible response and incomplete recovery.

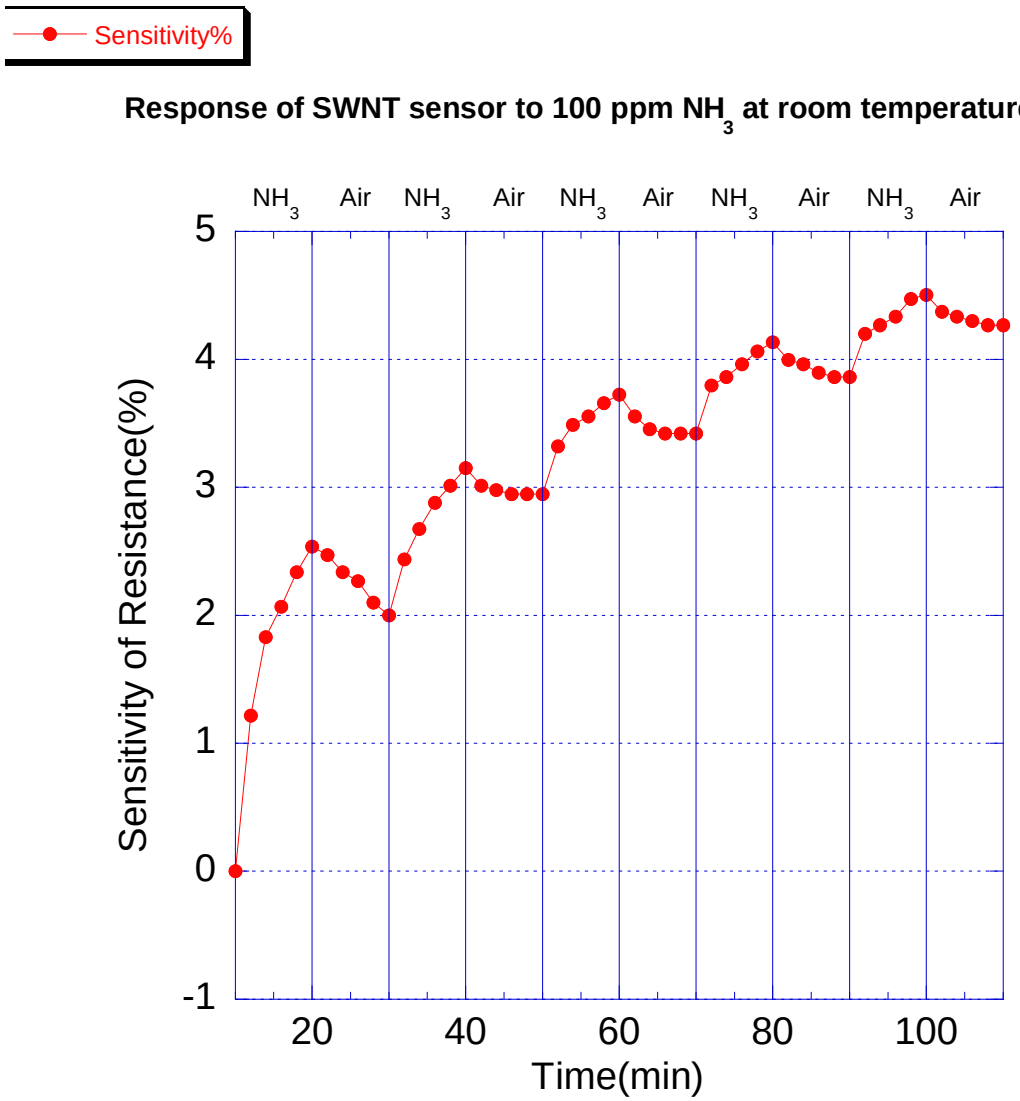

Figure 4.20: Measured resistance response as SWNT gas sensor is exposed to 100 ppm NH_3 and compressed air alternately for periods of 10 minutes each at room temperature. The sensor shows reversible response and incomplete recovery.

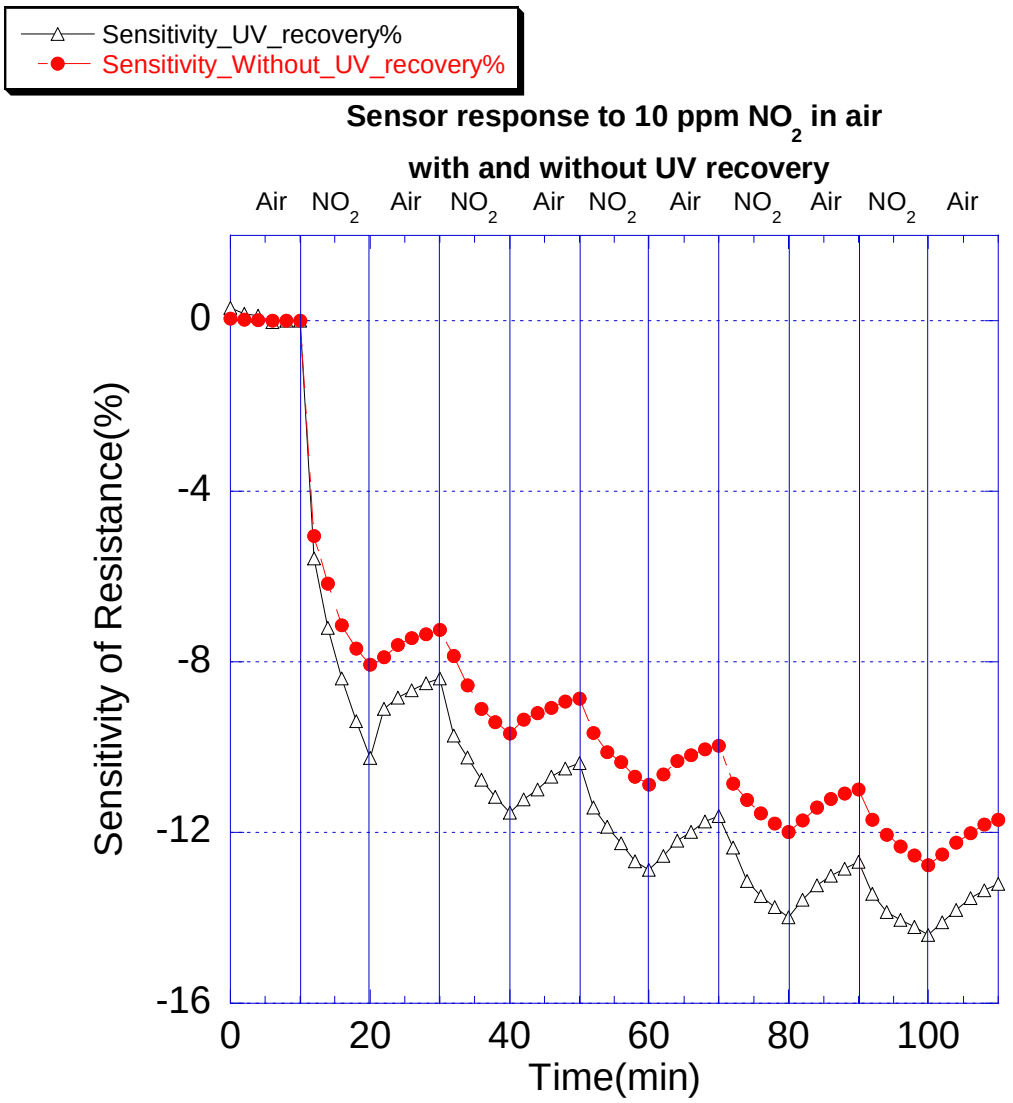

Figure 4.21: The effect of UV illumination on SWNT gas sensor recovery from 10 ppm NO_2 exposure in air. The red curve represents the sensor recovery in the flow of compressed air only. The black curve represents sensor recovery in the flow of compressed air with UV illumination.

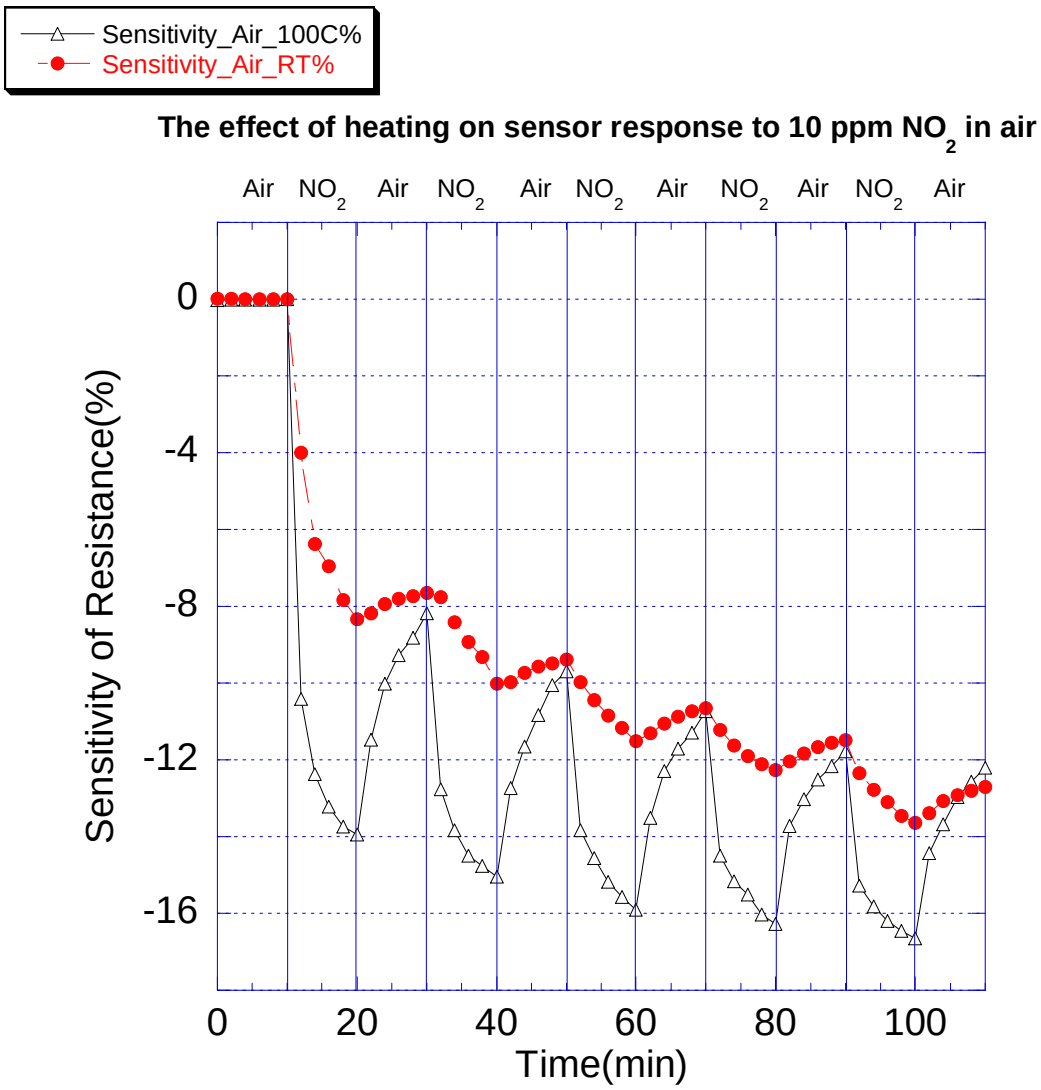

Figure 4.22: The effect of heating at 100ºC on SWNT gas sensor performance upon repeated 10 ppm NO_2 exposure in air. The red curve represents the sensor response at room temperature. The black curve represents the sensor response at 100ºC.

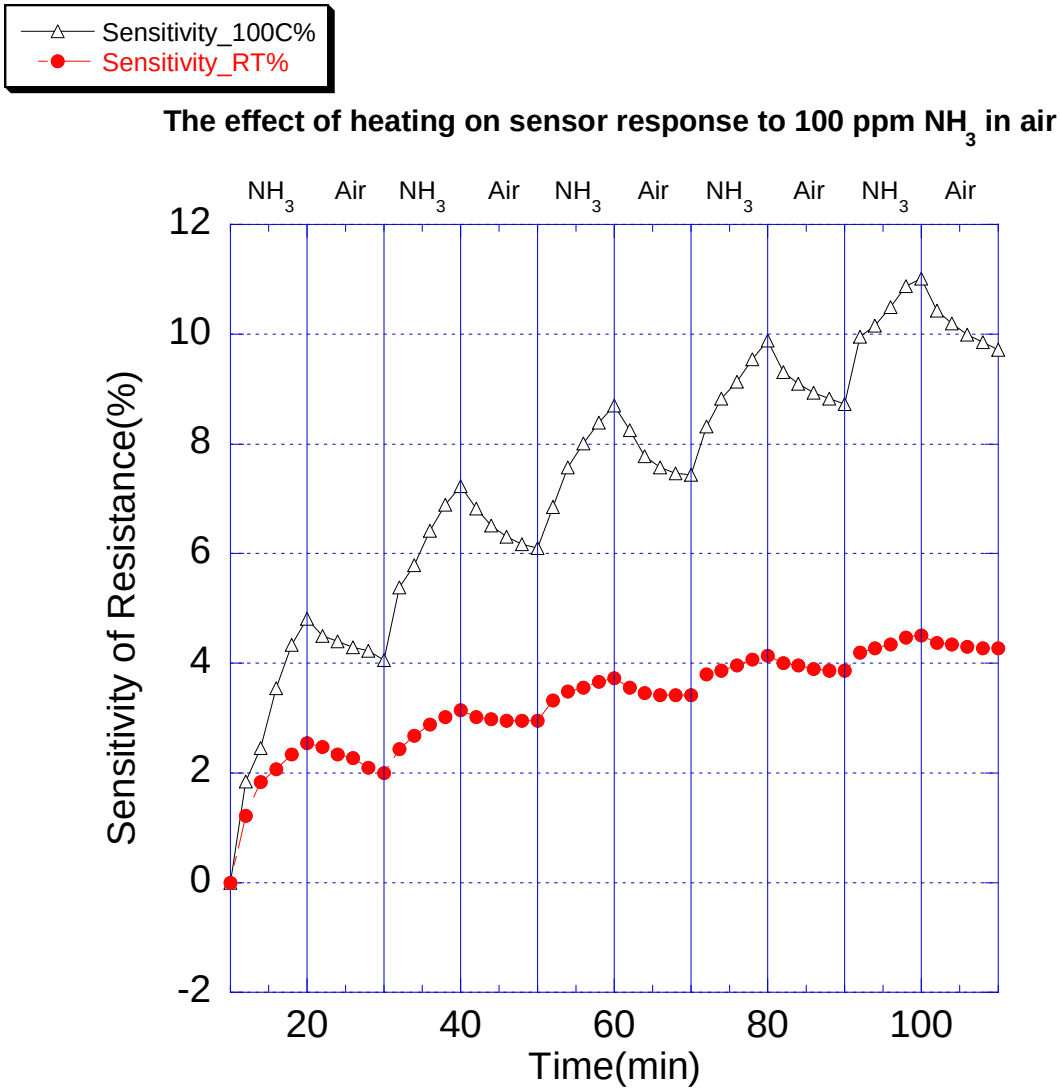

Figure 4.23: The effect of heating at 100ºC on SWNT gas sensor performance upon repeated 100 ppm NH_3 exposure in air. The red curve represents the sensor response at room temperature. The black curve represents the sensor response at 100ºC.

CHAPTER5: SUMMARY AND FUTURE WORK

5.1 Summary

This dissertation investigated the potential of carbon nanotubes as gas sensing materials at room temperature. An automated gas sensor testing system was designed and implemented, which features a PC controlled gas delivery system, real time electrical signal monitoring, data acquisition configuration, and LabVIEW programming. Resistive and capacitive gas sensors based on aligned MWNTs were fabricated and tested. It is the first report to construct a gas sensor device based on this unique CNT structure. The performance of a resistive sensor based on the mixture of low loading of SWNTs in organic binder was studied. To date, this is the lowest reported SWNT loading (1 wt %) for this type of sensor showing excellent response at room temperature.

Both MWNTs and SWNTs based gas sensors were designed, fabricated and tested in detection of common hazardous gases at room temperature. The carbon nanotubes employed in this work demonstrated p-type semiconducting characteristics and the sensors showed gas sensitivity at room temperature. The operating principles of the sensors were discussed in detail and techniques to improve the sensor performance were investigated.

5.1.1 Resistive sensing with aligned MWNTs

The amorphous carbon induced surface conductivity of the as-grown aligned MWNTs/AAO template was utilized to construct resistive sensor for preliminary gas detection. The results are as follows:

- At room temperature, the resistance of the as-grown MWNTs/AAO template shows an increase of 7.3% in the presence of 1% NH_3 gas for 60 minutes.
- The as-grown MWNTs/AAO template demonstrates reproducible, reversible as well as irreversible response to repeated 1% NH_3 exposure with an average sensitivity of 5.09%.

- The sensitivity increases as the NH_3 concentration increases. An average sensitivity of 10.9% was observed as the sample was subjected to multiple-cycled 5% NH_3 exposure at room temperature.
- The sample shows response to the presence of 100% CO_2 with an average sensitivity of 2.59%.
- The recovery is slow and incomplete. A strong humidity dependency was observed for the MWNTs based resistive sensor.
- Due to the strong humidity dependency and uncontrolled coverage of amorphous carbon on the surface of the as-grown MWNTs/AAO template, currently this type of material is only employed for preliminary gas sensing investigation instead of sensor device prototyping.

5.1.2 Capacitive sensing with aligned MWNTs

The amorphous carbon on the surface of as-grown MWNTs was removed by the method of plasma etching. Interdigitated capacitor was then patterned on the plasma-etched MWNTs/AAO template to form capacitive sensor for room temperature gas detection. The results are as follows:

- The MWNTs capacitive sensor demonstrates reproducible and reversible increase in capacitance to 1% NH_3 exposure with the sensitivity in the range of 0.25% to 0.3%.
- The sensitivity increases as the NH_3 concentration increases. An average sensitivity of 0.5% was observed as the sample was subjected to multiple-cycled 5% NH_3 exposure at room temperature.
- The sensor also demonstrated sensitivity to the presence of CO_2 and oxygen at room temperature.
- The in-depth investigation of the sensor electrical properties reveals that the sensor response was determined by the dielectric response instead of charge transfer between MWNTs and adsorbates.
- The magnitude of the capacitive sensitivity is restrained by the IDC electrode dimension, which is explained by the model of the capacitive sensor. In order to

improve the sensitivity, either the longer IDC electrodes or shorter distance between adjacent electrodes is required. Thus larger MWNTs/AAO sample size or finer pitch of IDC electrodes is essential to achieve better capacitive response.

- The MWNTs/AAO templates have demonstrated promising aspect for potential room temperature gas sensing applications. Some technical challenges have to be addressed, such as material reproducibility, structural robustness and batch productivity, in order to further investigate the possibility of device prototyping.

5.1.3 Resistive sensing with SWNTs

Resistive sensors were fabricated by coating the interdigitated electrodes with the mixture of SWNTs (1 wt% loading) and α-terpineol binder. The resistance of the sensor was monitored in the presence of various concentrations of NO_2 and NH_3 gas at room temperature. The results are as follows:

- The resistance of the SWNTs sensor undergoes drastic decrease in the presence of NO_2. It is decreased by an average of 11% in response to the exposure of 10 ppm NO_2 within 30 minutes.
- The sensor recovery is incomplete at room temperature. The incomplete recovery caused an undesirable, irreversible response as the sensor was employed for multiple cycle NO_2 detection.
- The sensitivity is nearly proportional to NO_2 concentrations with a lower detection limit of 1 ppm.
- The sensor demonstrates a 2.1% resistance increase in the presence of 100 ppm NH_3 at room temperature within 30 minutes.
- In response to repeated NH_3 exposure, the sensor shows both reversible and irreversible response. The irreversible response is due to the incomplete sensor recovery.
- The sensitivity increases corresponding to the increase of NH_3 concentration. The lower NH_3 detection limit is 10 ppm.
- The sensing mechanism of the SWNTs sensor can be explained by chemisorptions and physisorptions between nanotubes and gas molecules.

- The sensors demonstrate excellent sensitivity to both NO_2 and NH_3 in air as well as in N_2, which is a promising aspect towards device prototyping in the future.
- There is limited humidity dependency observed; however, the influence of temperature change on sensor performance needs in-depth study in the future.

5.1.4 Techniques to improve SWNTs sensor performance

The SWNT sensors demonstrate slow and incomplete recover characteristics, which in turn cause an undesirable drift of sensor resistance during the multiple-cycled gas detection. This incomplete recovery impairs the effectiveness of the gas sensing functionality towards practical applications. Hence UV illumination and moderate heating were investigated as the potential solutions to improve sensor recovery performance. The results are as follows:

- The UV illumination significantly enhanced the sensor recovery from NO_2 detection. The improved recovery is attributed to the photo-energy induced molecular desorption from SWNT sites. The adsorbed NO_2 molecules gain photon-energy from UV, overcome the desorption energy barrier and released from adsorption sites on SWNTs.
- During multiple-cycled NO_2 detection, the pre-depletion "cleaning effect" of UV illumination during sensor recovery creates additional adsorption sites for NO_2 gas molecules, and as a result, increased sensitivity.
- There is no positive impact of the UV illumination on sensor recovery during NH_3 detection, which is attributed to the effect of oxidized SWNTs. During recovery and under the impact of UV illumination, both NH_3 and oxygen desorbs from SWNTs. The desorption of NH_3 cause an increase of hole concentration in SWNTs, however it is counteracted by the desorption of oxygen which increases the electron concentration in nanotubes. Therefore for NH_3 detection, there is no enhancement in sensor recovery by the addition of UV illumination.
- By heating the sensor to a moderate temperature of 100ºC, both sensitivity and recovery have been significantly improved in NO_2 and NH_3 detection. Similar

observations were made when the gas detection was performed in air instead of N_2 ambient.

5.2 Future Work

There is substantial scope for carrying out further research that will extend the work presented in this dissertation. A few possible future directions are suggested as following:

- As discussed in section 3.3.2, the dimension of the IDC electrodes needs to be reduced in order to improve the gas sensitivity of the capacitive sensor which is based on MWNTs/AAO template. However the patterning techniques currently employed, including laser cut shadow mask and conductor paste screen printing, have limitations. In the future photo mask and photolithography could be upgraded options in consideration of the miniaturization process.
- The MWNTs resistive sensors show significant humidity dependency whereas the influence of humidity on the SWNTs resistive sensor is negligible. Further investigation is necessary to understand the mechanism and difference between them.
- Selectivity is an important aspect of sensor characteristic and should be studied in the future, particularly how the NO_2/NH_3 gas sensitivity will be affected by the presence of interference gases.
- A built-in heater could be incorporated into the existing SWNT sensor design. A serpentine platinum heater can be patterned on the back side of the ceramic sensor substrate thus the sensor can be heated to moderate temperature during operation to achieve better performance.
- A detailed investigation in the dependency of sensor performance on the SWNTs loading in sensing material would be necessary to gain better understanding of the sensing mechanism.

REFERENCES

[1] M. Madou, S. Morrison, Chemical sensing with solid state devices, Academic Press, Inc., San Diego, 1989.

[2] North American Gas Sensors and Gas Analyzers Markets, Published by Frost & Sullivan, 2004.

[3] S. Moulton, A. Minett, and G. wallace, Carbon nanotube based electronic and electrochemical sensors, Sensor Letters, 3 (2005) 183-193.

[4] Occupation Safety & Health Administration (OSHA), U. S. Department of Labor.

[5] S.M. Sze, Semiconductor sensors, John Wiley & Sons, Inc., New York, 1994.

[6] T. Seiyama, A. Kato, K. Fujushi, M. Nagatani, A new detector for gaseous components using semiconductive thin films, Anal. Chem. 34 (1962) 1502f.

[7] N. Taguchi, Japenese Patent 45-38200.

[8] N. Taguchi, Japenese Patent 47-38840.

[9] N. Taguchi, US Patent 3 644 795.

[10] P. R. Hauptmann, Selected examples of intelligent (micro) sensor systems: state-of the-art and tendencies, Meas. Sci. Technol., 17 (2006) 459–466.

[11] J.W. Gardner, and P.N. Bartlett, Electronic Noses Principles and Applications, Oxford University Press, New York, 1999.

[12] W. S. Lee, S. C. Lee, S. J. Lee, D. D. Lee, J. S. Huh, H. K. Jun, and J. C. Kim, The sensing behavior of SnO_2-based thick-film gas sensors at a low concentration of chemical agent simulants, Sensors and Actuators B, 108 (2005) 148–153.

[13] Application notes of International Sensor Technology (www.intlsensor.com).

[14] P. T. Moseley, J. Norris, and De Williams, Techniques and Mechanisms in Gas Sensing, Institute of Physics Publishing, 1991.

[15] Application notes of e2v Technologies PLC (www.e2v.com).

[16] K. Lundström, M. Shivaraman, and C. Svensson, A hydrogen-sensitive Pd-gate MOS transistor, J. Appl. Phys., 46 (1975) 3876-3881.

[17] D. Kohl, Function and applications of gas sensors, J. Phys. D: Appl. Phys. 34 (2001) R125-149.

[18] J. Ross, I. Robins, and B. Webb, The ammonia sensitivity of platinum-gate MOSFET devices: dependence on gate electrode morphology, Sens. Actuators. 11 (1987) 73-90.

[19] K. Lundström, M. Armgarth, A. Spetz, and F. Winquist, Gas sensors based on catalytic metal-gate field-effect devices, Sens. Actuators. 10 (1986) 399-421.

[20] N. Yamamoto, S. Tonomura, T. Matsuoka and H. Tsubomura, A study on a palladium-titanium oxide Schottky diode as a detector for gaseous components, Surf. Sci. 92 (1980) 400-406.

[21] G. Blackburn, M. Levy, and J. Janata, Field-effect transistor sensitive to dipolar molecules, Appl. Phys. Lett. 43 (1983) 700-701.

[22] P. Bergveld, J. Hendrikse, and W. Olthuis, Theory and application of the material work function for chemical sensors based on the field effect principle, Meas. Sci. Technol. 9 (1998) 1801–1808.

[23] D. McQuade, A. Pullen, and T. Swager, Conjugated polymer-based chemical sensors, Chem. Rev. 100 (2000) 2537–2574.

[24] M. Gerard, A. Chaubey, and B. Malhotra, Application of conducting polymers to biosensors, Biosens. Bioelectron.17 (2002) 345–359.

[25] Z. Deng, D. Stone, and M. Thompson, Poly N-(2-cyanoethyl) pyrrole as a selective film for the thickness-shear mode acoustic wave sensor, Can. J. Chem. 73 (1995) 1427-1435.

[26] M. Jocowicz, and J. Janata, Suspended gate field-effect transistor modified with poly (pyrrole) as alcohol sensor, Anal. Chem. 58 (1986) 514-517.

[27] P. T. Moseley, Solid state gas sensors, Meas. Sci. Technol. 8 (1997) 223–237.

[28] K. Drexler, Engines of creation: The Coming era of nanotechnology, Random House Inc., New York, 1987.

[29] S. Ijiima, Helical microtubules of graphitic carbon, Nature, 354 (1991) 56–58.

[30] R. Baughman, A. Zakhidov, and W. de Heer, Carbon nanotubes - the route toward applications, Science, 297 (2002) 787-792.

[31] J. Wildoer, L. Venema, A. Rinzler, R. Smalley, and C. Dekker, Electronic structure of atomically resolved carbon nanotubes, Nature, 391 (1998) 59-61.

[32] W. Hoenlein, F. Kreupl, G. Duesberg, A. Graham, M. Liebau, R. Seidel, and E. Unger, Carbon nanotubes for microelectronics: status and future prospects, Materials Science and Engineering, C23 (2003) 663-669.

[33] W. Liang, M. Bockrath, D. Bozovic, J. Hafner, M. Tinkham, and H. Park, Fabry - Perot interference in a nanotube electron waveguide, Nature, 411 (2001) 665-669.

[34] S. Frank, P. Poncharal, Z. Wang, and W. de Heer, Carbon nanotube quantum resistors, Science, 280 (1998) 1744-1746.

[35] P. Collins and P. Avouris, Nanotubes for electronics, Scientific American, 283 (2000) 62-69.

[36] P. Kim, L. Shi, A. Majumdar, and P. McEuen, Thermal transport measurements of individual multiwalled nanotubes, Phys. Rev. Lett., 87 (2001) 215502.

[37] M. Kociak, A. Kasumov, S. Guéron, B. Reulet, I. Khodos, Y. Gorbatov, V. Volkov, L. Vaccarini, and H. Bouchiat, Superconductivity in ropes of single-walled carbon nanotubes, Phys. Rev. Lett., 86 (2001) 2416–2419.

[38] Z. K. Tang, L. Zhang, N. Wang, X. X. Zhang, G. H. Wen, G. D. Li, J. N. Wang, C. T. Chan, and P. Sheng, Superconductivity in 4 angstrom single-walled carbon nanotubes, Science, 292 (2001) 2462-2465.

[39] G. Gao, T. Cagin, W. Goddard, Energetics, structure, mechanical and vibrational properties of single-walled carbon nanotubes, Nanotechnology, 9 (1998) 184-191.

[40] M. Yu, B. Files, S. Arepalli, and R. Ruoff, Tensile loading of ropes of single wall carbon nanotubes and their mechanical properties, Phys. Rev. Lett., 84 (2000) 5552-5555.

[41] M. Yu, O. Lourie, M. Dyer, K. Moloni, T. Kelly, and R. Ruoff, Strength and breaking mechanism of multiwalled carbon nanotubes under tensile load, Science, 287 (2000) 637-640.

[42] D. Qian, G. Wagner, W. Liu, M. Yu, and R. Ruoff, Mechanics of carbon nanotubes, Applied Mechanics Reviews, 55 (2002) 495-533.

[43] H. Dai, J. Hafner, A. Rinzler, D. Colbert, and R. Smalley, Nanotubes as nanoprobes in scanning probe microscopy, Nature, 384 (1996) 147-150.

[44] S. Wong, E. Joselevich, A. Woolley, C. Cheung, and C. Lieber, Covalently functionalized nanotubes as nanometre-sized probes in chemistry and biology, Nature, 394 (1998) 52-55.

[45] W de Heer, A. Chatelain, and D. Ugarte, A carbon nanotube field-emission electron source, Science, 270 (1995) 1179-1180.

[46] N. S. Lee, D. S. Chung, I. T. Han, J. H. Kang, Y. S. Choi, H. Y. Kim, S. H. Park, Y. W. Jin, W. K. Yi, M. J. Yun, J. E. Jung, C. J. Lee, J. H, You, S. H. Jo, C. G. Lee, and J. M. Kim, Application of carbon nanotubes to field emission displays, Diamond Relat. Materials, 10 (2001) 265-270.

[47] R. Baughman, C. Cui, A. Zakhidov, Z. Iqbal, J. Barisci, G. Spinks, G. Wallace, A. Mazzoldi, D. De Rossi, A. Rinzler, O. Jaschinski, S. Roth, and M. Kertesz, Carbon nanotube actuators, Science, 284 (1999) 1340-1344.

[48] S. Tans, A. Verschueren, and C. Dekker, Room-temperature transistor based on a single carbon nanotube, Nature, 393 (1998) 49-52.

[49] A. Bachthold, P. Hadley, T. Nakanishi, and C. Dekker, Logic circuits with carbon nanotube transistors, Science, 294 (2001) 1317-1320.

[50] S. Wind, J. Appenzeller, R. Martel, V. Derycke, and P. Avouris, Vertical scaling of carbon nanotube field-effect transistors using top gate electrodes, Appl. Phys. Lett., 80 (2002) 3817–3819.

[51] V. Derycke, R. Martel, J. Appenzeller, and P. Avouris, Carbon nanotube inter- and intramolecular gates, Nano Lett., 9 (2001) 453–456.

[52] www.fibrils.com.

[53] M. Biercuk, M. Llaguno, M. Radosavljevic, J. Hyun, and A. Johnson, Carbon nanotube composites for thermal management, Appl. Phys. Lett., 80 (2002) 2767–2769.

[54] M. Weisenberger, E. Grulke, D. Jacques, A. Rantell, and R. Andrews, Enhanced mechanical properties of polyacrylonitrile/multiwall carbon nanotube composite fibers, J. Nanosci. Nanotech., 3 (2003) 535-539.

[55] J. Kong, N. Franklin, C. Zhou, M. Chapline, S. Peng, K. Cho, and H. Dai, Nanotube molecular wires as chemical sensors, Science, 287 (2000) 622-625.

[56] P. Collins, K. Bradley, M. Ishigami, and A. Zettl, Extreme oxygen sensitivity of electronic properties of carbon nanotubes, Science, 287 (2000) 1801-1804.

[57] J. Li, Y. Lu, Q. Ye, M. Cinke, J. Han, and M. Meyyappan, Carbon nanotube sensors for gas and organic vapor detection, Nano Letters, 3 (2003) 929-933.

[58] R. Chen, N. Franklin, J. Kong, J. Cao, T. Tombler, Y. Zhang, and H. Dai, Molecular photodesorption from single-walled carbon nanotubes, Appl. Phys. Lett., 79 (2001) 2258-2260.

[59] J. Zhao, A. Buldum, J. Han, and J. Lu, Gas molecule adsorption in carbon nanotubes and nanotube bundles, Nanotechnology, 13 (2002) 195-200.

[60] K. Bradley, J. Gabriel, M. Briman, A. Star, and G. Gruner, Charge transfer from ammonia physisorbed on nanotubes, Phys. Rev. Lett., 91 (2003) 218301-1-4.

[61] P Qi, O. Vermesh, M. Grecu, A. Javey, Q Wang, and H Dai, Toward large arrays of multiplex functionalized carbon nanotube sensors for highly sensitive and selective molecular detection, Nano lett., 3 (2003) 347-351.

[62] H. Chang, J. Lee, S, Lee, and Y. lee, Adsorption of NH_3 and NO_2 molecules on carbon nanotubes, Appl. Phys. lett., 79 (2001) 3863-3865.

[63] C. Cantalini, L. Valentini, L. Lozzi, I. Armentano, J. Kenny, and S. Santucci, NO_2 gas sensitivity of carbon nanotubes obtained by plasma enhanced chemical vapor deposition, Sen. Actuators B, 93 (2003) 333-337.

[64] L. Valentini, I. Armentano, L. Lozzi, S. Santucchi, and J. Kenny, Interaction of methane with carbon nanotube thin films: role of defects and oxygen adsorption, Mater. Sci. Engin., C24 (2004) 527-533.

[65] S. Wang, Q. Zhang, D. Yang, P. Sellin, and G. Zhong, Multi-walled carbon nanotube-based gas sensors for NH_3 detection, Diamond and Related materials, 13 (2004) 1327-1332.

[66] E. Snow, F. Perkins, E. Houser, S. Badescu, and T. Reinecke, Chemical detection with a single-walled carbon nanotube capacitor, Science, 307 (2005) 1942-1945.

[67] E. Snow, F. Perkins, and J. Robinson, Chemical vapor detection using single-walled carbon nanotubes, Chem. Soc. Rev., 35 (2006) 790-798.

[68] O. Varghese, P. Kichambre, D. Gong, K. Ong, E. Dickey, and C. Grimes, Gas sensing characteristics of multi-wall carbon nanotubes , Sens and Actuat. B, 81 (2001) 32-41.

[69] K. Ong, K. Zeng, and C. Grimes, A wireless, passive carbon nanotubes-based gas sensor, IEEE Sensor Journal, 2 (2002) 82-88.

[70] S. Chopra, A. Pham, J. Gaillard, A. Parker, and A. Rao, carbon-nanotube-based resonant sensor for ammonia, Appl. Phys. lett. 80 (2002) 4632-4634.

[71] S. Chopra, K. McGuire, N. Gothard, A. Pham, and A. Rao, Selective gas detection using a carbon nanotube sensor, Appl. Phys. lett. 83 (2003) 2280-2282.

[72] V. jayaraman, Fabrication and characterization of porous alumina and cadmium sulfide for optoelectronic application, MS thesis, University of Kentucky Library, 2005.

[73] R. Andrews, D. Jacques, A. Rao, F. Derbyshire, D. Qian, X. Fan, E. Dickey and J. Chen, Continuous production of aligned carbon nanotubes: a step closer to commercial realization, Chem. Phys. Lett., 303 (1999) 467-474.

[74] K. Shelimov, D. Davydov, and M. Moskovits, Template-grown high-density nano-capacitor arrays, Appl. Phys. Lett., 77 (2000) 1722-1724.

[75] D. Ding, Z. Chen, S. Rajaputra, and V. Singh, Hydrogen sensors based on aligned carbon nanotubes in an anodic aluminum oxide template with palladium as a top electrode, Sensors and Actuators B, 124 (2007) 12-17.

[76] K. Ong, and C. Grimes, A carbon nanotube-based sensor for CO_2 monitoring, Sensors, 1 (2001) 193-205.

[77] K. Ong, and C. Grimes, A resonant printed-circuit sensor for remote query monitoring of environmental parameters, Smart Mater. Struct., 9 (2000) 421-428.

[78] K. Ong, C. Grimes, C. Robbins, and R. Singh, An inductor-capacitor resonant circuit remote query sensor: Design and application, Sens. Actuators A, 95 (2001) 33-43.

[79] C. Baird, Environmental chemistry, W.H. Freeman and Company, 1995.

[80] R. Moos, R. Muller, C. Plog, A. Knezevic, H. Leye, E. Irion, T. Braun, K. Marquardt, and K. Binder, Selective ammonia exhaust gas sensor for automotive applications, Sens. Actuators B, 83 (2002) 181-189.

[81] B. Timmer, W. Olthuis, and A. Berg, Ammonia sensors and their applications, Sens. Actuators B, 107 (2005) 666-677.

[82] T. Lindgren, D. Norback, K. Anderson, and B. Dammstrom, Cabin environment and perception of cabin air quality among commercial aircrew, Aviation Space and Environmental Medicine, 71 (2000) 774-782.

[83] S. Well, and J. DeSimone, CO_2 technology platform: an important tool for environmental problem solving, Angew. Chem. Int. Ed., 40 (2001) 518-527.

[84] P. Collis, M. Fuhrer, and A. Zettl, 1/f noise in carbon nanotubes, Appl. Phys. lett., 76 (2000) 894-896.

[85] H. Endres, and S. Drost, Optimization of the geometry of gas-sensitive interdigital capacitors, Sens. Actuators B, 4 (1991) 95-98.

[86] Adapted from University of Kentucky quarterly ACNP report, January, 2007.

[87] www.cheaptubesinc.com

[88] H. Q. Nguyen, V. T. Mai, B. H. Lee, and J. S. Huh, Effect of NH_3 gas on the electrical properties of single-walled carbon nanotubes bundles, Sens. Actuators B, 113 (2006) 341-346.

[89] H. Q. Nguyen, and J. S. Huh, Behavior of single-walled carbon nanotubes-base gas sensors at various temperatures of treatment and operation, Sens. Actuators B, 117 (2006) 426-430.

[90] W. Shi, and K. Johnson, Gas adsorption on heterogeneous single-walled carbon nanotubes bundles, Phys. Rev. Lett., 91 (1) (2003) 015504.

[91] M. Babaa, N. Dupont, E. Pavlovsky, K. McRae, and M. Varlot, Physical adsorption of carbon tetrachloride on as-produced and on mechanically opened single walled carbon nanotubes, Carbon, 42 (2004) 1549-1554.

[92] A. Kuznetsova, D. Mawhinney, V. Naumenko, J. Yates Jr., J. Liu, and R. Smalley, Enhancement of adsorption inside of single walled nanotubes: opening the entry port, Chem. Phys. Lett., 321 (2000) 292-296.

[93] M. Arab, F. Picaud, M. Devel, C. Ramseyer, and C. Giardet, Molecular selectivity due to adsorption properties in nanotubes, Phys. Rev. B, 69 (2004) 165401.

[94] M. Muris, N. Pavlovsky, M. Bienfait, and P. Zeppenfeld, Where are the molecules adsorbed on single-walled nanotubes, Surface Science, 492 (2001) 67-74.

[95] S. Santucci, S. Picozzi, F. Di Gregorio, L. Lozzi, C. Cantalini, L. Valentini, J. Kenny, and B. Delly, NO_2 and CO gas adsorption on carbon nanotubes: Experiment and theory, Journal of Chemical Physics, 119 (20) (2003) 10904-10910.

[96] H. Chang, J. Lee, S. Lee, and Y. Lee, Adsorption of NH_3 and NO_2 molecules on carbon nanotubes, Appl. Phys. Lett., 79 (23) (2001) 3863-3865.

[97] S. Jhi, S. Louie, and M. Cohen, Electronic properties of oxidized carbon nanotubes, Phys. Rev. Lett., 85 (8) (2000) 1710.

VITA

Ning was born on March 3, 1972 in Beijing, P. R. China. He earned his Bachelor's in Electrical Engineering from Nanjing University of Aeronautics & Astronautics in July 1994 and Master's in Electrical Engineering from University of Kentucky in May 2004, respectively. He worked as a senior Flight Safety Engineer at Air China in Beijing, China from August 1994 to July 2001. His research interests include gas sensors, MEMS, laser micromachining, and IC technologies.

Publications:

- Ning Ma and J. K. Lumpp, "SWNT-based Gas Sensor for NH_3 and NO_2 Detection," *Sensors & Actuators B: Chemical*, in revision.

- Ning Ma, S. Rajaputra, P. Clore, P. Sivakumar, J. K. Lumpp and V. Singh, "Design and Characterization of Aligned Carbon Nanotube based Gas Sensors," *Proceedings of 39th International Microelectronics and Packaging Symposium*, San Diego, California, October 2006.

- Suresh Rajaputra, Ning Ma, P. Clore, Dali Qian, R. Andrews, S. Phok, J. K. Lumpp and V. Singh, "Aligned Carbon Nanotube Arrays for Gas Sensing Applications," *Proceedings of Nanoelectronic Devices for Defense & Security Conference*, Crystal City, Virginia, June 2007.

- Suresh Rajaputra, Ning Ma, P. Clore, Dali Qian, R. Andrews, S. Phok, J. K. Lumpp and V. Singh, "Aligned Carbon Nanotube Arrays for Room Temperature Sensing of Ammonia and DMMP," accepted by *MRS Fall 2007 Meeting*, November 2007, Boston, MA.

- Jack Leifer, S.W. Smith, J. Black, Ning Ma, and J. K. Lumpp, "Measurement of In-plane Motion of Thin-film Structures using Videogrammetry," *Proceedings of 47th*

AIAA Structures, Structural Dynamics, and Materials Conference, vol. 2006-1805, May 2006, Newport, Rhode Island.

- Jack Leifer, S.W. Smith, J. Black, Ning Ma, and J. K. Lumpp, "Measurement of In-plane Motion of Thin-film Structures using Videogrammetry," *Journal of Spacecraft and Rockets*, vol. 44, No. 6, November/December 2007, in press.

- Ning Ma, "The study of excimer laser beam profile, homogenizer's beam shaping effect and fabrication of reflective patterned thin film test articles," Master's Thesis, Engineering Library, University of Kentucky, May 2004.

Ning Ma

12/04/2007